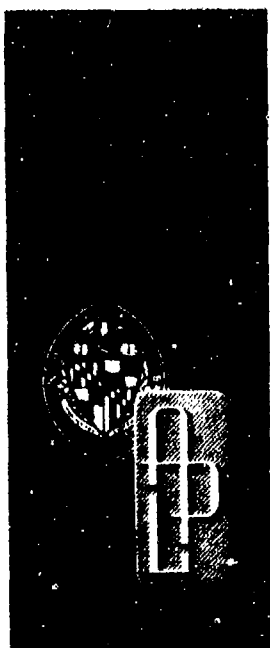


ADA 034213

APL/JHU  
TG 1283  
JULY 1976  
Copy No. 15



12 FG.

*Technical Memorandum*

# ANALYSIS OF A SINGLE-BIT DIGITAL RECEIVER FOR CARRIER AND CODE TRACKING

LARRY L. HOROWITZ

D D C  
RECEIVED  
JAN 11 1977  
R  
C

THE JOHNS HOPKINS UNIVERSITY - APPLIED PHYSICS LABORATORY

Approved for public release; distribution unlimited

REPORT DOCUMENTATION PAGE

1. REPORT NUMBER APL/JHU-TG-1283	2. GOVT ACCESSION NO	3. RECIPIENT'S CATALOG NUMBER 9
4. TITLE (and Subtitle) ANALYSIS OF A SINGLE-BIT DIGITAL RECEIVER FOR CARRIER AND CODE TRACKING	5. TYPE OF REPORT & PERIOD COVERED Technical Report	
7. AUTHOR(s) Larry L. Horowitz	6. PERFORMING ORG. REPORT NUMBER TG 1283	8. CONTRACT OR GRANT NUMBER(s) 15 N00017-72-c-4401
9. PERFORMING ORGANIZATION NAME & ADDRESS The Johns Hopkins University Applied Physics Laboratory Johns Hopkins Road Laurel, Maryland 20810	10. PROGRAM ELEMENT, PROJECT, TASK AREA & WORK UNIT NUMBERS Task P810	
11. CONTROLLING OFFICE NAME & ADDRESS Strategic Systems Project Office, SP-25 Washington, DC 20376	12. REPORT DATE 11 July 1976	13. NUMBER OF PAGES 139
14. MONITORING AGENCY NAME & ADDRESS Naval Plant Representative Office Johns Hopkins Road Laurel, MD 20810 12 141p.	15. SECURITY CLASS. (of this report) Unclassified	
16. DISTRIBUTION STATEMENT (of this Report) Approved for public release; distribution unlimited.	15a. DECLASSIFICATION/DOWNGRADING SCHEDULE NA D D C RECEIVED JAN 11 1977 REGULATORY	
17. DISTRIBUTION STATEMENT (of the abstract entered in Block 20, if different from Report) NA		
18. SUPPLEMENTARY NOTES NA		
19. KEY WORDS (Continue on reverse side if necessary and identify by block number) SATRACK Phase-locked loop Delay-locked loop Hard limiter		
20. ABSTRACT (Continue on reverse side if necessary and identify by block number) Post-flight processing of spread-spectrum signals often requires high-rate data recording. One way to lessen the recording rate requirement is to use single-bit quantization of the sampled signal in the recording. The performance of an aided digital post-flight receiver for carrier and code tracking when single-bit quantization is utilized in the data recording is here analyzed. The assumed signal structure is used in the SATRACK-GPS program.		

APL/JHU  
TG 1283  
JULY 1976

*Technical Memorandum*

**ANALYSIS OF A SINGLE-BIT  
DIGITAL RECEIVER FOR CARRIER AND  
CODE TRACKING**

LARRY L. HOROWITZ

ASSIGNED TO:  Wired System  Self Storage

NWS  
DPC  
TRANSMISSION  
JUSTIFICATION

BY: DISTRICT ENGINEER/QUALITY CONTROL

DATE: \_\_\_\_\_

*M*

THE JOHNS HOPKINS UNIVERSITY ■ APPLIED PHYSICS LABORATORY  
Johns Hopkins Road, Laurel, Maryland 20810  
Operating under Contract N00017-72-C-4401 with the Department of the Navy

Approved for public release; distribution unlimited

CONTENTS

List of Illustrations . . . . .	4
1. Introduction . . . . .	7
2. Description of the Shipboard Received Signal in the SATRACK Program . . . . .	8
3. Shipboard Preprocessor . . . . .	9
4. Postflight Digital Receiver . . . . .	10
5. Performance of the First Stage of the Digital Receiver . .	12
6. Performance of the Second Stage of the Digital Receiver .	19
7. Loop Gain Control . . . . .	22
8. Effects of Antenna Switching . . . . .	23
9. Conclusions and Suggestions for Future Work . . . . .	25
References . . . . .	26
Appendix A: Diagrams Related to the Digital Receiver . . .	27
Appendix B: An Example of Digital Receiver Performance . . . . .	37
Appendix C: SATRACK Carrier and PRN Processing Using an Analog Receiver Model . . . . .	45
Appendix D: A Single-Bit Processing Scheme for SATRACK-GPS Carrier Tracking . . . . .	69
Appendix E: Performance Analysis of the Coherent Binary Delay-Locked Loop for the SATRACK Digital Receiver . . . . .	109
Appendix F: Performance Analysis of the Noncoherent Carrier and Code Tracking Loops for the SATRACK Digital Receiver . . . . .	123
Appendix G: Some Practical Simplifications . . . . .	137

ILLUSTRATIONS

1	Performance Degradation Factors as a Function of Sampling Rate: (a) Factor for Eq. 3 (i.e., noncoherent delay-locked loop); (b) Factor for Eq. 11 and Eq. 18 (i.e., suppressed-carrier tracking loop or phase-locked loop) . . . . .	13
2	Performance Degradation Factor in Eq. 19, as a Function of Sampling Rate . . . . .	20
A-1	Preprocessing Aboard Range Ship . . . . .	29
A-2	The $i^{\text{th}}$ Postflight Receiver for $x(t)$ . . . . .	30
A-3	Noncoherent Delay-Locked Loop . . . . .	31
A-4	Suppressed-Carrier Tracking Loop. (Abbreviated signal components are included in diagram to aid in reading.).	33
A-5	Digital Phased-Locked Loop . . . . .	35
A-6	Binary Phase-Locked Loop . . . . .	36
C-1	The $i^{\text{th}}$ Postflight Receiver for $x(t)$ . . . . .	48
C-2	Noncoherent Delay-Locked Loop . . . . .	49
C-3	The Squaring Loop and Frequency Divider . . . . .	53
C-4	Phase-Locked Loop/Coherent Delay-Locked Loop . . . . .	58
C-5	Costas Loop . . . . .	63
C-6	Decision-Feedback Loop . . . . .	63
D-1	Preprocessing Aboard Range Ship . . . . .	70
D-2	IF Mixer and Digital Phase-Locked Loop (DPLL) . . . . .	71
D-3	Multiplication in a Phase Detector Gate: (a) Time Axis; (b) 100-kHz Sinusoid; (c) 100-kHz Sinusoid $90^\circ$ Offset from b; (d) 100-kHz Sinusoid $72^\circ$ Offset from b ( $18^\circ$ offset from perfect track); (e) Product of b and c in Phase Detector (sum of samples balanced to 0); (f) Product of b and d in Phase Detector (sum of samples is net positive, indicating relative position shift of b compared with d)	73

D-4	Response (in counts) of the Phase Detector for Different Relative Phase Shifts of the Input Waves from Perfect Tracking (90° offset) . . . . .	74
D-5	Response of Analog Loop Filter to a Step Function: (a) Analog Step Function; (b) Step Response of Filter .	76
D-6	Phase of Step Response of Analog VCO and Digital VCO .	77
D-7	Model of Noise-Free Digital Phase-Locked Loop . . . . .	78
D-8	Linearized Model of Noise-Free Digital Phase-Locked Loop ( $\tau = 0.75$ ) . . . . .	78
D-9	Effect of Input Noise on Sampled Data: (a) Sinusoidal Carrier Wave; (b) 1-Bit Quantized Samples of Sinusoid; (c) Sinusoid with Additive Input Noise; (d) 1-Bit Quantized Samples of Sinusoid with Noise . . . . .	81
D-10	Effect of Input Noise with Phase Comparator: (a) Noiseless Input Sinusoidal Wave; (b) 1-Bit Quantized Version of Sinusoid; (c) Squarewave Tracking Input Sinusoid; (d) Squarewave Slightly Offset in Phase from Perfect Track of Input Sinusoid; (e) Output of Phase Comparator for Inputs b and c; (f) Output of Phase Comparator for Inputs b and d; (g) Sinusoid from a, but Shaded Where Result of e is Positive; (h) Sinusoid from a, but Shaded Where Result of f is Positive . . . . .	83
D-11	Comparison of Power Spectral Densities: (a) Power Spectral Density of $n(t)$ ; (b) Power Spectral Density of $n_1(t)$ , $n_2(t)$ . . . . .	85
D-12	PSD of Double Frequency (200 MHz) Noise Term in the Output of Gate 5. (This noise is caused by the overlap of a box 2-MHz wide centered at 200 kHz and a box 2-MHz wide centered at -200 kHz) . . . . .	87
D-13	Relation Between the Phase Uncertainty (per hertz of loop bandwidth) at the VCO Output Caused by the Input and Input Noise (carrier power/noise spectral density) Ratio, $A^2/(N_0/2)$ . (log-log scale) . . . . .	91
D-14	Phase Variance at Output of 2-Hz Loop as a Function of Shipboard Sampling Rate . . . . .	93
D-15	Postulated Mean Response of Phase Detector to Phase Offsets, with $\gamma$ (= Input SNR) as a Parameter . . . . .	94

D-16	Relation of the Input Squarewave Reference to the BRM and the Output: (a) Input Squarewave Reference to BRM; (b) Output of 6-Bit BRM with Gate Set to 43 . . . . .	99
D-17	Output of Multiplier for Sinusoidal Inputs $[y(t)]$ and for 1-Bit Quantized Sinusoidal Inputs $[y_q(t)]$ . . . . .	103
E-1	Binary Delay-Locked Loop and Associated Processing . . . . .	111
E-2	Normalized Delay Variance at Output at 0.5-Hz Loop as a Function of Shipboard Sampling Rate. (log-log scale) . . . . .	119
E-3	Normalized Delay Variance at Output of 5-Hz Loop as a Function of Shipboard Sampling Rate. (linear scale) . . . . .	120
F-1	The Noncoherent Delay-Locked Loop . . . . .	125
F-2	Degradation of Signal/Noise Density Ratio in Eq. F-4 as a Function of Sampling Rate . . . . .	128
F-3	The Suppressed-Carrier Tracking Loop. (Abbreviated signal components are included in diagram to aid in reading.) . . . . .	131

## 1. INTRODUCTION

Postflight processing of spread-spectrum signals often requires high-rate data recording. One way to reduce the recording rate requirement is to use single-bit quantization (i.e., hard limiting) of the sampled signal in the recording.

The performance of an aided digital postflight receiver for carrier and code tracking when single-bit quantization is utilized in the data recording is here analyzed. The assumed signal structure is that used in the SATRACK-GPS program.

In the SATRACK scheme, signals originating from  $N$  in-view satellites ( $N \leq 7$ ) are transponded by a missile to receivers on range ships. The  $N$  satellites consist of  $N - 1$  Global Positioning System (GPS) satellites and one pseudosatellite (i.e., a range ship imitating a satellite). The signal received by the range ship is assumed to be single-bit quantized before being sampled and recorded for postflight processing. Telemetry and ground station data are used to aid the various tracking loops in the postflight receiver, permitting the bandwidths of these loops to be narrowed.

The body of this report combines the results of Appendixes D, E, and F, where investigations are made into the performance of component loops of the receiver. Detailed diagrams of the component loops of the receiver are given in Appendix A. An example of the performance of the receiver for a given set of input parameters and a given shipboard sampling rate is shown in Appendix B. The performance of an analog model of this receiver (continuous-time input, no quantization) is analyzed in Appendix C. Appendixes C, D, E, and F report the results of separate investigations carried out at different stages of the overall work. Thus at times the notations, system parameters, and receiver diagrams given in these appendixes differ from those given in the text and Appendix A.

The analysis in Sections 2 through 7 is for an uninterrupted input signal. In actuality, the SATRACK missile transponder switches between two pairs of receiving antennas every 1.152 ms. The received signal from each antenna pair is tracked by its own receiver, hence the input signal to the receiver is on for 1.152 ms, off for 1.152 ms, etc. The effect of this antenna switching and shipboard receiving antenna polarization are both discussed in Section 8.

## 2. DESCRIPTION OF THE SHIPBOARD RECEIVED SIGNAL IN THE SATRACK PROGRAM

In the SATRACK scheme, signals originating from  $N - 1$  in-view Global Positioning System satellites ( $N \leq 7$ ), and one pseudosatellite, are transponded by a missile to receivers on range ships. The signal received by a given range ship has the form,

$$x(t) = \sum_{i=1}^N \left\{ \sqrt{2} A_i(t) \text{PRN}_i(t - \lambda_i) m_i(t - \lambda_i) \sin[\omega_0 t + \phi_i(t)] \right\} + n(t), \quad (1)$$

where  $\lambda_i$  denotes the total time delay from signal transmission by satellite (i) to final signal reception by the ship; the function  $\text{PRN}_i(t)$  is a pseudorandom sequence (Gold code) of  $\pm 1$ 's with a bit (chip) length of  $\Delta = 10^{-6}/1.023$  second, and a sequence repetition rate (epoch rate) of 1 kHz (i.e., 1023 chips per epoch); the function  $m_i(t)$  is also a sequence of  $\pm 1$ 's, which among other things carries satellite orbit data; the chip length of  $m_i(t)$  is  $\Delta_m = 20$  ms; the phase function  $\phi_i(t)$  is the result of doppler shifts caused by satellite, missile, and range ship movement; and the noise function  $n(t)$  is white noise, which is bandlimited by the shipboard receiver, to  $\pm 1.073$  MHz about the missile transmission frequency,  $f_0 = 2200$  MHz. A  $\pm 1.073$  MHz bandwidth is chosen to allow room for the code width of 1.023 MHz, and a maximum doppler shift of  $\pm 50$  kHz. The power spectral density (PSD) of  $n(t)$  is given by  $N_0/2 = 10^{-17.2}$  (mW/Hz). The noise function may be written

$$n(t) = \sqrt{2} [n_1(t) \sin \omega_0 t + n_2(t) \cos \omega_0 t],$$

where  $n_1(t)$  and  $n_2(t)$  are independent white Gaussian noises, of power spectral density  $N_0/2$ , which are bandlimited to  $|f| \leq 1.073$  MHz. The carrier power for the  $i$ th signal,  $A_i^2$ , can range between  $10^{-14.7}$  and  $10^{-12.5}$  mW. The code sequences,  $\text{PRN}_i(t)$ , and their epoch times (as transmitted by the satellites) are known by the postflight receiver, although the delays  $\{\lambda_i\}$  are not known a priori. However, telemetry and ground station data are available to the receiver, and are converted into aiding information for the various receiver tracking loops. The data  $m_i(t)$  may be partially known a priori, but will be treated here as totally unknown.

### 3. SHIPBOARD PREPROCESSOR

The carrier signal received by the ship is first heterodyned down to 100 MHz and then input to the preprocessing scheme shown in Appendix A, Fig. A-1. The input signal to the preprocessor is heterodyned to a center frequency of 100 kHz. The doppler shift is expected to be less than 50 kHz on either side of this center frequency. The 2.146 MHz signal bandwidth is necessary because of the code width ( $\pm 1.023$  MHz) and the doppler shift. A 100 MHz low-pass filter is used to reject the double-angle signal and noise resulting from the mixing operation. The shipboard IF frequency was chosen at 100 MHz to avoid averaging the output of the mixer in the low-pass filter over any time period larger than that over which the low frequency component of this output (which has a bandwidth of 1.073 MHz) will change by 0.25 radian (Ref. 1). The I (in-phase) and Q (quadrature) channel signals recorded on the ship are given by

$$\begin{aligned}
 I: & \text{Sign} \left\{ A_1(t_n) m_1(t_n - \lambda_1) \text{PRN}_1(t_n - \lambda_1) \cos[\phi_1(t_n) + \omega_2 t_n - \theta] \right. \\
 & \quad \left. + n_1(t_n) \cos(\omega_2 t_n - \theta) - n_2(t_n) \sin(\omega_2 t_n - \theta) \right\} \\
 Q: & \text{Sign} \left\{ A_1(t_n) m_1(t_n - \lambda_1) \text{PRN}_1(t_n - \lambda_1) \sin[\phi_1(t_n) + \omega_2 t_n - \theta] \right. \\
 & \quad \left. + n_1(t_n) \sin(\omega_2 t_n - \theta) + n_2(t_n) \cos(\omega_2 t_n - \theta) \right\} .
 \end{aligned}$$

---

Ref. 1. W. E. Larimore, "Design and Performance of a Second-Order Digital Phase-Locked Loop," Symposium on Computer Processing in Communications, Polytechnic Institute of Brooklyn, 1969, pp. 343-356.

#### 4. POSTFLIGHT DIGITAL RECEIVER

The signal recorded on the range ship is processed at APL in the postflight digital receiver. The object of the receiver is to track the carrier doppler shifts of the signals from the various satellites, and the different delays of the PRN sequences. Telemetry and surface station data from the flight are provided to the postflight receiver to aid in this task.

The accuracy of the aiding signals determines the dynamics that the receiver loops must track. Given the order of a loop, the dynamics to be tracked essentially present a lower bound on the usable loop bandwidth. It is assumed that the accuracy of the aiding signals is sufficient to ensure that the loop bandwidths chosen in the examples are above these lower bounds.

Each of the  $N$  delays  $\{\lambda_i\}$  and doppler shifts  $\{\phi_i(t)\}$  are tracked with a separate receiver. The  $i$ th receiver uses its knowledge of the  $i$ th code sequence  $PRN_i(t)$  to separate its signal component from the other  $N - 1$  signal components in  $x(t)$  (see Eq. (1)). The interference in the  $i$ th receiver from the other  $N - 1$  signal components in  $x(t)$  will affect the performance of the receiver, and will superpose its effect with that caused by the noise  $n(t)$ . The effects of interference are deterministic in nature, and can perhaps be attenuated by, for example, processing the strongest signal first, and then compensating the receivers for the other signals with the information obtained about the strongest signal, etc. Concentration here will be on the effects of input noise. Thus we will deal with the signal  $x(t)$  as though it were in fact given by  $x_i(t)$ , a fictitious signal, defined as

$$x_i(t) = \sqrt{2}A_i(t)PRN_i(t - \lambda_i)m_i(t - \lambda_i)\sin[\omega_0 t + \phi_i(t)] + n(t) \quad (2)$$

The  $i$ th postflight receiver has the form shown in Appendix A, Fig. A-2. Note that the computer aids obtained from telemetry and ground station data are used in both stages of the receiver. The first stage of the receiver estimates the function  $m_i(t - \lambda_i)$  and stores it on tape. This modulation is then stripped off the input signal for use by the second stage. The first stage also obtains information on code epoch synchronization and carrier phase, which may be used in the second stage, along with (or combined with) the computer aids obtained from telemetry and ground station data. The second stage of the receiver uses the outputs of the first stage to aid the precision estimation of  $\phi_i(t)$  and the delay  $\lambda_i$ . If the information on code epochs and carrier phase is combined with the computer aids, off-line processing is required. For this

reason we show  $\hat{m}_1(t - \lambda_1)$  being put on tape, and the two stages of the receiver do not run concurrently. The various components pictured in Fig. A-2 are given in more detail in other figures of Appendix A. As to the performance of the receiver, the relationships given in the following discussion are valid for signal parameters within a few orders of magnitude of the SATRACK values (yielding quasilinear performance in the tracking loops). Very low signal levels cause threshold effects that are not accounted for here. High signal levels cause a decrease in the input-noise effects, bringing them down to the levels of the effects of noises generated internally by the tracking loops (e.g., see Appendix D). Signal power levels comparable to the input noise power (in a  $\pm 1.073$  MHz bandwidth) cause a loss of the dither provided by the input noise, and a consequent increase in nonlinear phenomena. A detailed example of the type of analysis used to obtain the following results is given in Appendix E.

## 5. PERFORMANCE OF THE FIRST STAGE OF THE DIGITAL RECEIVER

The main purpose of the first stage of the digital receiver is to estimate the data modulation,  $m_1(t - \lambda_1)$ . The first component of this stage of the digital receiver is the noncoherent delay-locked loop (DLL) (Appendix A, Fig. A-3). The purpose of this loop is to lock onto the PRN modulation and to remove it from the input signal (see Eq. (8)). The input signal is first heterodyned down to 0 frequency by an aided signal designed to also remove as much doppler shift as possible. The performance of this loop is analyzed in Appendix F. The rms delay error,  $\epsilon_1(t) = \lambda_1(t) - \hat{\lambda}_1(t)$ , at the loop output is given by

$$\frac{\sigma(\epsilon_1)}{\Delta} = \left\{ \left[ \frac{N_o (10^{0.19991})}{2A_1^2 (0.9029)} + 4 \left( \frac{N_o (10^{0.19991})}{2A_1^2 (0.9029)} \right)^2 (2B_w) \right] \left( \frac{B_{N1}}{2} \right) \right\}^{1/2}, \quad (3)$$

where  $B_w$  is the one-sided bandwidth of lowpass filters preceding the squarers. This width must be sufficient to pass both the data (50 Hz) and the aided doppler shift (say 20 Hz, although preliminary simulations show that 3 Hz is probably sufficient). Thus  $B_w$  could be chosen to be 70 Hz (a 1/140 second averager). The factors of 0.9029 represent the degradation in power caused by passing the data through a filter that passes only the first major lobe of the data power spectrum. This number represents the value of  $E[m_{1LP}]^2$  where  $m_{1LP}(Lt - \lambda_1)$  is the filtered data. The value 0.9029 is obtained by modeling the data as having a triangular autocorrelation function (see Appendix F). If the data were in fact a 40 ms square wave (the worst possible case), this factor would change to 0.81059.  $B_{N1}$  is the two-sided loop noise bandwidth. This parameter may be chosen to give the desired error performance, with the constraint that too small a value of  $B_{N1}$  will allow noises generated within the loop (not discussed here) to become significant factors. Note that, as discussed in Appendix D, local clock phase jitter is not a significant noise source, because of the synchronous control of the local clock, the loop sampling mechanism, and the reading of the input tape. The factor of  $10^{0.19991}$  is a function of the sampling rate, which is assumed here to be 2.5 MHz. In Fig. 1 the variation of this factor with sampling rate is plotted. Note that at 2.5 MHz the factor is 1.9991 dB below the line in Fig. 1 for analog continuous time processing, accounting for our factor of  $10^{0.19991}$  in Eq. (3). An ideal shipboard bandpass filter ( $\pm 1.073$  MHz) was assumed in the analysis. A comparison of Eq. (3) with the result of Gill (Ref. 2) for analog continuous time processing

---

Ref. 2. W. J. Gill, "A Comparison of Binary Delay-Lock Tracking Loop Implementations," IEEE Transactions on Aerospace and Electronic Systems, Vol. AES-2, No. 4, July 1966, pp. 415-424.

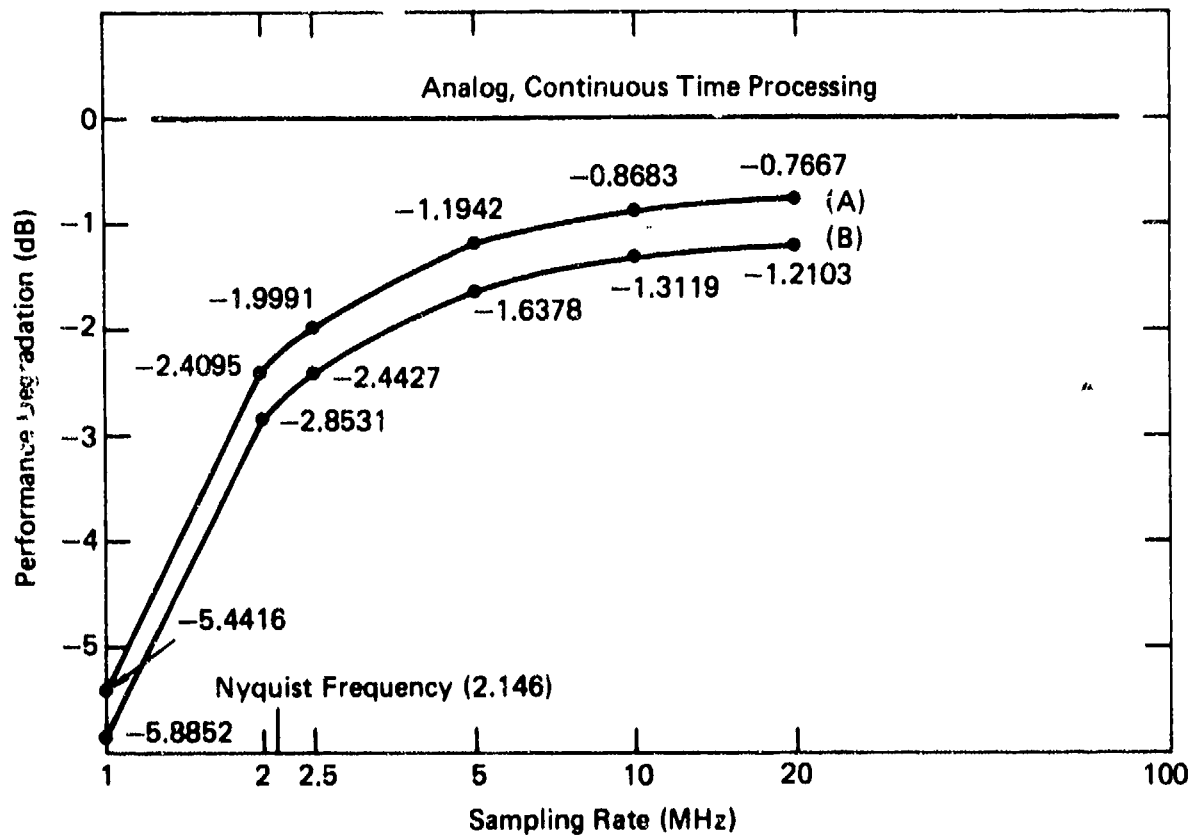


Fig. 1 Performance Degradation Factors as a Function of Sampling Rate: (a) Factor for Eq. 3 (i.e., noncoherent delay-locked loop); (b) Factor for Eq. 11 and Eq. 18 (i.e., suppressed-carrier tracking loop or phase-locked loop)

shows that the degradation caused by the shipboard bandpass filtering and single-bit processing is embodied in the factors of  $10^{0.19991}$  in Eq. (3). The multiplication of the band limited input noise by the reference code causes a 0.4436 dB decrease in noise power spectral density. The effect of this noise decrease is cancelled by a 0.4436 dB decrease in the slope of the code cross-correlation function, which, in turn, is caused by band limiting of the input signal (to be discussed). Thus shipboard band limiting produces no net effect. Consequently the factors of  $10^{0.19991}$  in Eq. (3) represent the effects of single-bit processing alone.

We find it useful later to calculate  $E[R_{PRN_1}(\epsilon_1)]$ , where  $R_{PRN_1}(\cdot)$  is the  $i$ th code autocorrelation function. Modeling  $\epsilon_1$  as Gaussian,

$$E[R_{PRN_1}(\epsilon_1)] \approx 1 - \left( \frac{2}{\sqrt{2\pi}} \right) \left( \frac{\sigma(\epsilon_1)}{\Delta} \right), \quad (4)$$

where  $\sigma(\epsilon_1)$  is obtained from Eq. (3).

Because of the single-bit processing, the mean output of the delay detector is decreased below the output that would be observed if there were no input noise. The factor of reduction is inversely proportional to the signal/noise variance ratio ( $SNR_1$ ) on the input signal, for the low SNR values that concern us. In our case, with a -147 dBm signal,  $SNR_1$  is given by

$$\frac{A_1^2}{\left(\frac{N_0}{2}\right)(2)\left(\text{recorded bandwidth}\right)} = \frac{A_1^2}{\left(\frac{N_0}{2}\right)(2)(2.146 \times 10^6)} = \frac{10^{-14.7}}{(10^{-17.2})(2)(2.146 \times 10^6)}$$

$$= -41.3266 \text{ dB}, \quad (5)$$

and we find that the scale factor with this ratio is 26490.8. Thus, if the signal level were in fact -135 dBm, then  $SNR_1$  would be -40.1266, and the scale factor would be

$$(26490.8) 10^{+4.01266 - 4.13266} = 20095.3 \quad (6)$$

We will discuss the internal loop signals as though sampling in the loops were being carried out at the same rate as the shipboard sampling. In fact, the loop sampling rates are variable, and the shipboard recorded signal is held at a constant level between its samples.

With 2.5 MHz sampling and a counter cycle of 1/139.997 second, the maximum count that could be observed at the output of Lowpass (1) in Appendix A, Fig. A-3 is  $(2.5 \times 10^6) (1/139.997) (2) = 35\,715$  counts. In the no-noise case, the signal that would be observed at this point is

$$(35715) m_{1LP}(t - \lambda_1) R_{PRN_1}(\lambda_1 - \hat{\lambda}_1) \left( 1 - \left| \left\{ -\pi + \left[ \phi_{d_1}(t) + \pi \right]_{\text{mod } 2\pi} \right\} \left( \frac{2}{\pi} \right) \right| \right), \quad (7)$$

where  $\phi_{d_1}(t) \triangleq \phi_1(t) - \phi_{\text{ref}_1}(t)$ ,  $m_{1LP}(t - \lambda_1)$  represents the filtered data, and  $R_{PRN_1}(\cdot)$  is the  $i$ th code autocorrelation function. The third factor in Eq. (7) is a cosine wave with triangular lobes. With input noise present, and a -147 dBm signal, there is a scale factor of  $\sqrt{26490.8} = 162.760$  associated with this signal [at  $\phi_{d_1}(t) = 0$ ]. So we would observe

$$35715 (\sqrt{26490.8})^{-1} m_{1LP}(t - \lambda_1) R_{PRN_1}(\lambda_1 - \hat{\lambda}_1) \cos \left[ \phi_{d_1}(t) \right] + n_{a1}(t) \quad (8a)$$

The transformation of the triangular wave to a cosine is discussed in Appendix D. The output of Lowpass (2) is given by

$$35715 (\sqrt{26490.8})^{-1} m_{1LP}(t - \lambda_1) R_{PRN_1}(\lambda_1 - \hat{\lambda}_1) \sin \left[ \phi_{d_1}(t) \right] + n_{b1}(t), \quad (8b)$$

where noise terms  $n_{a1}(t)$  and  $n_{b1}(t)$  are in quadrature. The signals in Eq. (8) are multilevel quantized and take new values every  $(139.997)^{-1}$  second. They will be referred to collectively as  $y_{11}(t)$ . The signal/noise density ratio in Eqs. (8a) and (8b) is given by

$$\frac{(10^{-0.24427}) (1/2) A_1^2}{\frac{N_o}{2}}$$

(The signal/noise density ratio of these signals without shipboard hard-limiting and sampling would have been  $(1/2) (A_1^2) (N_o/2)^{-1}$ ). The variation of the factor  $10^{-0.24427}$  with shipboard sampling rate is shown in Fig. 1. Thus we may determine the variance of  $n_{a1}(t)$  that would be observed at the output of Lowpass (1).

$$\frac{\text{signal power}}{\text{noise density}} = \frac{(1/2) [(35715) (\sqrt{26490.8})^{-1}]^2}{(139.997)^{-1} \sigma^2[n_{a1}(t)]} = \frac{(10^{-0.24427}) (1/2) (A_1^2)}{\frac{N_o}{2}},$$

thus

$$\sigma^2[n_{a1}(t)] = \sigma^2[n_{b1}(t)] = 37410.6 \text{ counts}^2 \quad (9)$$

The next phase of the tracking is a suppressed-carrier tracking loop. The intent is to track the phase angle in Eq. (8) in order to remove the sinusoids from the data modulation. (Recall that the PRN code has been removed by the noncoherent DLL.)

The suppressed-carrier tracking loop is shown in Appendix A, Fig. A-4. The output signals of the noncoherent delay-locked loop are first heterodyned up to a 25 Hz IF frequency so that the suppressed-carrier loop will not have to track near zero frequency. The loop itself is a combination of a squaring loop and a Costas loop. The combination is needed because the input signal from the ship is recorded at low enough frequency to have noise terms overlapping zero frequency. The output of this loop is two signals given by

$$y_{21}(t) = \begin{cases} \cos[\omega_1 t - \phi_{d1}(t) + n_{31}(t)] \\ \sin[\omega_1 t - \phi_{d1}(t) + n_{31}(t)] \end{cases}, \quad (10)$$

where  $n_{31}(t)$  is the phase tracking error. The rms value of  $n_{31}(t)$  is given by (see Appendix F)

$$n_{31}(t)_{\text{rms}} = \left\{ \left[ \frac{N_o (10^{0.24427})}{2A_1^2 (E[R_{\text{PRN}_1}(\epsilon_1)])^2 (0.9029)} + \left( \frac{N_o (10^{0.24427})}{2A_1^2 (E[R_{\text{PRN}_1}(\epsilon_1)])^2 (0.9029)} \right)^2 (2B_w) \right] B_{N2} \right\}^{1/2} \text{ rad}, \quad (11)$$

where  $B_{N2}$  is the two-sided loop bandwidth of the suppressed carrier loop, and  $E[R_{\text{PRN}_1}(\epsilon_1)]$  was evaluated in Eq. (4). The effect of changes in sampling rate on Eq. (11) is given in Fig. 1, analogously to the effect on Eq. (3). The factor  $10^{0.24427}$  in Eq. (11) represents 0.4436 dB more degradation than does the factor  $10^{0.19991}$  in Eq. (3). This difference is the result of ship-board bandpass filtering of the input signal. Here the effects of this operation are analyzed differently and more accurately than they are in Appendix F. The bandpass filtering affects the multiplications of the input signal by reference codes in the receiver. The cross correlation of the band limited input code with the reference code is a distorted version of the code autocorrelation function. The degradation in the peak value of the autocorrelation function affects the operation of any carrier tracking loops that follow code removal. The degradation in the slope of the autocorrelation function (in the neighborhood of  $+0.5\Delta$  and  $-0.5\Delta$  from the peak value) affects the operation of the delay-locked loops. For an ideal bandpass filter at the chip rate, the degradation in peak values is found to be 0.8872 dB. The degradation in slope is calculated for a causal first-order bandpass filter. (The causality seems to be important for this result.) The slope degradation is

approximately one-half of the peak value degradation, or 0.4436 dB. The result given in Appendix F (i.e., 1.999 dB degradation) included a 0.4436 dB degradation for both the phase-locked loops and the delay-locked loops. This is accurate for the delay-locked loops, but another 0.4436 dB must be subtracted for the phase-locked loops. This explains the extra factor of  $10^{0.04436}$  in Eq. (11), compared with Eq. (3).

Equation (11) may be compared with Eq. (10.52) in Ref. 3 where a suppressed carrier loop with analog continuous-time processing is analyzed. We see then that the factors of  $10^{0.24427}$  represent the degradation caused by shipboard bandpass filtering and single-bit quantization. As described above, the effects of shipboard band limiting are a 0.4436 dB decrease in noise power spectral density and a 0.8872 dB decrease in code cross correlation peak. Thus we may attribute a net degradation of 0.4436 dB to the shipboard bandpass filtering. This leaves a factor of  $10^{0.24427 - 0.04436} = 1.9991$  dB caused by the single-bit processing alone, as in Eq. (3).

It is useful to evaluate  $E \cos[n_{31}(t)]$  later. Modeling  $n_{31}(t)$  as Gaussian, we obtain

$$E \cos[n_{31}(t)] = \exp\left(-\frac{\sigma^2[n_{31}(t)]}{2}\right), \quad (12)$$

where  $\sigma^2[n_{31}(t)]$  is obtained from Eq. (11). The outputs of the carrier loop are mixed with the quantities in Eq. (8) as shown in Appendix A, Fig. A-4. This removes the carrier from the data. The result is given by

$$y_{31}(t) = m_{1,LP}(t - \lambda_1) \cos n_{31}(t) R_{PRN_1}[e_1(t)] + n_{41}(t), \quad (13)$$

where  $n_{41}(t)$  is a lowpass Gaussian process of 70 Hz bandwidth and  $10^{0.24427} (N_0/2A_1^2)$  power spectral density. There is a 180° phase ambiguity in  $y_{11}(t)$ ; thus the data sequence and its inverse are mutually indistinguishable. This has no effect on receiver performance, however, and will be ignored. Note that the data modulation on the signal transmitted by the satellite is the source of this 180° phase ambiguity. Because of differential encoding of the data, message estimation is also not affected. Appendix C describes both the technique for synchronizing the data clock (data transitions occur once every 20 code epochs, and are aligned with the code epochs) and the technique for estimating the bits in  $m_1(t - \lambda_1)$  given Eq. (13).

---

Ref. 3. A. J. Viterbi, Principles of Coherent Communication, McGraw-Hill Book Co., New York, 1966.

We obtain the following bit-estimation error probability:

$$P(E) \triangleq P \left[ \begin{array}{c} \hat{m}_1(t - \lambda_1) \\ \text{bit \#k} \end{array} \neq \begin{array}{c} m_1(t - \lambda_1) \\ \text{bit \#k} \end{array} \right] \approx 1/2 \left[ 1 - \operatorname{erf} \left( \sqrt{R'_{b1}} \left\{ E[R_{PRN_1}(\epsilon_1)] \right\} \left\{ E[\cos n_{31}(t)] \right\} \right) \right] \quad (14)$$

where

$$R'_{b1} = \left( \frac{A_1^2}{N_0 (10^{0.24427})} \right) (\Delta_m) \quad (15)$$

(Recall that  $(\Delta_m = 20 \text{ ms})$  and that  $\sigma(\epsilon_1)$  is given by Eq. (3).) The quantities in Eq. (14) are found in Eqs. (15), (4), and (12), respectively. The  $\operatorname{erf}(\cdot)$  is the tabulated error function. (In Eq. (14) any intersymbol interference effects and the fact that the signal in Eq. (13) only changes value every 1/140 second have been ignored.) It is useful to evaluate  $E[\hat{m}_1(t - \lambda_1) m_1(t - \lambda_1)]$ . First we must realize that, because of the code epoch estimation error, the probability that  $m_1(t - \lambda_1) \neq \hat{m}_1(t - \lambda_1)$  at any specific time is not equal to the bit-estimation error probability. Instead,

$$P(m \neq \hat{m}) \triangleq \operatorname{Prob} [\hat{m}_1(t - \lambda_1) \neq m_1(t - \lambda_1)] \approx [P(E)] \left( \frac{\Delta_m - \sigma(\epsilon_1)}{\Delta_m} \right) + 1/2 \left( \frac{\sigma(\epsilon_1)}{\Delta_m} \right) \quad (16)$$

We may then write

$$E(m\hat{m}) \triangleq E[\hat{m}_1(t - \lambda_1) m_1(t - \lambda_1)] = 1 \times P(m = \hat{m}) - 1 \times P(m \neq \hat{m}) \quad (17)$$

Equation (17) yields an important quantity for determining the operation of the second stage of the digital receiver. Incidentally, this quantity can be seriously degraded by the presence of cycle slips in the suppressed-carrier tracking loops. Thus this phenomenon must be avoided as much as possible. Some important simplifications possible in Fig. A-4 (Appendix A) and the data estimation are given in Appendix G.

An example of the determination of the performance of the entire receiver, given a set of sample signal parameters and a sampling rate, is done in Appendix B. In the next section, the second stage of the digital receiver is discussed.

## 6. PERFORMANCE OF THE SECOND STAGE OF THE DIGITAL RECEIVER

The phase-locked loop and coherent delay-locked loop that comprise the second stage of the postflight receiver for  $x_1(t)$  are here discussed. This stage performs the precision tracking of the doppler shift ( $\phi_1(t)$ ) and the delay ( $\lambda_1$ ). The operation of this stage will be aided by the value of  $\hat{m}_1(t - \lambda_1)$  determined by stage 1, and by the combination of carrier and code aids formed from both the output of stage 1 and the telemetry and ground station data (see Appendix A, Fig. A-2). The errors in this stage can be determined by iteratively solving a pair of simultaneous equations. The digital phase-locked loop is shown in Appendix A, Fig. A-5. If given the value of the delay error,  $\epsilon_{a1}(t) \triangleq \lambda_1(t) - \hat{\lambda}_{1a}(t)$ , of the coherent delay-locked loop, then the rms value of the phase error,  $\phi_{e1}(t) \triangleq \phi_1(t) - \hat{\phi}_{1a}(t)$ , of the phase-locked loop is given by

$$\sigma[\phi_{e1}(t)] = \left[ \left( \frac{N_o (10^{0.24427})}{2A_1^2} \right) \left( \frac{1}{\{E\{R_{PRN_1}[\epsilon_{a1}(t)]\}\}^2 [E(\hat{m}\hat{m})]^2} \right) B_{N4} \right]^{1/2} \text{ rad, (18)}$$

where  $B_{N4}$  is the loop noise bandwidth of the phase-locked loop.  $E[\hat{m}\hat{m}]$  was determined in Eq. (17), and  $E\{R_{PRN_1}[\epsilon_{a1}(t)]\}$  may be obtained by applying Eq. (4) to the rms value of  $\epsilon_{a1}(t)$ . The factor of  $10^{0.24427}$  is again a function of sampling rate, as shown in Fig. 1. Given  $\phi_{e1}(t)$ , the rms value of  $\epsilon_{a1}(t)$  in the delay-locked loop (Appendix A, Fig. A-6) may be obtained from

$$\frac{\sigma[\epsilon_{a1}(t)]}{\Delta} = \left[ \left( \frac{N_o (10^{0.18067})}{2A_1^2} \right) \left( \frac{1}{\{E[\cos \phi_{e1}(t)]\}^2 [E(\hat{m}\hat{m})]^2} \right) \left( \frac{B_{N3}}{2} \right) \right]^{1/2}, \quad (19)$$

where  $B_{N3}$  is the two-sided loop noise bandwidth of the delay-locked loop.  $E \cos \phi_{e1}(t)$  may be determined from the rms value of  $\phi_{e1}(t)$  by using Eq. (12). The factor  $10^{0.18067}$  is valid for 2.5 MHz sampling. The variation of this factor with sampling rate is given in Fig. 2. Note that for sampling at 20 MHz the degradation is 0.5043 dB. This checks well with the result of Spilker (Ref. 4), who finds a 0.414 dB degradation in binary delay-locked loop performance with continuous time processing following hard limiting. Also note from Fig. 1 that the phase-locked loop degradation with 20 MHz sampling is 1.2103 dB. As described

Ref. 4. J. J. Spilker, Jr., "Delay Lock Tracking of Binary Signals," IEEE Trans. on Space Electronics and Telemetry, Vol. SET-9, March 1963, pp. 1-8.

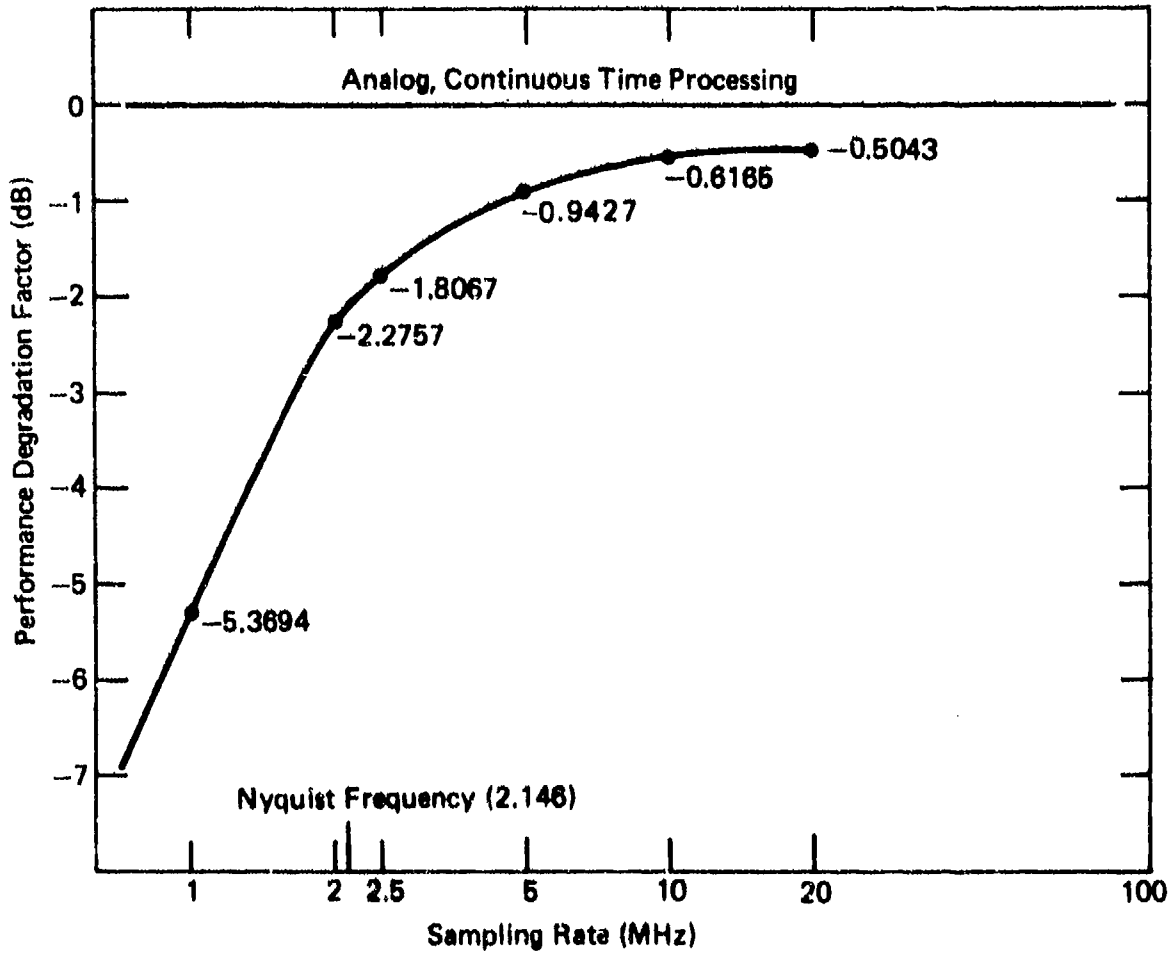


Fig. 2 Performance Degradation Factor in Eq. 19, as a Function of Sampling Rate

in Section 5, 0.4436 dB of this degradation is due to the shipboard bandpass filtering, leaving 0.7667 dB caused by single-bit quantization. This checks well with the results of Springett and Simon (Ref. 5), who found a 0.645 dB degradation under somewhat similar circumstances with continuous time processing. Equations (18) and (19) are simultaneous equations for  $\sigma[\phi_{e1}(t)]$  and  $\sigma[\epsilon_{a1}(t)]$ . These two equations can be solved by starting with  $E[R_{PRN1}(\epsilon_1)] \approx 1$ , obtaining  $\sigma[\phi_{e1}(t)]$  from Eq. (18), substituting this into Eq. (19) to get  $\sigma[\epsilon_{a1}(t)]$ , and proceeding iteratively until  $\sigma[\phi_{e1}(t)]$  and  $\sigma[\epsilon_{a1}(t)]$  converge.

Incidentally, Eq. (19) is derived by adding 0.4436 dB to the degradation given in Appendix E. This is necessitated by the bandpass filtering of the input code, not accounted for in Appendix E. Equation (18) is obtained from Appendixes D and F. The degradation determined in Appendix D was calculated in the absence of PRN modulation, which was included in obtaining Eq. (F-5) (Appendix F), which we use to get Eq. (18).

The scale factor degradation (caused by single-bit processing) in the output of the delay detector in the coherent DLL is given by the square root of the degradation found in Section 5 for the noncoherent DLL. Thus, if  $SNR_1 = -41.3266$  dB, then this scale factor is  $\sqrt{26490.8}$ . This factor is inversely proportional to  $\sqrt{SNR_1}$  in the coherent delay-locked loop. In the phase-locked loop, the scale factor is less than this by a factor of  $2/\pi$ , so it is given by  $(2/\pi)\sqrt{26490.8}$  for  $SNR_1 = -41.3266$  dB. Again, the factor is inversely proportional to  $\sqrt{SNR_1}$ . The physical cause of the  $\pi/2$  factor in mean phase detector output is that the recorded samples used to detect phase shifts in a coherent phase detector are the samples near the peaks of the received sinusoid, which are the most reliable samples in a noisy environment (Appendix D). The samples used to detect delay shifts in a delay detector are distributed among reliable and unreliable samples. An example of the determination of the performance of the digital receiver, given a set of sample signal parameters and a sampling rate, is done in Appendix B.

---

Ref. 5. J. C. Springett and M. K. Simon, "An Analysis of the Phase Coherent-Incoherent Output of the Bandpass Limiter," IEEE Trans. on Communication Technology, Vol. COM-19, No. 1, February 1971, pp. 42-49.

## 7. LOOP GAIN CONTROL

In the noncoherent delay-locked loop and the suppressed-carrier tracking loop, the scale factors affecting the detector outputs are inversely proportional to input  $\text{SNR}_1$ . In the coherent delay-locked loop and the phase-locked loop, the scale factors affecting the detector outputs are inversely proportional to  $\sqrt{\text{SNR}_1}$ . Thus, if it were desired to have constant bandwidths in each of these four loops it would be necessary to provide a factor proportional to  $1/(\text{SNR}_1)$  in the noncoherent loops, and proportional to  $1/\sqrt{\text{SNR}_1}$  in the coherent loops. A signal proportional to  $\text{SNR}_1$  is found at node (A) in Fig. A-4. This signal may be inverted to yield a number proportional to  $1/(\text{SNR})$  for use in the noncoherent loops. A signal proportional to  $\sqrt{\text{SNR}_1}$  is found at node (A) in Fig. A-6. This signal may be inverted to yield a number proportional to  $1/\sqrt{\text{SNR}_1}$  for use in the coherent loops. More details of the gain control in our example will be discussed in Appendix B.

## 8. EFFECTS OF ANTENNA SWITCHING

As mentioned in Section 1, the missile transponder switches its input between two separate pairs of receiving antennas every 1.152 ms. Synchronous modulation on a pilot carrier signal transmitted by the missile indicates when switching occurs. The signal from each pair of antennas will be tracked using its own receiver. The error detectors in the various component loops of the receiver tracking a specific pair of antennas will be turned off while the other pair of antennas is in use. The aiding signals will, however, continue to be input to the loops during these periods of no signal input.

It is presumed that the difference between the actual input phase (or delay) and the aiding signals is low frequency in nature. The switching rate is much faster than any of the receiver loop bandwidths, tending to minimize the dynamic effects of the switching on the receiver errors. Switching transients will have an effect, but that effect will not be treated here. Under these circumstances, the effect of the antenna switching is a 3 dB loss in each tracking loop (due to the effective decrease of integration time).

Thus, with 2.5 MHz sampling, Eq. (3) is replaced by

$$\frac{\sigma(\epsilon_1)}{\Delta} = \sqrt{2} \left\{ \left[ \frac{N_o (10^{0.19991})}{2A_1^2 (0.9029)} + \left( \frac{N_o (10^{0.19991})}{A_1^2 (0.9029)} \right)^2 (2B_w) \right] \left( \frac{B_{N1}}{2} \right) \right\}^{1/2}; \quad (20)$$

Equation (11) is replaced by

$$[n_{31}(t)]_{\text{rms}} = \sqrt{2} \left\{ \left[ \frac{N_o (10^{0.24427})}{2A_1^2 \{E[R_{\text{PRN}_1}(\epsilon_1)]\}^2 (0.9029)} + \left( \frac{N_o (10^{0.24427})}{2A_1^2 \{E[R_{\text{PRN}_1}(\epsilon_1)]\}^2 (0.9029)} \right)^2 (2B_w) \right] \left( \frac{B_{N2}}{2} \right) \right\}^{1/2} \text{ rad}; \quad (21)$$

Equation (15) is replaced by

$$R'_{b1} = \left( \frac{A_1^2}{N_o (10^{0.24427})} \right) \quad (22)$$

Equation (18) is replaced by

$$\sigma[\phi_{e1}(t)] = \sqrt{2} \left\{ \left( \frac{N_o (10^{0.24427})}{2A_1^2} \right) \left( \frac{1}{\{E[R_{PRN_1}(\epsilon_1)]\}^2 [E(\hat{m})]^2} \right) \left( B_{N4} \right) \right\}^{1/2} \text{ rad ;} \quad (23)$$

and Eq. (19) is replaced by

$$\frac{\sigma[\epsilon_{a1}(t)]}{\Delta} = \sqrt{2} \left\{ \left( \frac{N_o (10^{0.18067})}{2A_1^2} \right) \left( \frac{1}{\{E[\cos[\phi_{e1}(t)]]\}^2 [E(\hat{m})]^2} \right) \left( \frac{B_{N3}}{2} \right) \right\}^{1/2} \quad (24)$$

The results of right-circularly polarized shipboard reception and left-circularly polarized shipboard reception of the input signal are recorded separately on the ship. These receptions may be tracked separately by the postflight receiver. The result is a total of four tracking receivers (2 antenna pairs  $\times$  2 polarizations) for each satellite signal transponded by a given missile.

## 9. CONCLUSIONS AND SUGGESTIONS FOR FUTURE WORK

In this report the performance of a single-bit digital receiver for carrier and code processing has been analyzed. We have thus demonstrated the feasibility of single-bit quantization in the recording of spread-spectrum signals for postflight processing. Diagrams pertaining to the digital receiver were given.

The following facets of receiver performance were not discussed here, and are suggested for future investigations.

1. Acquisition behavior: The digital tracking loops, when operated in quasilinear regions, are expected to exhibit acquisition behavior analogous to the behavior of analog loops. Nonetheless, investigation here would be useful.
2. Nonlinear phenomena: Nonlinear performance may be caused both by low signal levels (threshold effects and cycle-slippage) and by high signal levels (loss of dither from input noise). These phenomena in the digital loops are still to be investigated.

REFERENCES

1. W. E. Larimore, "Design and Performance of a Second-Order Digital Phase-Locked Loop," Symposium on Computer Processing in Communications, Polytechnic Institute of Brooklyn, 1969, pp. 343-356.
2. W. J. Gill, "A Comparison of Binary Delay-Lock Tracking Loop Implementations," IEEE Transactions on Aerospace and Electronic Systems, Vol. AES-2, No. 4, July 1966, pp. 415-424.
3. A. J. Viterbi, Principles of Coherent Communication, McGraw-Hill Book Co., New York, 1966.
4. J. J. Spilker, Jr., "Delay Lock Tracking of Binary Signals," IEEE Trans. on Space Electronics and Telemetry, Vol. SET-9, March 1963, pp. 1-8.
5. J. C. Springett and M. K. Simon, "An Analysis of the Phase Coherent-Incoherent Output of the Bandpass Limiter," IEEE Trans. on Communication Technology, Vol. COM-19, No. 1, February 1971, pp. 42-49.
6. W. C. Lindsey and M. K. Simon, Telecommunication Systems Engineering, Prentice-Hall, Inc., New Jersey, 1973.
7. J. M. Wozencraft and L. M. Jacobs, Principles of Communication Engineering, John Wiley & Sons, New York, p. 2.5, 1967.
8. R. Jaffee and E. Rehtin, "Design and Performance of Phase Lock Circuits Capable of Near-Optimum Performance Over a Wide Range of Input Signal and Noise Levels," IRE Trans. on Information Theory, Vol. IT-1, March 1955, pp. 66-72.
9. R. Sydnor, J. J. Caldwell, and B. E. Rose, "Frequency Stability Requirements for Space Communications and Tracking Systems," Proc. IEEE, Vol. 54, No. 2, February 1966, pp. 231-236.
10. A. Papoulis, Probability, Random Variables, and Stochastic Processes, McGraw-Hill Book Co., New York, 1965, pp. 483-484.
11. R. W. Levinge, "Frequency Control Using Binary Rate Multipliers for Automatic Testing on CW Radar Systems," Proc. IEE, Vol. 121, No. 10, October 1974, pp. 1059-1966.

Appendix A

DIAGRAMS RELATED TO THE DIGITAL RECEIVER

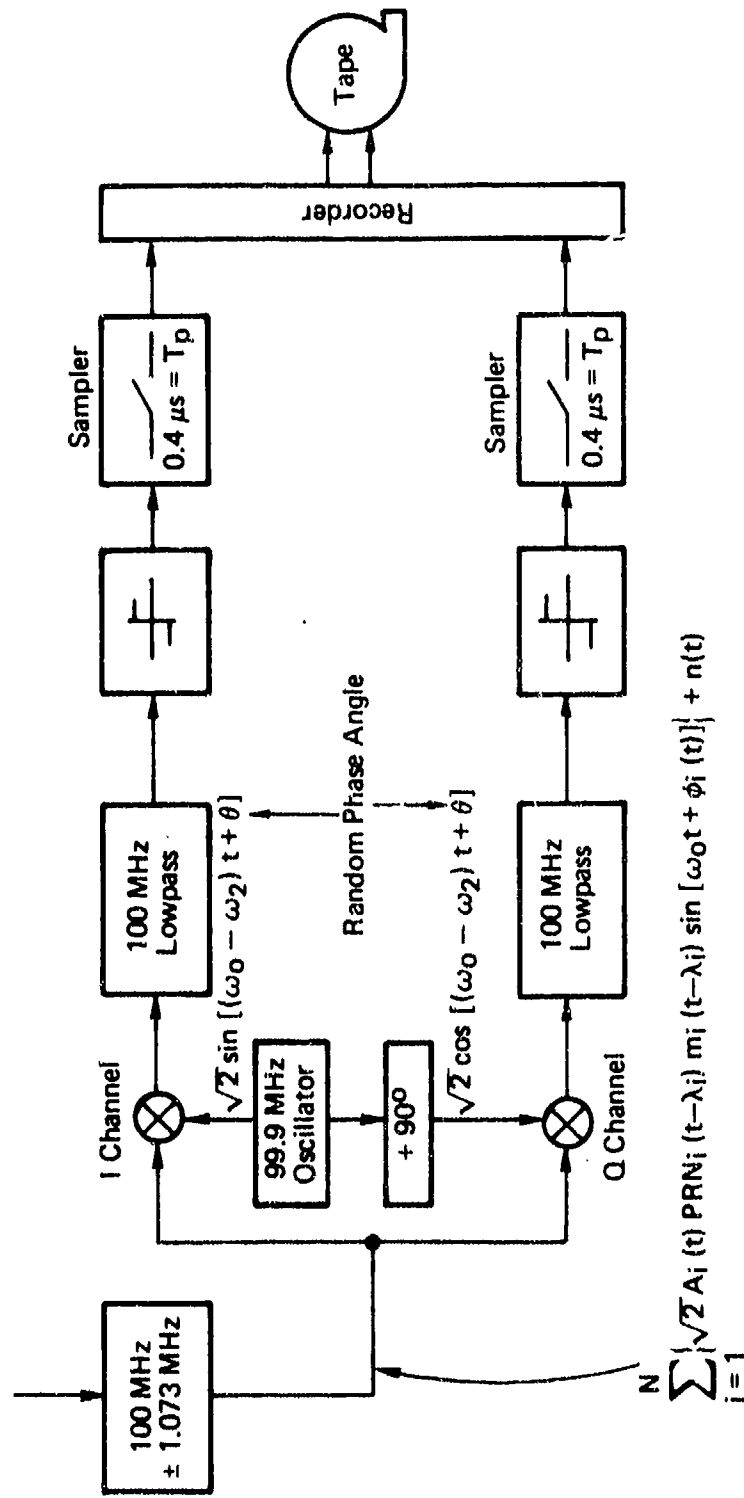


Fig. A-1 Preprocessing Aboard Range Ship

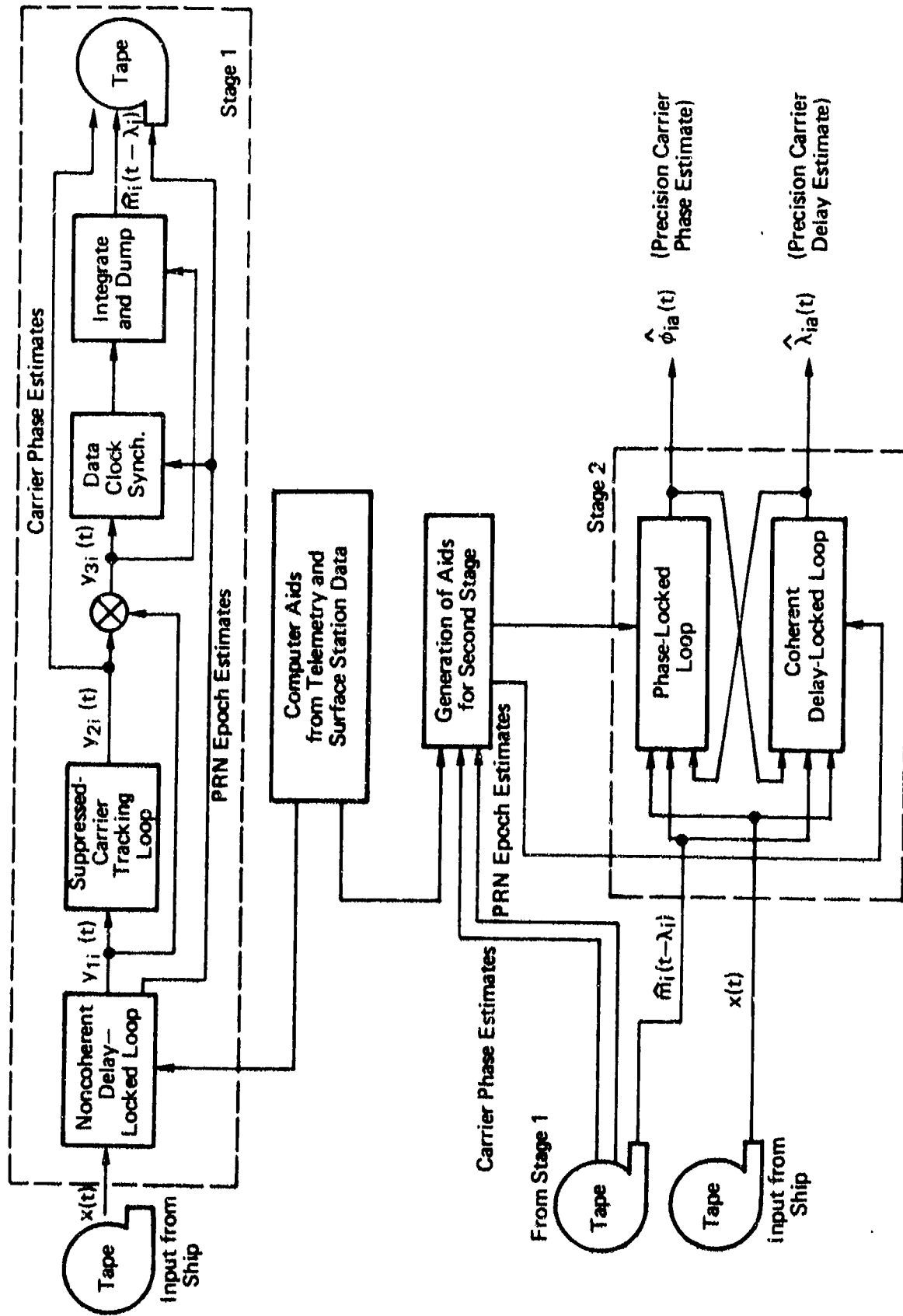


Fig. A-2 The  $i$ th Postflight Receiver for  $x(t)$

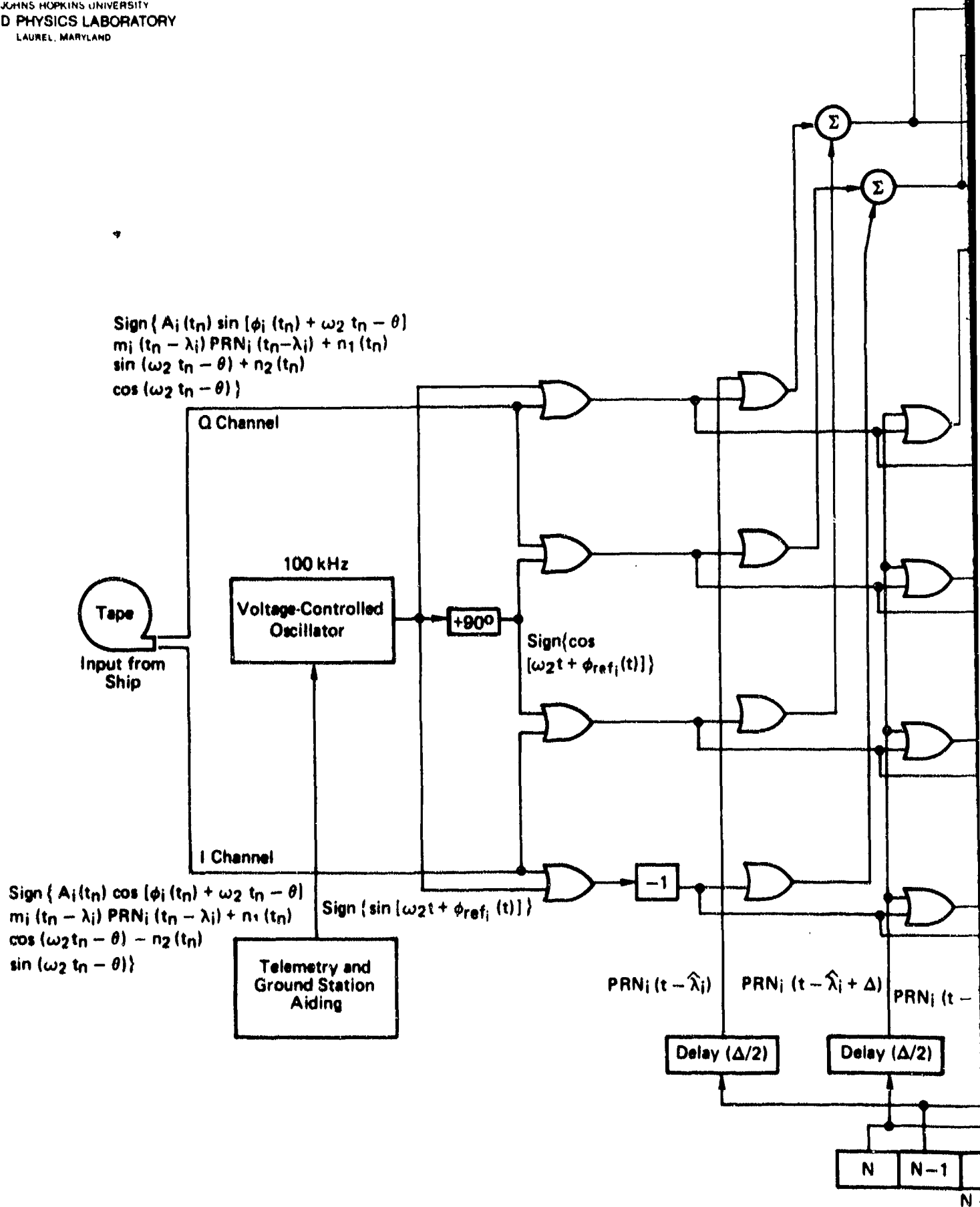


Fig. A-3 Noncoherent Delay-Locked Loop



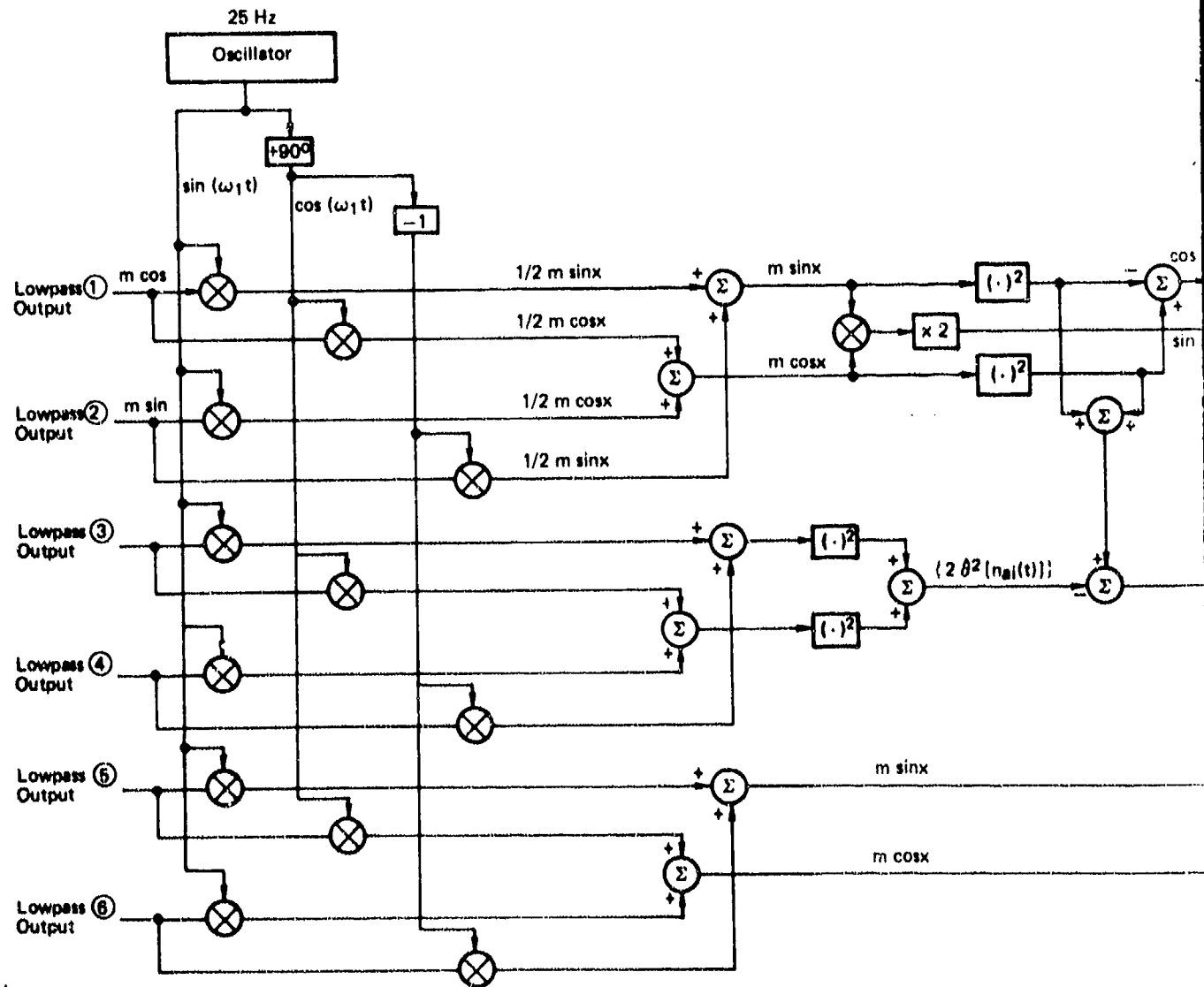
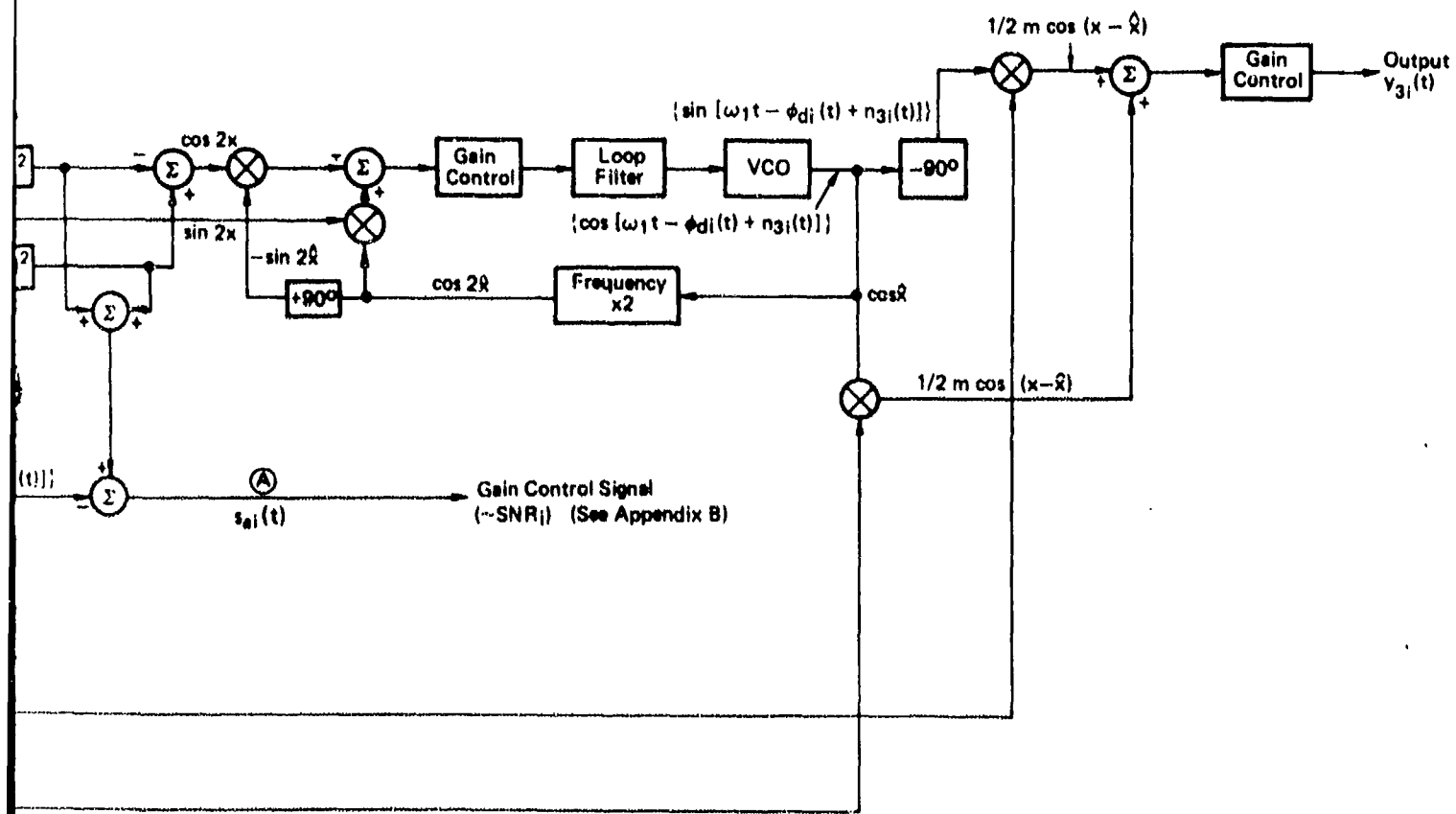


Fig. A-4 Suppressed-Carrier Tracking Loop  
 Elements are Included in Diagram to



Carrier Tracking Loop. (Abbreviated Signal Component in Diagram to Aid in Reading)

2

PRECEDING PAGE BLANK NOT FILMED

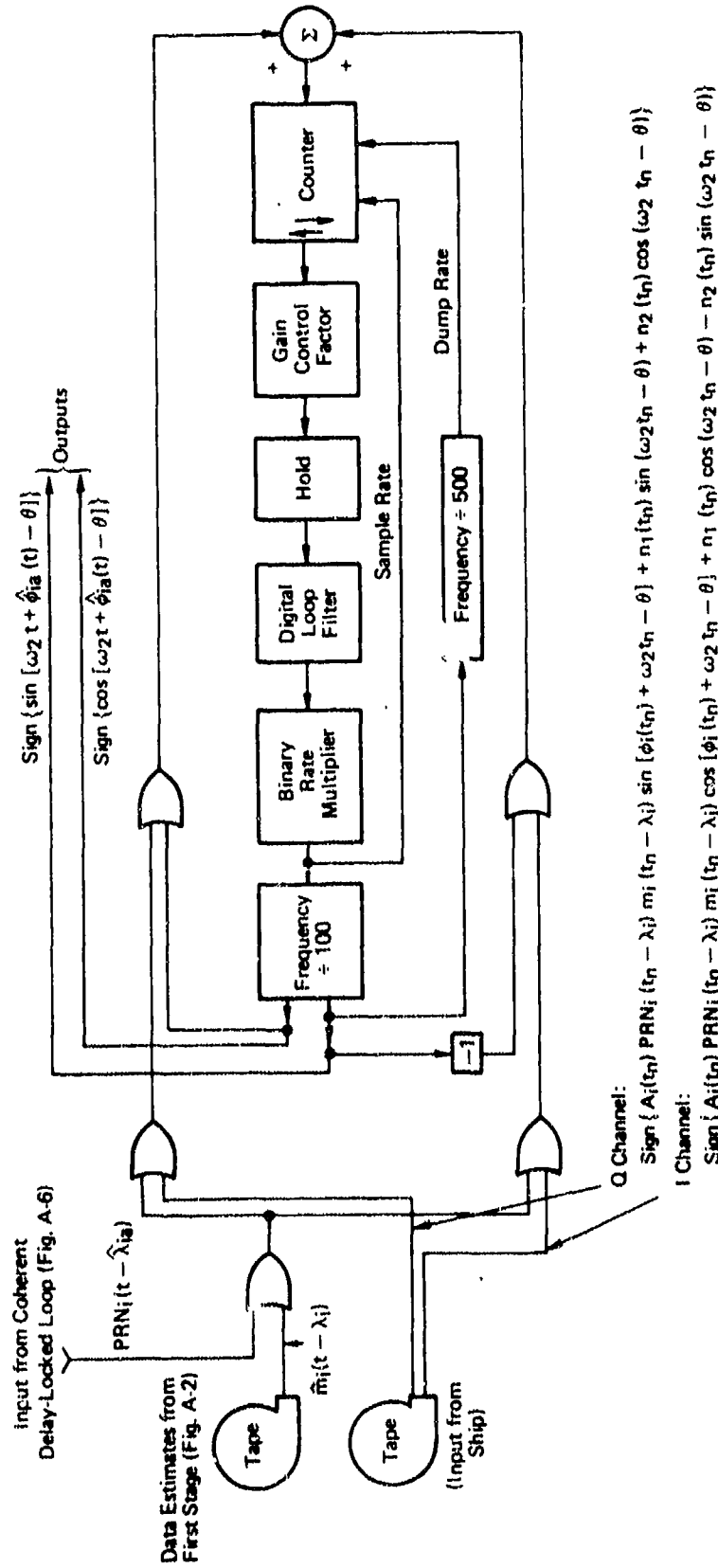


Fig. A-5 Digital Phase-Locked Loop

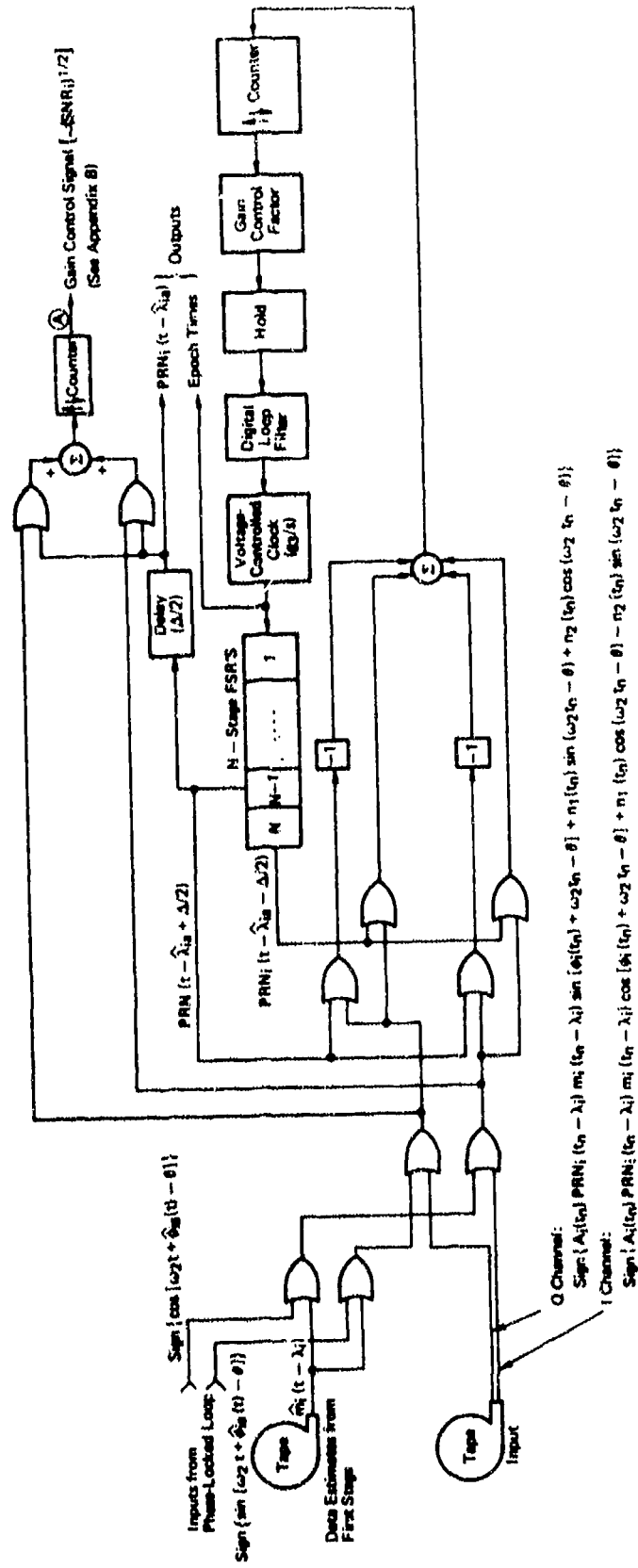


Fig. A-6 Binary Delay-Locked Loop

Appendix B

AN EXAMPLE OF DIGITAL RECEIVER PERFORMANCE

In this appendix the performance of the digital receiver is determined with sample values of the relevant parameters. Let the signal power be -130 dBm, the noise power spectral density (PSD) be  $N_0/2 = 10^{-17.2}$  mW, and the sampling rate be 5 MHz. The shipboard receiver bandwidth is still taken to be  $\pm 1.073$  MHz. The following analysis is done in the absence of antenna switching. (The effect of antenna switching is given in Section 8 of the main text.)  $SNR_1$  is given by

$$\frac{A_1^2}{\left(\frac{N_0}{2}\right)(2)(2.146 \times 10^6)} = \frac{10^{-13.0}}{(10^{-17.2})(2)(2.146 \times 10^6)} = -24.3266 \text{ dB} \quad (\text{B-1})$$

Thus, as demonstrated in Eq. (6), the scale factor affecting the mean output of the delay detector in the noncoherent delay-locked loop is

$$(26490.8)(10^{2.43266 - 4.13266}) = 528.561 \quad (\text{B-2})$$

The scale factor in the coherent delay-locked loop is the square root of this quantity, or 22.990. The scale factor in the phase-locked loop is  $(2/\pi)(22.990) = 14.636$ .

The outputs of Lowpass ① and Lowpass ② in Fig. A-3 are given by

$$(71430) \left( \frac{SNR_1}{(10^{-2.43266})(528.561)} \right)^{1/2} m_{iLP}(t - \lambda_1) R_{PRN_1}(\lambda_1 - \hat{\lambda}_1) \cos[\phi_{d_1}(t)] + n_{d_1}(t)$$

$$(71430) \left( \frac{SNR_1}{(10^{-2.43266})(528.561)} \right)^{1/2} m_{iLP}(t - \lambda_1) R_{PRN_1}(\lambda_1 - \hat{\lambda}_1) \sin[\phi_{d_1}(t)] + n_{d_1}(t) \quad (\text{B-3})$$

where 71430 is the maximum possible number of counts at the outputs of Lowpass ① or Lowpass ② after  $139.997^{-1}$  second. The variance of  $n_{ai}(t)$  may be found as in Eq. (9)

$$\frac{\text{Signal Power}}{\text{Noise Density}} = \frac{\left(\frac{1}{2}\right)(71430)^2 \left( \frac{\text{SNR}_1}{(10^{-2.43266})(528.561)} \right)}{(139.997)^{-1} \sigma^2[n_{ai}(t)]}$$

$$= \frac{(10^{-0.16378}) \left(\frac{1}{2}\right) A_1^2}{\left(\frac{N_0}{2}\right)} \quad (\text{B-4})$$

$$\sigma^2[n_{ai}(t)] = \sigma^2[n_{bi}(t)]$$

$$= 124326.8 \text{ counts}^2 \quad (\text{B-5})$$

Thus  $n_{ai}(t)$  has a PSD of  $(124326.8)(139.997)^{-1} = 888.07$  (counts<sup>2</sup>/Hz). The variance of  $n_{ai}(t)$ , and its PSD, are independent of the SNR, as can be seen from Eq. (B-4). They are functions only of the sampling rate and the accumulation time of the low-pass filter. We have assumed the loop sampling rates to be equal to the shipboard sampling rate. If the sampling rates internal to the loops are faster than the shipboard sampling rate, the signal means will change in predictable manners. The signal power/noise density ratios will remain constant, so that the noise variances may again be determined, using Eq. (9), for example, in this particular case. The signal at node ① in Fig. A-4 is given by

$$s_{ai}(t) = (71430)^2 \left( \frac{\text{SNR}_1}{(10^{-2.43266})(528.561)} \right) m_{1LP}^2 R_{PRN1}^2 (\lambda_1 - \hat{\lambda}_1)$$

$$- (71430)^2 \left( \frac{\text{SNR}_1}{(10^{-2.43266})(528.561)} \right) m_{1LP}^2 R_{PRN1}^2 (\lambda - \hat{\lambda}_1 + \Delta)$$

$$+ n_{gli}(t) \quad (\text{B-6})$$

For  $\hat{\lambda}_1 \approx \lambda_1$ ,  $R_{PRN1}^2(\lambda_1 - \hat{\lambda}_1) \approx 1$ , and  $R_{PRN1}^2(\lambda - \hat{\lambda}_1 + \Delta) \approx 0$ . Also  $m_{1LP}^2 \approx 0.9029$ , and  $n_{gli}(t)$  has PSD given by

$$8(888.07)^2(139.997) + 4(71430)^2 \left( \frac{\text{SNR}_1}{(10^{-2.43266}) (528.561)} \right) \\
 \times m_{LP}^2 R_{PRN_1}^2 (\lambda_1 - \hat{\lambda}_1) (888.07) \text{ counts}^2/\text{Hz} . \quad (\text{B-7})$$

Equation (B-6) may be rewritten as

$$s_{ai}(t) \approx (71430)^2 \left( \frac{\text{SNR}_1}{(10^{-2.43266}) (528.561)} \right) (0.9029) + n_{gli}(t) ,$$

where the PSD of  $n_{gli}(t)$  is given by

$$8(888.07)^2(139.997) + 4(71430)^2 \left( \frac{\text{SNR}_1}{(10^{-2.43266}) (528.561)} \right) (0.9029) (888.07) . \quad (\text{B-8})$$

Thus, if  $s_{ai}(t)$  is averaged for  $T_a$  seconds, its mean value will be given by

$$(71430)^2 \left( \frac{\text{SNR}_1}{(10^{-2.43266}) (528.561)} \right) (0.9029) \quad (\text{B-9})$$

and the rms noise on this observation will be

$$\left\{ \left[ 8(888.07)^2(139.997) + 4(71430)^2 \left( \frac{\text{SNR}_1}{(10^{-2.43266}) (528.561)} \right) (0.9029) (888.07) \right] \left( \frac{1}{T_a} \right) \right\}^{1/2} \text{ counts} . \quad (\text{B-10})$$

For  $\text{SNR}_1$  in the neighborhood of -24.3266 dB, the rms error (with 0.1 second averaging) is  $5.6 \times 10^5$  counts. This gives a relative precision of 6% in the estimation of  $\text{SNR}_1$  in this neighborhood; that is,

$$\frac{5.6 \times 10^5}{\left( \frac{(71430)^2(0.9029)}{(10^{-2.43266}) (528.561)} \right) (10^{-2.43266})} \approx 0.06$$

In place of that part of the gain control circuitry in Fig. A-3 and Fig. A-4 that estimates  $2\sigma^2[n_{ai}(t)]$ , it is possible instead to use the analytically determined value in Eq. (B-5). The first noise term in Eq. (B-10) would then be reduced by a factor of 2; however, in this case, if the loop sampling rate is variable, it would then be necessary to

average  $\sigma^2[n_{a1}(t)]$  over the interval of interest, as the sampling rate changes. Gain control proportional to  $(\text{SNR}_1)^{-1}$  is necessary in the noncoherent DLL, in the suppressed-carrier loop, and at the output of the suppressed-carrier loop.

Next, the performance of the first stage of the digital receiver will be determined. Using Eq. (3), we find that (with 5 MHz sampling, and  $B_{N1} = 1$  Hz):

$$\frac{\sigma(\epsilon_1)}{\Delta} = \left\{ \left[ \frac{(10^{-17.2})(10^{0.11942})}{(10^{-13.0})(0.9029)} \right. \right. \\ \left. \left. + 4 \left( \frac{(10^{-17.2})(10^{0.11942})}{(10^{-13.0})(0.9029)} \right)^2 (140) \right] (0.5) \right\}^{1/2}$$

$$\frac{\sigma(\epsilon_1)}{\Delta} = (6.955 \times 10^{-3}) \Delta = 6.799 \text{ ns} . \quad (\text{B-11})$$

Then, from Eq. (4)

$$E[R_{\text{PRN}_1}(\epsilon_1)] = 1 - \left( \frac{2}{\sqrt{2\pi}} \right) (6.955 \times 10^{-3}) = 0.99445 \quad (\text{B-12})$$

Further, from Eq. (11) we have (let  $B_{N2} = 1$  Hz)

$$[n_{31}(t)]_{\text{rms}} = \left\{ \left[ \frac{(10^{-17.2})(10^{0.16378})}{(10^{-13.0})(0.99445)^2(0.9029)} \right. \right. \\ \left. \left. + \left( \frac{(10^{-17.2})(10^{0.16378})}{(10^{-13.0})(0.99445)^2(0.9029)} \right)^2 (140) \right] (1) \right\}^{1/2}$$

$$[n_{31}(t)]_{\text{rms}} = 0.01022 \times 10^{-3} \text{ rad} = 0.5858^\circ , \quad (\text{B-13})$$

and obtain from Eq. (12)

$$E\{\cos[n_{31}(t)]\} = \exp \left[ -\frac{(0.01022)^2}{2} \right] = 0.999948 . \quad (\text{B-14})$$

For the operation of the bit estimator, we obtain from Eq. (15)

$$R'_{bi} = \left( \frac{10^{-13.0}}{(2 \times 10^{-17.2})(10^{0.16378})} \right) (20 \times 10^{-3})$$

$$R'_{bi} = 108.698 ; \quad (B-15)$$

then from Eq. (14),

$$P(E) \approx \frac{1}{2} \left\{ 1 - \operatorname{erf} \left[ (\sqrt{108.698})(0.99445)(0.999948) \right] \right\}$$

$$P(E) \approx \frac{1}{2} \left[ 1 - \operatorname{erf} (10.3674) \right]$$

$$P(E) \approx 5.6744 \times 10^{-49} \quad (B-16)$$

and from Eq. (16)

$$P(m \neq \hat{m}) \approx (5.6744 \times 10^{-49}) \left( \frac{20 \times 10^{-3} - 6.799 \times 10^{-9}}{20 \times 10^{-3}} \right)$$

$$\left( + \frac{1}{2} \frac{6.799 \times 10^{-9}}{20 \times 10^{-3}} \right)$$

$$P(m \neq \hat{m}) \approx 1.69975 \times 10^{-7} . \quad (B-17)$$

Finally, from Eq. (17),

$$E(m\hat{m}) = (1 - 3.3995 \times 10^{-7}) \approx 1$$

$$E(m\hat{m}) \approx 1 . \quad (B-18)$$

This value of  $E(m\hat{m})$  indicates that the data estimation is essentially perfect, so far as the second stage of the receiver is concerned. For smaller signal power/noise density ratios  $E(m\hat{m})$  is smaller.

Next, the operation of the second stage of the receiver is discussed. As mentioned in Section 8 of the main report, the gain control signal for the coherent loops is found at node (A) in Fig. A-6. If the cycle time of the counter at this node is given by 0.1 second, then the

maximum possible number of counts observable there is

$$(0.1)(5 \times 10^6)(2) = 10^6 .$$

The signal at node  $\textcircled{A}$  is analogous to that at the output of Lowpass

$\textcircled{1}$  in Fig. A-3, as described in Eq. (B-3):

$$(10^6) \left( \frac{\text{SNR}_1}{(10^{-2.43266})(528.561)} \right)^{1/2} m_{1\text{LP}}(t - \lambda_1) \hat{m}_{1\text{LP}}(t - \lambda_1) R_{\text{PRN}_1}(\lambda_1 - \hat{\lambda}_{1a}) \cos \phi_{e1}(t) + n_{g21}(t) \quad (\text{B-19})$$

The signal power/noise density ratio is the same as in Eq. (B-4). We may thus determine  $\sigma^2[n_{g21}(t)]$ .

$$\begin{aligned} \frac{\text{Signal Power}}{\text{Noise Density}} &= \frac{(\frac{1}{2} \times 10^6) \left( \frac{\text{SNR}_1}{(10^{-2.43266})(477.2388)} \right)}{(0.1)\sigma^2(n_{g21}(t))} \\ &= \frac{(10^{-0.11942})(\frac{1}{2})(A_1^2)}{(\frac{\sigma}{2})} \end{aligned} \quad (\text{B-20})$$

$$\sigma^2[n_{g21}(t)] = 1740541 \quad (\text{B-21})$$

For  $\lambda_1(t) \approx \hat{\lambda}_1(t)$  and  $\phi_{e1}(t) \approx 0$ , we have that  $R_{\text{PRN}_1}(\lambda_1 - \hat{\lambda}_{1a}) \approx 1$ , and  $\cos \phi_{e1}(t) \approx 1$ . The value of  $m_{1\text{LP}}(t - \lambda_1)m_{1\text{LP}}(t - \lambda_1)$  is itself a weak function of  $\text{SNR}_1$ , a fact that we will ignore and merely assign it the value 1, as determined earlier in this appendix. For  $\text{SNR}$  in the neighborhood of -24.3266, and with 0.1-second averaging, the rms noise on the measurement is  $\sqrt{1740541} = 1319$  counts, and the relative precision of the estimate of  $(\text{SNR}_1)^{1/2}$  is 3%.

The performance of the second stage of the receiver is determined next. We first rewrite Eqs. (18) and (19), the simultaneous equations for the rms errors of the second-stage tracking loops. Recall that the 5 MHz sampling rate changes a factor in these equations, as given in Figs. 1 and 2.

We will solve these equations

$$\sigma[\phi_{ei}(t)] = \left[ \left( \frac{N_o(10^{0.16378})}{2A_1^2} \right) \left( \frac{1}{(E\{R_{PRN_1}[\epsilon_{ai}(t)]\})^2 (E[\hat{m}\hat{m}])^2} \right) \left( \frac{B_{N4}}{2} \right) \right]^{1/2} \text{ rad} \quad (\text{B-22})$$

$$\frac{\sigma[\epsilon_{ai}(t)]}{\Delta} = \left[ \left( \frac{N_o(10^{0.09427})}{2A_1^2} \right) \left( \frac{1}{(E\{\cos[\phi_{ei}(t)]\})^2 (E[\hat{m}\hat{m}])^2} \right) \left( \frac{B_{N3}}{2} \right) \right]^{1/2} \quad (\text{B-23})$$

We will solve these equations iteratively. Start by setting  $E\{R_{PRN_1}[\epsilon_{ai}(t)]\} = 1$  in Eq. (B-22). Then, using Eq. (B-18) and letting  $B_{N4} = 1$  Hz we obtain

$$\sigma[\phi_{ei}(t)] = \left[ \left( \frac{(10^{-17.2})(10^{0.16378})}{10^{-13.0}} \right) (1) (1) \right]^{1/2} \text{ rad} ,$$

$$\sigma[\phi_{ei}(t)] = 9.592 \times 10^{-3} \text{ rad} = 0.5755^\circ . \quad (\text{B-24})$$

Substituting Eq. (B-24) into Eq. (12), we obtain

$$E[\cos n_{31}(t)] = 0.999954 . \quad (\text{B-25})$$

Substituting Eq. (B-25) into Eq. (B-23), and letting  $B_{N3} = 1$  Hz, we have

$$\frac{\sigma[\epsilon_{ai}(t)]}{\Delta} = \left[ \left( \frac{(10^{-17.2})(10^{0.09427})}{10^{-13.0}} \right) \left( \frac{1}{(0.999954)(1)} \right) (0.5) \right]^{1/2}$$

$$\frac{\sigma[\epsilon_{ai}(t)]}{\Delta} = 6.261 \times 10^{-3} . \quad (\text{B-26})$$

We then use this quantity in Eq. (4) to obtain

$$E\{R_{PRN_1}[\epsilon_{ai}(t)]\} = 0.99500 . \quad (\text{B-27})$$

By substituting Eq. (B-27) into Eq. (B-22), we now obtain

$$\sigma[\phi_{ei}(t)] = 9.640 \times 10^{-3} = 0.5523^\circ . \quad (\text{B-28})$$

The iteration is continued until  $\sigma[\epsilon_{ei}(t)]$  and  $\sigma[\phi_{ei}(t)]$  converge, which has already happened here, because substituting Eq. (B-28) into Eq. (12) yields  $E[\cos n_{31}(t)] = 0.999954$ , which is the value in Eq. (B-25). Thus,

$$\sigma[\phi_{ei}(t)] = 0.5523^\circ \quad (\text{B-29})$$

$$\sigma[\epsilon_{ei}(t)] = 6.261 \times 10^{-3} \Delta = 6.12 \text{ ns} . \quad (\text{B-30})$$

These quantities characterize the performance of the digital receiver, given the signal parameters, sampling rate, and receiver parameters assumed in this appendix.

This performance characterization accounts for errors caused by input noise only. As mentioned in Section 4 of the main report, high signal levels can attenuate the effects of input noise to the order of the effects of noises generated internally by the tracking loops. It is shown in Appendix D that the noise generated internally by the phase-locked loop is approximately  $0.6^\circ$  rms, independent of the signal level. Thus the rms noise at the output of the phase-locked loop is in fact given by

$$\sigma[\phi_{ei}(t)] = \sqrt{0.5523^2 + 0.6^2} = 0.815^\circ \quad (\text{B-31})$$

A similar result would apply to the delay-locked loop. The internal noise levels in the loops depend on the specific hardware implementations, as discussed in Appendix D.

Appendix C

SATRACK CARRIER AND PRN PROCESSING USING  
 AN ANALOG RECEIVER MODEL

Presented here is a receiver design for SATRACK carrier and code processing. The discussion is in terms of an analog input signal (not sampled, not quantized). In the SATRACK scheme a sum of carrier signals is transponded by the missile from the satellites to the range ship. These carriers are suppressed by pseudorandom noise (PRN) biphasic modulation ( $\pm 1$  amplitude modulation, with a different sequence for each satellite), and  $\pm 1$  data modulation. In the postflight receiver it is desired to track the carrier doppler shifts and the different delays of the PRN sequences. Telemetry and surface station data from the flight is provided to the postflight receiver to aid in this task. This appendix discusses a proposed design for a postflight receiver and analyzes its performance.

A RECEIVER DESIGN FOR SATRACK CARRIER AND CODE PROCESSING

The signal transponded by the missile from the  $N$  in-view satellites to the range ship in the SATRACK scheme is received by the ship in the form:

$$x(t) = \sum_{i=1}^N \left\{ \sqrt{2P_{s1}} \text{PRN}_i(t - \lambda_i) m_i(t - \lambda_i) \cos[\omega_0 t + \phi_i(t)] \right\} + n(t) . \quad (C-1)$$

Here,  $\lambda_i$  denotes the total time delay from transmission of the signal by satellite ( $i$ ) to its final reception by the ship. The function  $\text{PRN}_i(t)$  is a pseudorandom sequence of  $\pm 1$ 's with a bit (chip) length of  $\Delta = 10^{-6}/1.023$  second and a sequence repetition rate (epoch rate) of 1 kHz (i.e., 1023 chips per epoch). The function  $m_i(t)$  is also a sequence of  $\pm 1$ 's, which carries satellite orbit data, among other things. The chip length of  $m_i(t)$  is  $\Delta_m = 20$  ms. The phase function  $\phi_i(t)$  is the result of the doppler shifts caused by satellite, missile, and range ship movement. The noise function  $n(t)$  is white noise, which is bandwidth limited, by the shipboard receiver, to  $\pm 1$  MHz about the missile transmission frequency of  $f_0 = 2200$  MHz. The power spectral density (PSD) of  $n(t)$  is given by  $(N_0/2) = 10^{-17.2}$  mW/Hz. The normal carrier power for the  $i$ th signal,  $P_{s1}$ , is given by  $10^{-14.7}$  mW, although a wide variation

may be observed in the signal power received from the different satellites. The nominal signal power/noise density ratio is thus given by  $2P_{s_i}/N_0 = 25 \text{ dB}\cdot\text{Hz}$ . The code sequences,  $\text{PRN}_i(t)$ , and their epoch times (as transmitted by the satellites) are known by the postflight receiver, although the delays  $\{\lambda_i\}$  are not known a priori. The doppler shifts  $\{\phi_i(t)\}$  are also not known a priori. However, telemetry and ground station data are available to the receiver, and are converted into aiding information for the various receiver tracking loops. The data  $m_i(t)$  may be partially known a priori, but will be treated here as totally unknown, causing a very small deterioration in code and carrier tracking performance.

The received signal  $x(t)$  is heterodyned by 2200 MHz to a nominal zero center frequency by the shipboard preprocessor and then hard limited, sampled, and recorded for later processing by the postflight receiver (Appendix D). Here the single-bit quantization (hard limiting) and sampling of  $x(t)$  is ignored, and an analog receiver that will perform the objectives stated above is discussed. The performance of a specific design for this receiver will be analyzed, in the expectation that the performance of a digital receiver operating on the heterodyned, single-bit quantized, sampled version of  $x(t)$  will be much like the performance of the analog receiver. This expectation is not unfounded, because in Appendix D it is concluded that one component of this system, a single-bit quantized digital phase-locked loop, will perform in the same manner as an analog phase-locked loop, suffering only a 1.15 dB degradation in output phase variance.

Each of the  $N$  delays  $\{\lambda_i\}$  and doppler shifts  $\{\phi_i(t)\}$  are tracked with a separate receiver. The  $i$ th receiver uses its knowledge of the  $i$ th code sequence  $\text{PRN}_i(t)$  to separate its signal component from the other  $N-1$  signal components in  $x(t)$  (see Eq. (C-1)). The interference in the  $i$ th receiver from the other  $N-1$  signal components in  $x(t)$  will affect the performance of the receiver, and will superpose its effect with that caused by the noise  $n(t)$ .

This appendix is limited to analyzing the effects of the noise  $n(t)$  on the performance of the  $i$ th receiver. Thus the signal  $x(t)$ , which is input to the  $i$ th receiver, will be dealt with as though it were in fact  $x_i(t)$ , a fictitious signal defined here as:

$$x_i(t) \triangleq \sqrt{2P_{s_i}} \text{PRN}_i(t - \lambda_i) m_i(t - \lambda_i) \cos[\omega_0 t + \phi_i(t)] + n(t) \quad (\text{C-2})$$

After  $x(t)$  is processed through the  $N$  receivers it might be possible to make a second pass through  $x(t)$  with each receiver having its input,  $x(t)$ , altered to remove the interfering signal components, using information supplied by the  $N-1$  other receivers from the first pass through  $x(t)$ .

The  $i$ th analog postflight receiver has the form shown in Fig. C-1. The first stage of the receiver estimates the function  $m_i(t - \lambda_i)$ , and stores it on tape. The second stage of the receiver uses this tape to aid in estimating  $\phi_i(t)$  and the delay,  $\lambda_i$ , in the reception of  $PRN_i(t)$ . The computer aids obtained from telemetry and ground station data are used in both stages of the receiver. Detailed diagrams of the various components in Fig. C-1 will be given along with the discussion of receiver performance.

#### ESTIMATION OF $m_i(t - \lambda_i)$

The first processing performed by the  $i$ th receiver on the input signal  $x(t)$  is done with a noncoherent delay-locked loop (Ref. C-1), as pictured in Fig. C-2. (Recall that we are working with  $x_i(t)$  rather than  $x(t)$  in our analysis of the effects of noise on system performance.) This loop locks onto the delay  $\lambda_i$  in the code  $PRN_i(t - \lambda_i)$ , using a feedback shift register (FSR) code generator that reproduces the pseudo-random sequence  $PRN_i$ . The operation of the loop is noncoherent with respect to both the input carrier phase  $\phi_i(t)$  and the data  $m_i(t - \lambda_i)$ , both of which are unknown at this stage in the processing. Define the error in delay tracking as

$$\epsilon_i \triangleq \lambda_i - \hat{\lambda}_i,$$

where  $\hat{\lambda}_i$  is the estimate of delay  $\lambda_i$  generated by the loop. It is shown in Ref. C-1 that (see Fig. C-2):

$$e(\epsilon_i) = P_{s1}(\epsilon_i/\Delta); |\epsilon_i| \leq \Delta/2. \quad (C-3)$$

We choose for the closed loop a transfer function that is optimum in terms of total mean-squared delay error for ramp inputs of delay in the presence of noise. This transfer function is given by

---

Ref. C-1. W. J. Gill, "A Comparison of Binary Delay-Lock Tracking Loop Implementations," IEEE Transactions on Aerospace and Electronic Systems, Vol. AES-2, No. 4, July 1966, pp. 415-424.

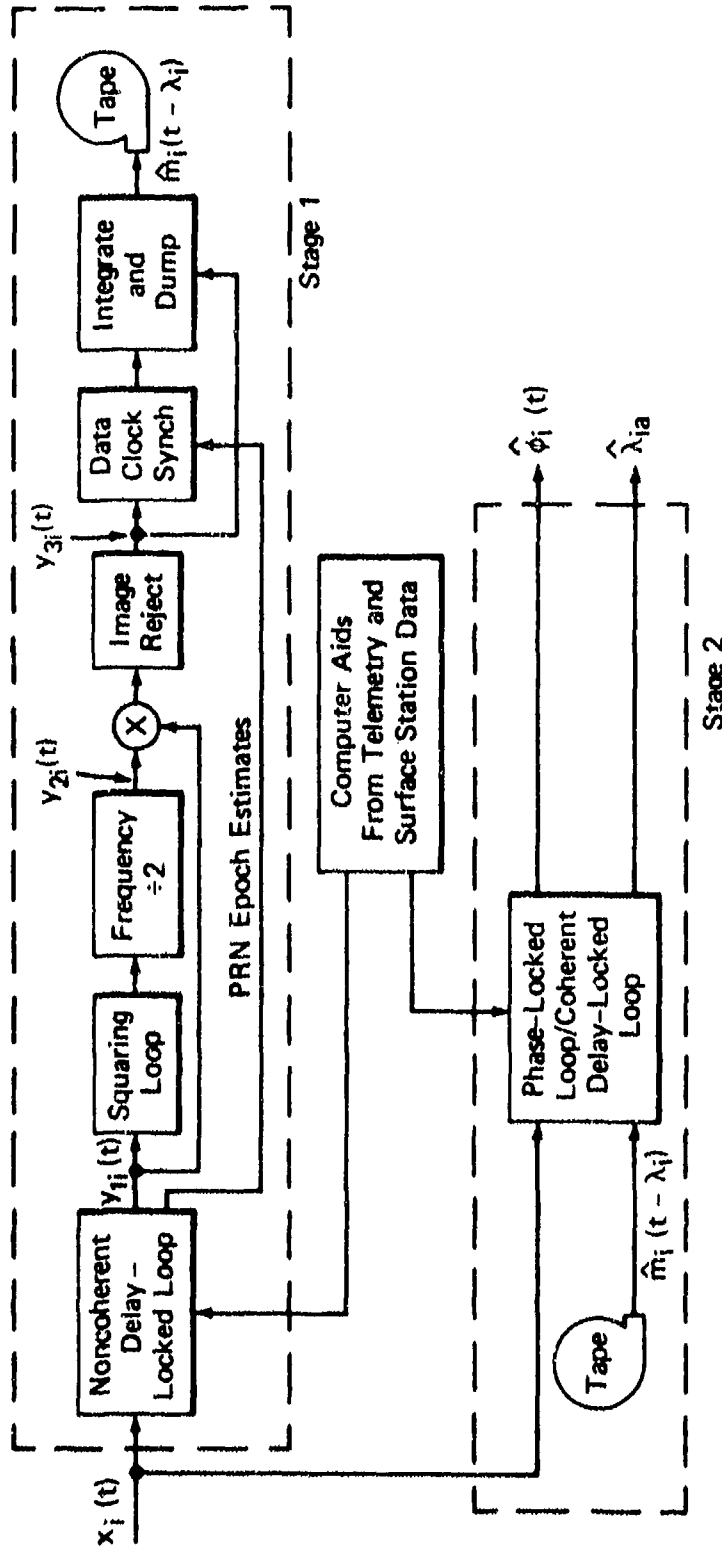


Fig. C-1 The  $i$ -th Postflight Receiver for  $x(t)$

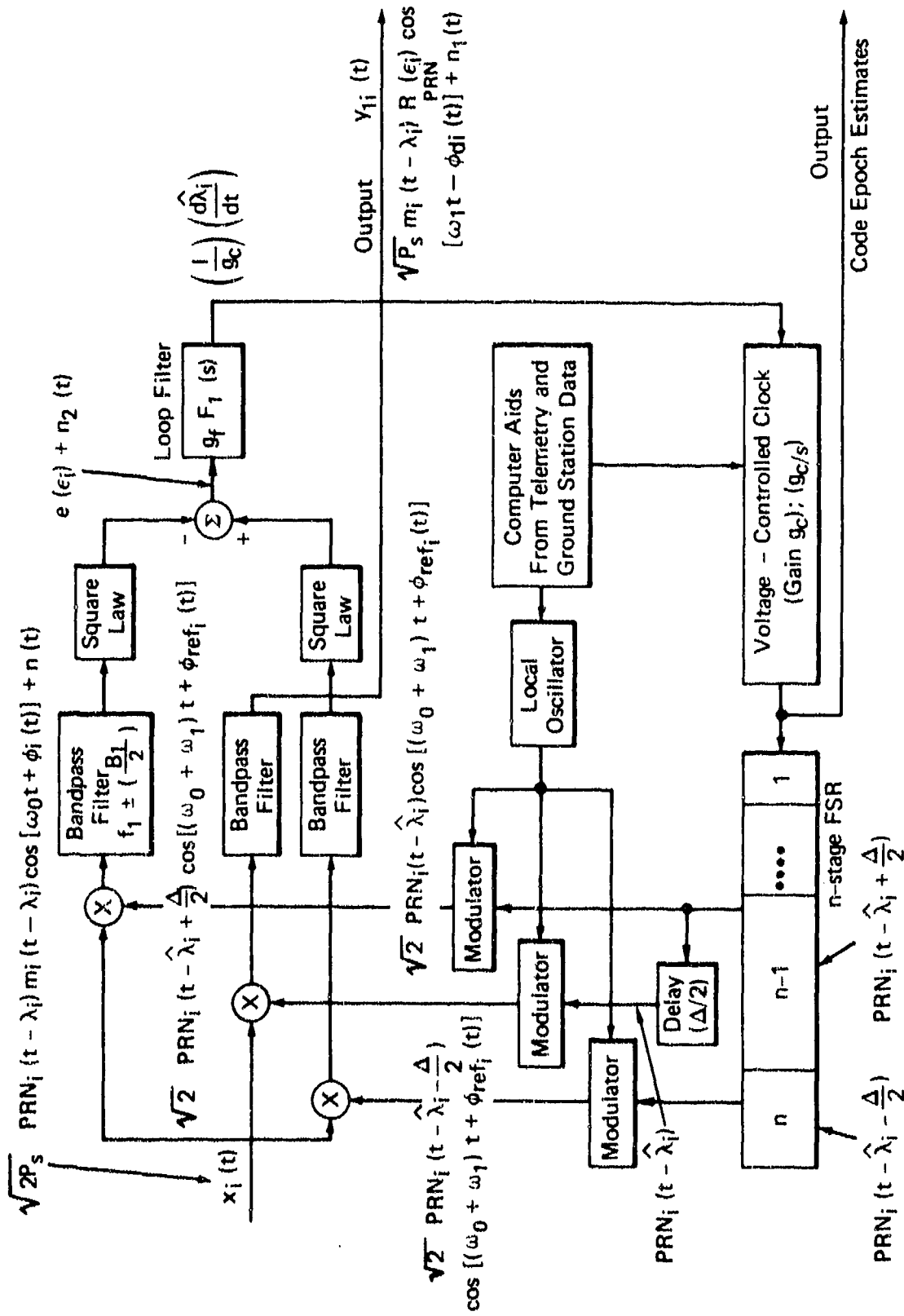


Fig. C-2 Noncoherent Delay-Locked Loop

$$\frac{\hat{\lambda}_1(s)}{\lambda_1(s)} \Delta H_1(s) = \frac{(1 + \sqrt{2s/\rho_0})}{[1 + \sqrt{2s/\rho_0} + (s/\rho_0)^2]} \quad (C-4)$$

and the two-sided closed loop noise bandwidth is given by

$$B_{N1} = 1.06 \rho_0 \text{ Hz} . \quad (C-5)$$

The transfer function in Eq. (C-4) can be approximated by choosing as the transfer function for the loop filter

$$F_1(s) = \frac{(1 + \sqrt{2s/\rho_0})}{(1 + gs/\rho_0)} , \quad (C-6)$$

where  $g$  is a normalized gain constant defined by

$$g = \frac{P_{si} g_f g_c}{\rho_0} , \quad (C-7)$$

and  $g$  is chosen to be large by making  $g_f$  large. It is then shown in Ref. C-1 that the rms value of the normalized error of the loop delay estimate,  $\epsilon_1(t)/\Delta$ , is given by

$$\frac{\sigma_\epsilon}{\Delta} = (\epsilon_1/\Delta)_{\text{rms}} = \sqrt{\left( \frac{N_o}{2P_{si}} + \frac{N_o^2 B_1}{P_{si}^2} \right) \left( \frac{B_{N1}}{2} \right)} , \quad (C-8)$$

where  $B_1$  is the bandwidth of the bandpass filters preceding the square law devices in Fig. C-2. A lower limit of 0.1 Hz is set on loop-noise bandwidth for any of the loops to be discussed. For lesser bandwidths there is danger of having noises generated within the loops (which will not be accounted for in the present analysis) dominating the error performance. It is obvious from Eq. (C-8) that the smaller  $B_1$  is made, the better will be the loop performance. In fact, considering a value of  $\sigma_\epsilon = 0.3\Delta$  to be the threshold value for proper loop operation (Ref. C-2) we find that it is necessary to keep  $B_1$  low in order to guarantee proper performance and the maintenance of loop delay lock. The bandpass filters must be wide enough to pass  $m_1(t - \lambda_1)$  relatively unchanged, so that  $m_1(t - \lambda_1)$  disappears in the square law devices. Also, their pass-band must be wide enough to always encompass the output frequency of the

---

Ref. C-2. J. J. Spilker, Jr., "Delay Lock Tracking of Binary Signals," IEEE Trans. on Space Electronics and Telemetry, Vol. SET-9, March 1963, pp. 1-8.

mixers, which varies with the doppler shift of the input signal. The  $m_1(t - \lambda_1)$  requires a bandpass of  $B_1 = 100$  Hz. The input doppler shift can be as much as  $\pm 100$  kHz. Using Eq. (8), given the nominal SATRACK signal and noise levels and the lower limit  $B_{N1} = 0.1$  Hz, the maximum allowable value of  $B_1$  for  $\sigma_\epsilon = 0.3\Delta$  may be determined, which is  $B_{1max} = 44$  kHz. This bandwidth will not accommodate the doppler shift. Therefore aiding information must be provided to force the local oscillator to follow the doppler shift of the input signal to some degree.

There are a number of alternative methods to provide the aiding. For the present discussion the telemetry and ground station data that are provided to the postflight processor are utilized. These data force the local oscillator in the envelope correlator to follow the input doppler frequency with a nominal offset of fixed frequency  $f_1$ , and a phase error of

$$\phi_{d_1}(t) \stackrel{\Delta}{=} \phi_1(t) - \phi_{ref_1}(t), \quad (C-9)$$

where  $\phi_{ref_1}(t)$  is the computer phase aiding, which is of sufficient accuracy to ensure that  $\dot{\phi}_{d_1}(t) \ll 2\pi \cdot 100$  rad/s. Thus,  $B_1$  is set equal to 100 Hz, the value required to pass  $m_1(t - \lambda_1)$ . Then  $B_{N1}$  is arbitrarily chosen as 2 Hz, such that from Eq. (C-8)  $\sigma_\epsilon = 0.08463\Delta$ , well within threshold. Thus the code epoch estimates are accurate to an rms error of  $\sigma_\epsilon = 0.08463\Delta = 82.73$  ns. The output of the noncoherent delay-locked loop is given, Ref. C-1, by

$$y_{11}(t) = \sqrt{P_{s1}} m_1(t - \lambda_1) R_{PRN}[\epsilon_1(t)] \cos[\omega_1 t - \phi_{d_1}(t)] + n_1(t), \quad (C-10)$$

where

$$R_{PRN}(\epsilon) \approx 1 - \frac{|\epsilon|}{\Delta}; \quad |\epsilon| < \Delta, \quad (C-11)$$

---

Ref. C-3. W. C. Lindsey and M. K. Simon, Telecommunication Systems Engineering, Prentice-Hall, Inc., New Jersey, 1973.

and  $n_1(t)$  is white noise of spectral height  $N_0/4$ , which is band-limited to  $f_1 - (B_1/2) \leq |f| \leq f_1 + (B_1/2)$ . By making the approximation that  $\epsilon_1(t)$  is a Gaussian random process, it is found that

$$E[R_{PRN}(\epsilon_1(t))] = 0.93247 \quad (C-12)$$

so that Eq. (C-10) may be replaced with

$$y_{11}(t) = \sqrt{P_{s1}} m_1(t - \lambda_1)(0.93247)\cos[\omega_1 t - \phi_{d_1}(t)] + n_1(t), \quad (C-13)$$

where Eq. (C-13) in the following discussion is justified whenever the noise bandwidths of the various loops are much narrower than the frequency content of  $R_{PRN}[\epsilon_1(t)]$ .

The next step in obtaining an estimate of  $m_1(t - \lambda_1)$  is to remove the cosine in Eq. (C-13) from  $y_{11}(t)$ . This factor is effectively a carrier wave, which is suppressed by  $m_1(t - \lambda_1)$ . Thus it is necessary to employ a suppressed carrier tracking loop to recover this cosine. Assume that a squaring loop (which gives equivalent performance to a Costas loop) is used. A decision-feedback loop could be used here, with slight improvement in overall system performance, but the loop acquisition problem would then be complicated by the initial lack of data clock synchronization, which is required for decision feedback. A diagram of a squaring loop, Ref. C-3, is given in Fig. C-3. The bandpass filter,  $D_2(s)$ , must be wide enough to pass both  $m_1(t - \lambda_1)$  and the cosine (i.e., 100 Hz as before). The second bandpass filter,  $D_3(s)$ , is centered at frequency  $2f_1$ , and must be wide enough to pass the component of  $y_{11}^2(t)$  at  $2f_1$ . A 100 Hz bandwidth is assumed sufficient here also. The output of the squaring loop and frequency divider is

$$y_{21}(t) = 2\cos[\omega_1 t - \phi_{d_1}(t) + n_3(t)], \quad (C-14)$$

where  $n_3(t)$  is the phase tracking error. Using the discussion of suppressed carrier tracking loops in this appendix, it is found that the rms value of  $n_3(t)$  becomes

$$[n_3(t)]_{\text{rms}} = \left\{ \left[ \frac{N_0}{2P_s \cdot (0.93247)^2} + \left( \frac{N_0}{2P_s \cdot (0.93247)^2} \right)^2 \cdot 100 \right] \cdot B_{N2} \right\}^{1/2} \text{ rad}, \quad (C-15)$$

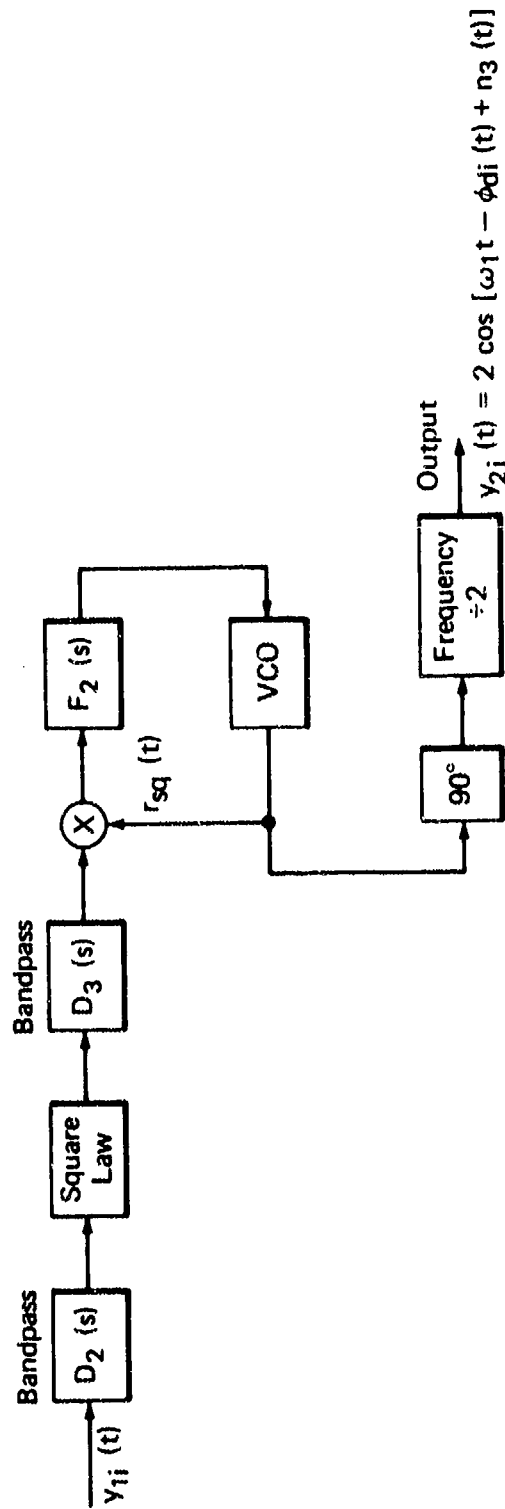


Fig. C-3 The Squaring Loop and Frequency Divider

where  $B_{N2}$  is the loop noise bandwidth of the squaring loop, which is assumed to be 1 Hz. We obtain

$$[n_3(t)]_{\text{rms}} = 0.07042 \text{ rad} = 4.0350^\circ \quad (\text{C-16})$$

As indicated in Fig. C-1,  $y_{11}(t)$  is multiplied by  $y_{21}(t)$  to obtain

$$y_{31}(t) = \sqrt{P_{\text{SI}}} m_1(t - \lambda_1) [\cos n_3(t)] R_{\text{PRN}}[e_1(t)] + n_4(t), \quad (\text{C-17})$$

where  $n_4(t)$  is white noise of spectral density  $N_0/2$ , bandlimited to  $|f| \leq (B_1/2)$ , ( $B_1 = 100$  Hz).

The signal  $y_{31}(t)$  is next put into the data clock synchronizer. The data  $m_1(t)$ , when modulated onto the signal  $x_1(t)$  before transmission by the satellite, has its transitions at the exact time of  $\text{PRN}_1(t)$  epochs. Because the chip length of  $m_1(t)$  is exactly 20 times the epoch length of  $\text{PRN}_1(t)$ , which one of 20 possible PRN epoch times is aligned with the  $m(t)$  chip must be determined. In order to do this, the following test is performed. The signal  $y_{31}(t)$  is integrated over each PRN epoch, as determined in the noncoherent delay-lock loop, to obtain

$$y_{31}^j = \int_{j \times 10^{-3}}^{(j+1) \times 10^{-3}} y_{31}(t) dt; \quad j = 0, \dots, (T_p \times 10^3 - 1), \quad (\text{C-18})$$

where  $T_p$  is the length in seconds of the combined satellite-missile pass ( $\approx 300$  s). Thus there are  $T_p \times 10^3$  separate intervals over which  $y_{31}(t)$  is integrated. The values of  $\{y_{31}^j\}$  may be stored on tape, to avoid recomputing them. The alignment of  $m_1(t)$  with  $\text{PRN}_1(t)$  may occur at any of the first 20 epochs of  $\text{PRN}_1(t)$ . If we are testing for whether the  $l$ th epoch is correct, the following summation must be computed:

$$s_l = \left\{ \left| \sum_{j=0}^{l-1} y_{31}^j \right| \right\} + \left\{ \sum_{k=0}^{\left(\frac{T_p \times 10^3}{20}\right) - 2} \left| \sum_{j=20k+l}^{20(k+1)+l-1} y_{31}^j \right| \right\} + \left\{ \left| \sum_{j=T_p \times 10^3 - 20 + l}^{T_p \times 10^3 - 1} y_{31}^j \right| \right\} \quad (\text{C-19})$$

Whichever value of  $\ell$  yields the highest value of  $g_\ell$  is chosen for the alignment of  $m_1(t - \lambda_1)$  with the epochs of  $\text{PRN}_1(t - \lambda_1)$ . The section of this appendix on data clock synchronization shows that the probability of choosing the wrong value of  $\ell$  for the synchronization of the data bits with the code epochs is low enough that computing time may be saved by using only 150 seconds of data (instead of  $T_p \approx 300$  s) in the synchronization process, while still having a probability of synch error on the order of  $10^{-6}$ , which can be ignored. Of course, the estimates of the code epoch are in error by an rms value of 82.73 ns, so that the data bits will also be off in alignment by this amount. The integration of  $y_{31}(t)$  over each data chip interval determines whether  $\hat{m}_1(t - \lambda_1)$  is positive or negative over that chip. These integrals are given by

$$b_k = \sum_{i=20k+\ell}^{20(k+1)+\ell-1} y_{31}^j \quad (C-20)$$

The probability of incorrectly determining  $m_1(t - \lambda_1)$  through integration over a chip interval ( $\Delta_m = 20$  ms), if the starting time of the interval were exactly known, is given from Eq. (C-17), using Ref. C-3, pp. 305-319.

$$\begin{aligned} \text{Prob} [\hat{m}_1(t - \lambda_1) \neq m_1(t - \lambda_1)] \\ = E \left[ \frac{1}{2} \left( 1 - \text{erf} \left\{ \sqrt{R_b} R_{\text{PRN}} [\epsilon_1(t)] \cos n_3(t) \right\} \right) \right], \quad (C-21) \end{aligned}$$

where it is assumed that  $\epsilon_1(t)$  and  $n_3(t)$  are relatively constant for 20 ms, and

$$R_b \triangleq \frac{P_s \Delta_m}{N_o} = \frac{P_s \times 20 \times 10^{-3}}{N_o} \quad (C-22)$$

However, because there is an rms offset of 82.73 ns in the alignment time,  $R_b$  effectively becomes,

$$R_b' = \frac{P_s (20 \times 10^{-3} - 82.73 \times 10^{-9})}{N_o} = 3.1622 \quad (C-23)$$

Next the quantity in Eq. (C-21) will be evaluated. The random variable  $g$  is defined as

$$g \triangleq \sqrt{R_b} R_{PRN}[\epsilon_1(t)] \cos n_3(t) \quad (C-24)$$

To find the mean value of  $g$  it is assumed that  $\epsilon_1(t)$  and  $n_3(t)$  are independent. Using Eq. (11) and assuming that  $\epsilon(t)$  is Gaussian,

$$ER_{PRN}[\epsilon_1(t)] = 0.93247 \quad (C-25)$$

has already been obtained. Assuming  $n_3(t)$  is Gaussian, and using the definition of the characteristic function of a Gaussian random variable  $n_3 \approx N(0, \sigma^2)$ ,

$$\phi(n_3) \triangleq Ee^{j\omega n_3} = \exp\left(\frac{-\sigma^2 \omega^2}{2}\right) \quad (C-26)$$

and

$$E \cos n_3(t) = 0.99752 \quad (C-27)$$

Thus,

$$Eg = \sqrt{R_b} ER_{PRN}[\epsilon_1(t)] E \cos n_3(t) \\ Eg = 1.6541 \quad (C-28)$$

Because  $\text{erf}(z)$  is quite linear near  $z = 1.6541$ , and  $g$  is nearly evenly distributed in probability about  $Eg$ , the approximation is made that

$$E[\text{erf}(g)] = \text{erf}(Eg) \quad (C-29)$$

Hence, we find from Eqs. (C-21), (C-24), (C-28), and (C-29) that

$$P[\hat{m}_1(t - \lambda_1) \neq m_1(t - \lambda_1)] = \frac{1}{2}[1 - \text{erf}(1.6541)] \\ = 9.6632 \times 10^{-3} \quad (C-30)$$

The quantity  $E[\hat{m}_1(t - \lambda_1)m(t - \lambda_1)]$ , which will be used later, is evaluated using Eq. (C-30).

$$\begin{aligned}
 E[\hat{m}_1(t - \lambda_1)m_1(t - \lambda_1)] &= 1 \times \text{Prob}(m = \hat{m})^{-1} \times \text{Prob}(m \neq \hat{m}) \\
 &= 1 \cdot \left[ (1 - 9.6632 \times 10^{-3}) \left( \frac{20 \times 10^{-3} - 82.73 \times 10^{-9}}{20 \times 10^{-3}} \right) \right. \\
 &\quad \left. + \frac{1}{2} \left( \frac{82.73 \times 10^{-9}}{20 \times 10^{-3}} \right) \right] \\
 &= 1 \cdot \left[ (9.6632 \times 10^{-3}) \left( \frac{20 \times 10^{-3} - 82.73 \times 10^{-9}}{20 \times 10^{-3}} \right) \right. \\
 &\quad \left. + \frac{1}{2} \left( \frac{82.73 \times 10^{-9}}{20 \times 10^{-3}} \right) \right]
 \end{aligned}$$

$$E[\hat{m}_1(t - \lambda_1)m_1(t - \lambda_1)] = 0.98067 \quad (\text{C-31})$$

#### COHERENT TRACKING OF $\phi_1(t)$ AND $\lambda_1$

The operation of the phase-locked loop/coherent delay-locked loop (PLL/DLL), which comprises stage 2 of the postflight receiver for  $x_1(t)$ , will be aided by the value of  $m_1(t - \lambda_1)$  determined by stage 1, the code epoch synchronization performed in stage 1 (which will aid in the code acquisition of the delay-locked loop), and the telemetry and ground station data available to the postflight receiver. The PLL/DLL loop is shown in Fig. C-4. The errors in this loop will be determined iteratively. If given that the phase-locked loop tracks with error

$\phi_e(t) \triangleq \phi_1(t) - \hat{\phi}_1(t)$ , then the normalized rms value of the delay error  $\epsilon_a(t) \triangleq \lambda_1(t) - \hat{\lambda}_{1a}(t)$  of the the delay-locked loop is given (Fig. C-4 and Ref. C-1) by

$$\frac{\sigma_{\epsilon_a}}{\Delta} = \sqrt{\frac{B_{N3}N_o}{4P_s [E \cos \phi_e(t)]^2 \{E[m(t - \lambda_1)\hat{m}(t - \lambda_1)]\}^2}} \quad (\text{C-32})$$

where  $B_{N3}$  is the loop noise bandwidth of the delay-locked loop. We use expectations in Eq. (C-32) under the assumption that  $B_{N3}$  is narrower than the frequency content of  $\phi_e(t)$  and  $m(t - \lambda_1)\hat{m}(t - \lambda_1)$ . Also assume that  $\phi_e(t)$  and  $\hat{m}(t - \lambda_1)$  are independent. Further, if given a delay error



$\epsilon_a(t)$  in the output of the delay-locked loop, then we obtain from phase-locked loop theory, Ref. C-3, p. 29, that the rms phase error at the output of the phase-locked loop is given approximately by

$$\sigma_{\phi_e} = \sqrt{\frac{B_{N4} N_o}{2P_s \{ ER_{PRN}[\epsilon_a(t)] \}^2 [Em(t - \lambda_1) \hat{m}(t - \lambda_1)]^2}} \text{ rad}, \quad (C-33)$$

where  $B_{N4}$  is the loop noise bandwidth of the phase-locked loop. It is assumed that  $B_{N3} = 0.2$  Hz,  $B_{N4} = 1$  Hz, and will now determine  $\sigma_{\epsilon_a}$  and  $\sigma_{\phi_e}$  iteratively. First let  $R_{PRN}[\epsilon_a(t)] = 1$  in Eq. (C-33). Then obtain  $\sigma_{\phi_e} = 0.057342$  rad and approximate  $\phi_e(t)$  as Gaussian. Then  $E \cos \phi_e(t) = 0.99836$ . Using this and Eq. (C-31) in Eq. (C-32) there obtains  $\sigma_{\epsilon_a} = 0.018163\Delta$ . This quantity is then put back into Eq. (C-33).

Approximating  $\epsilon_a(t)$  as Gaussian, and using Eq. (C-11)  $E\{R_{PRN}[\epsilon_a(t)]\} = 0.98551$ . Substituting this value into Eq. (C-33),  $\sigma_{\phi_e} = 0.05816$  rad. The iteration between Eq. (C-32) and Eq. (C-33) is reiterated until estimates of  $\sigma_{\phi_e}$  and  $\sigma_{\epsilon_a}$  converge (to five significant digits), which happens on the next iteration. Then

$$\sigma_{\epsilon_a} = 0.018164\Delta = 17.76 \text{ ns} \quad (C-34)$$

and

$$\sigma_{\phi_e} = 0.058186 \text{ rad} = 3.334^\circ \quad (C-35)$$

These answers then are the rms values of the errors in the receiver estimates of  $\phi_1(t)$  and  $\lambda_1$ . Note that only errors caused by input noise have been considered, so that both noise generated internally by the various loops and errors caused by signal dynamics have been neglected.

#### SUPPRESSED CARRIER TRACKING LOOPS

In this section three types of suppressed carrier tracking loops are discussed: the squaring loop, the Costas loop, and the decision-feedback loop. The analysis is based on linearization of the equations given in Ref. C-3. Comparison will be made of the operation of these three loops when the following input signal is applied to them.

$$y(t) = \sqrt{2P_s} d(t) \sin[\omega_0 t + \theta(t)] + n_w(t), \quad (C-36)$$

where  $d(t)$  is modulation in the form of a  $\pm 1$  pulse train with bit interval  $T_d$ , and  $n_w(t)$  is white noise of spectral density  $(N_0/2)$ .

A diagram of a squaring loop is given in Fig. C-3. The first bandpass filter,  $D_2(s)$  (bandwidth  $B_2$ ), changes  $n_w(t)$  from white noise to bandlimited white noise,  $n_{w1}(t)$ , over frequencies

$$f_0 - B_2/2 \leq |f| \leq f_0 + B_2/2,$$

while passing  $d(t)$  relatively unchanged. Thus the output of the filter  $D_2(s)$  may be written

$$z(t) = \sqrt{2P_s} d(t) \sin[\omega_0 t + \theta(t)] + n_{w1}(t), \quad (C-37)$$

and  $n_{w1}(t)$  may be written

$$n_{w1}(t) = \sqrt{2}[n_c(t) \cos \omega_0 t - n_g(t) \sin \omega_0 t], \quad (C-38)$$

where  $n_c(t)$  and  $n_g(t)$  are independent white noise processes of power spectral density  $N_0/2$ , bandlimited to  $|f| \leq (B_2/2)$ . Alternatively,  $n_{w1}(t)$  may be written

$$n_{w1}(t) = \sqrt{2} \left\{ N_c(t) \cos[\omega_0 t + \theta(t)] - N_g(t) \sin[\omega_0 t + \theta(t)] \right\}, \quad (C-39)$$

where

$$\begin{aligned} N_c(t) &= n_c(t) \cos \theta(t) + n_g(t) \sin \theta(t) \\ N_g(t) &= -n_c(t) \sin \theta(t) + n_g(t) \cos \theta(t) \end{aligned} \quad (C-40)$$

and  $N_c(t)$ ,  $N_g(t)$  are independent white noise processes of power spectral density  $N_0/2$ , bandlimited to  $|f| \leq B_2/2$ . Let  $\psi(t) \triangleq \theta(t) - \hat{\theta}(t)$ , where  $\hat{\theta}(t)$  may be obtained by frequency division of the output,  $r_{sq}(t)$ , of the squaring loop

$$r_{sq}(t) = 2K_1 \sin[2\omega_0 t + 2\hat{\theta}(t)]. \quad (C-41)$$

The differential equation for the operation of the squaring loop is then given in Ref. C-3, p. 59 by

$$\dot{2\psi}(t) = 2\dot{\theta}(t) - KF_2(s)\{P_s d^2(t) \sin 2\psi(t) + v_2[t, 2\psi(t)]\} \quad (C-42)$$

The noise term,  $v_2[t, 2\psi(t)]$ , is characterized by (see Ref. C-3, p. 80)

$$R_{v_2}(\tau) \triangleq E[v_2(t, 2\psi)v_2(t + \tau, 2\psi)] = 4[P_s R_{N_c}(\tau) + R_{N_c}^2(\tau)] \quad (C-43)$$

where in the derivation of Eq. (C-43) it is assumed that  $T_d \gg \tau_n$ , and  $\tau_n$  is the correlation time of the bandlimited input noise  $n_{\omega 1}(t)$ , so that  $m(t) = m(t + \tau)$  for all values of  $\tau$  of interest, and that  $\psi(t)$  is relatively constant over such values of  $\tau$ . If the loop bandwidth  $B_N$  is much narrower than  $B_2$ , then the only portion of  $v_2(t)$  of interest is the value at zero frequency, which is

$$S_{v_2}(f=0) = 4 \left[ \frac{P_s N_o}{2} + \left( \frac{N_o}{2} \right)^2 \right] B_2 \quad (C-44)$$

In an ordinary phase-locked loop, the equation of operation is (see Ref. C-3, p. 28)

$$\dot{\psi}(t) = \dot{\theta}(t) - KF_2(s)\{\sqrt{P_s} \sin \psi(t) + N[t, \psi(t)]\} \quad (C-45)$$

where the PSD of  $N[t, \psi(t)]$  is  $N_o/2$  at  $f = 0$ . For such a loop, the rms value of the output phase error is found to be, using linearization (i.e.,  $\sin \psi \approx \psi$ ), (see Ref. C-3, p. 29)

$$\psi(t)_{\text{rms}} = \sqrt{\left( \frac{N_o}{2P_s} \right) B_N} \text{ rad} \quad (C-46)$$

Thus, by analogy between Eq. (C-42) and Eq. (C-45), the output phase error of the squaring loop is

$$2\psi(t)_{\text{rms}} = \sqrt{4 \left[ \frac{P_s N_o}{2} + \left( \frac{N_o}{2} \right)^2 \right] B_2} \left( \frac{1}{P_s} \right) B_N \text{ rad} \quad (C-47)$$

so that

$$\phi(t)_{\text{rms}} = \sqrt{\left[ \frac{N_o}{2P_s} + \left( \frac{N_o}{2P_s} \right)^2 \right] B_2} B_N \text{ rad} \quad (C-48)$$

As discussed in Ref. C-3, p. 63, the Costas loop (see Fig. C-5), is theoretically equivalent to the squaring loop, so long as the shaping provided by  $G(s)$  in Fig. C-5 is equivalent to that produced by the low-pass equivalent of  $D_2(s)$  in Fig. C-3. Thus Eq. (C-48) also characterizes the performance of the Costas loop.

The decision-feedback loop (Fig. C-6) offers improved performance over both the squaring and the Costas loop. It makes use of an ordinary phase-locked loop with incorporated delay,  $T_d$ . The  $\pm 1$  modulation  $d(t)$  is removed from the input carrier by the output of a modulation estimator. The modulation estimator is a matched filter set up to detect a  $\pm 1$  over a bit interval  $T_d$ . This matched filter is merely an integrate-and-dump circuit followed by a hard limiter. The delay in the phase-locked loop is needed to allow the modulation estimator to make its decision on the current bit before any attempt is made to remove the bit from the carrier in the multiplier. The differential equation of the decision-feedback loop is (see Ref. C-3, p. 65)

$$\dot{\psi}(t) = \dot{\theta}(t) - KF_2(s) \left( \sqrt{P_s} \{1 - 2P_E[\psi(t)]\} \sin \psi(t) + d_{\text{est}}(t) N_{\ell}[t, \psi(t)] \right) \quad (C-49)$$

where the delay  $T_d$  has been ignored, on the presumption that  $B_N \ll T_d^{-1}$ .  $N_{\ell}[t, \psi(t)]$  is modeled exactly as  $N[t, \psi(t)]$  in Eq. (C-45).  $P_E[\psi(t)]$  is the error probability of the modulation estimator, conditioned on the loop phase error.  $P_E[\psi(t)]$  is given by

$$P_E[\psi(t)] = \frac{1}{2} \left\{ 1 - \text{erf} \sqrt{R_b} \cos[\psi(t)] \right\} \quad (C-50)$$

where

$$R_b \triangleq \frac{P_s T_d}{N_0} \quad (C-51)$$

and

$$\text{erf}(\alpha) \triangleq \frac{2}{\sqrt{\pi}} \int_{\alpha}^{\infty} \exp(-\beta^2) d\beta \quad (C-52)$$

In the frequency region of interest (near zero frequency)  $N_{\ell}[t, \psi(t)]$  is white. Further, if the spectrum of  $d_{\text{est}}(t)$  is not wider than that of  $N_{\ell}[t, \psi(t)]$  then the noise term  $d_{\text{est}}(t) N_{\ell}[t, \psi(t)]$  in Eq. (C-49) is also white near zero frequency, with PSD given by the product of the PSD of  $N_{\ell}[t, \psi(t)]$  (i.e.,  $N_0/2$ ) with the power in  $d_{\text{est}}(t)$  (i.e., unity). Thus this noise term has spectral height  $N_0/2$ , as did  $N_{\ell}[t, \psi(t)]$ . We make the approximation in Eq. (C-49) that  $P_E[\psi(t)]$  can be replaced with its

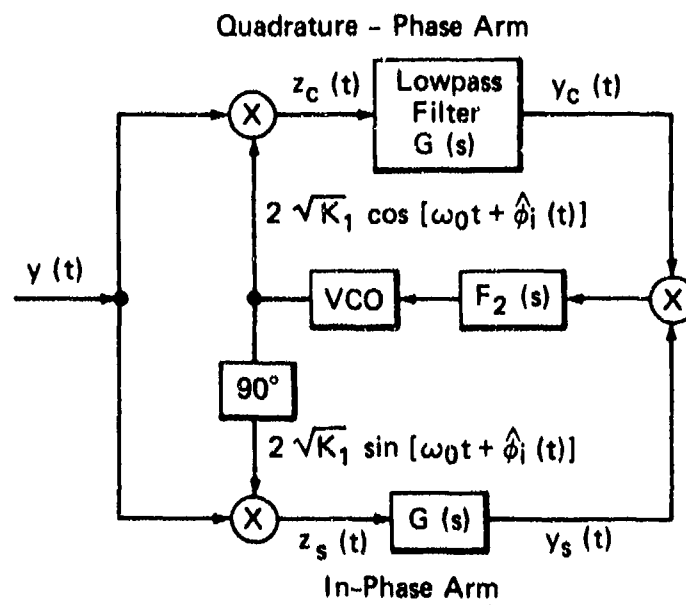


Fig. C-5 Costas Loop

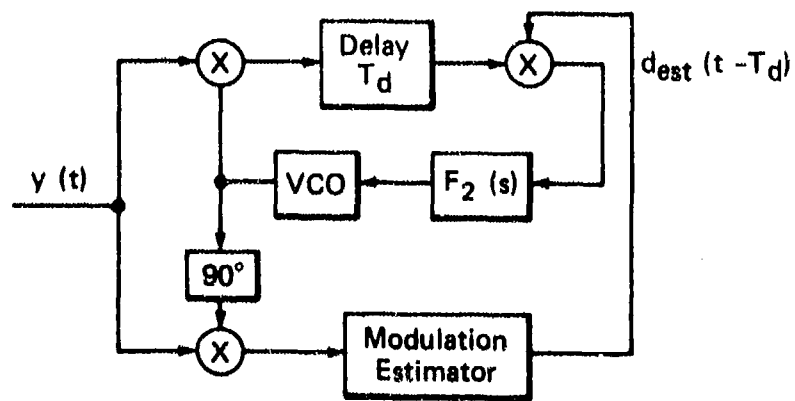


Fig. C-6 Decision-Feedback Loop

expected value, which is certainly true for small  $\psi(t)$ . Then the rms phase error at the loop output, after linearization of the loop, is given by

$$\psi(t)_{\text{rms}} = \sqrt{\left(\frac{N_o}{2P_s}\right) \left(\frac{1}{E \operatorname{erf}[\sqrt{R_b} \cos \psi(t)]}\right)^2} B_N \text{ rad} , \quad (\text{C-53})$$

where  $B_N$  is the loop bandwidth of the phase-locked loop component of the decision-feedback loop. If  $\psi(t)$  is small, which we may verify, then we may approximate  $\cos \psi \approx 1$ , so that Eq. (C-53) becomes

$$\psi(t)_{\text{rms}} = \sqrt{\left(\frac{N_o}{2P_s}\right) \left(\frac{1}{\operatorname{erf}(\sqrt{R_b})}\right)^2} B_N \text{ rad} . \quad (\text{C-54})$$

The answers obtained in Eqs. (C-48) and (C-54) through linearization agree quite well with those displayed in Ref. C-3, which were computed using the nonlinear theory.

#### PERFORMANCE OF DATA CLOCK SYNCHRONIZATION

In this section we evaluate the probability that the determination of the synchronization of the data clock with the code epochs (as described in the text) will be in error. The input to this procedure is given in Eq. (C-17) as:

$$y_{31}(t) = \sqrt{P_{s1}} m_1(t - \lambda_1) \cos[n_3(t)] R_{\text{PRN}}[e_1(t)] + n_4(t) . \quad (\text{C-55})$$

Because of the low frequency nature of the procedure used, Eq. (C-55) may be replaced by

$$y_{31}(t) = \sqrt{P_{s1}} m_1(t - \lambda_1) E \cos[n_3(t)] E R_{\text{PRN}}[e_1(t)] + n_4(t) . \quad (\text{C-56})$$

Then, using Eqs. (C-12) and (C-27), Eq. (C-56) may be replaced by

$$y_{31}(t) = \sqrt{P_{s1}} (0.93016) m_1(t - \lambda_1) + n_4(t) \quad (\text{C-57})$$

If  $T$  seconds of data are used (instead of  $T_p$ , as in Eq. (C-19)), and the procedure outlined earlier is used, then

$$g_\ell = E(g_\ell) + n_\ell \quad (\text{C-58})$$

(call  $\ell^*$  the value of  $\ell$  for proper synchronization). Then

$$E(g_{\ell}) \approx \int_0^T 0.93016 \sqrt{P_{si}} \left( \frac{20 \times 10^{-3} - 82.73 \times 10^{-9}}{20 \times 10^{-3}} \right) dt, \quad (C-59)$$

where the code epochs themselves have an rms estimation error of 82.73 ns. If  $\ell$  is in error by  $k$  out of 20 epochs ( $k = -10, -9, \dots, 0, 1, \dots, 9$ ), then

$$E(g_{\ell}) = \left( \frac{20 - |k|}{20} \right) \int_0^T 0.93016 \sqrt{P_{si}} \left( \frac{20 \times 10^{-3} - 82.73 \times 10^{-9}}{20 \times 10^{-3}} \right) dt,$$

$$E(g_{\ell}) = \left( \frac{20 - |k|}{20} \right) 0.930156 \sqrt{P_{si}} T. \quad (C-60)$$

The noise,  $n_{\ell}$ , is given by

$$n_{\ell} = \int_0^T n_4(t) h_{\ell}(t) dt, \quad (C-61)$$

where  $h_{\ell}(t)$  is a sequence of  $\pm 1$ 's, determined by the signs of the  $\{y_{31}^j\}$  in Eq. (C-18). The variance of  $n_{\ell}$  is then

$$\left( \sigma_{n_{\ell}} \right)^2 = E \int_0^T \int_0^T n_4(t) n_4(\gamma) h_{\ell}(t) h_{\ell}(\gamma) dt d\gamma, \quad (C-62)$$

Because of the long integration time of our process, the 50 Hz bandwidth of  $n_4(t)$  is ignored, and it is treated as though it were white, with PSD of  $N_0/2$ . Thus Eq. (C-62) is evaluated,

$$\left( \sigma_{n_{\ell}} \right)^2 = \int_0^T \int_0^T \left( \frac{N_0}{2} \right) \delta(t - \gamma) dt d\gamma = \left( \frac{N_0}{2} \right) T \quad (C-63)$$

Using signal space theory, Ref. C-4, pp. 77-82, the probability of the estimation of the data clock synchronization being off by one code epoch in a given direction is the same as the probability of mistaking two signals space apart by  $(1/20)(0.930156)(\sqrt{P_{s1}})T$  in noise of variance  $TN_0/2$ , which is

$$Q \left[ \left( \frac{1}{2} \right)^2 \left[ \left( \frac{1}{20} \right) (0.930156) \sqrt{P_{s1}} T \right]^2 \cdot \left( \frac{2}{TN_0} \right) \right]^{1/2}, \quad (C-64)$$

where

$$Q(\alpha) \triangleq \int_{\alpha}^{\infty} \left( \frac{1}{\sqrt{2\pi}} \right) \exp(-\beta^2/2) d\beta. \quad (C-65)$$

For  $T = 150$  sec, the quantity in Eq. (C-65) is given by  $Q(5.063) \approx 3 \times 10^{-7}$ .

This quantity is the probability of being off by one code epoch in a given direction. For both directions, the probability is twice this, or approximately  $6 \times 10^{-7}$ . For larger offsets the probability is much smaller. This then is approximately the probability that the synchronization of the data bits with the code epoch times will be incorrect.

---

Ref. C-4. J. M. Wozencraft and L. M. Jacobs, Principles of Communication Engineering, John Wiley & Sons, New York, 1967.

Appendix C

REFERENCES

- C-1. W. J. Gill, "A Comparison of Binary Delay-Lock Tracking Loop Implementations," IEEE Transactions on Aerospace and Electronic Systems, Vol. AES-2, No. 4, July 1966, pp. 415-424.
- C-2. J. J. Spilker, Jr., "Delay Lock Tracking of Binary Signals," IEEE Trans. on Space Electronics and Telemetry, Vol. SET-9, March 1963, pp. 1-8.
- C-3. W. C. Lindsey and M. K. Simon, Telecommunication Systems Engineering, Prentice-Hall, Inc., New Jersey, 1973.
- C-4. J. M. Wozencraft and L. M. Jacobs, Principles of Communication Engineering, John Wiley & Sons, New York, 1967,

## Appendix D

### A SINGLE-BIT PROCESSING SCHEME FOR SATRACK-GPS CARRIER TRACKING

This appendix presents the results of the first phase of the investigation of the digital receiver. Three main topics are treated. First, single-bit-quantized shipboard preprocessing of the doppler carrier signal is discussed. Second, a specific design for a single-bit-quantized second-order digital phase-locked loop (one component of the digital receiver) is presented. Third, models are derived for the various noises present in this tracking loop, both those noises inherent in the input signal and those due to single-bit quantization in the tracking loop.

#### SHIPBOARD PREPROCESSING AND THE DIGITAL PHASE-LOCKED LOOP

In the SATRACK scheme a sum of carrier signals is transponded by the missile from the satellites to the range ship. These carriers are suppressed by pseudorandom noise (PRN) biphase modulation ( $\pm 1$  amplitude modulation, with a different sequence for each satellite) and  $\pm 1$  data modulation. In the postflight receiver it is desired to track the carrier doppler shifts and the different delays of the PRN sequences. Telemetry and surface station data from the flight is provided to the postflight receiver to aid in this task. The signals transponded by the missiles and received by the ships will be multiplied by in-phase and quadrature sinusoids of fixed frequency, sampled, quantized, and stored on tape for postflight processing at APL. In the investigation to be pursued in this paper, it is assumed that single-bit quantization is used, and there follows the analytical exploration of the receiver performance that would then be obtained. Specifically, the performance of the digital phase-locked loop, one component of the digital receiver, will be discussed.

The shipboard preprocessing and digital phase-locked loop (DPLL) have the structure shown in Figs. D-1 and D-2. In this paper the data modulation has been ignored and it has been assumed that the PRN used for ranging has been completely removed from the single-bit-quantized doppler signal before processing in the DPLL.

#### THE SHIPBOARD PREPROCESSOR

The carrier signal received by the ship is first heterodyned to 50 MHz and then input to the preprocessing scheme shown in Fig. D-1. The

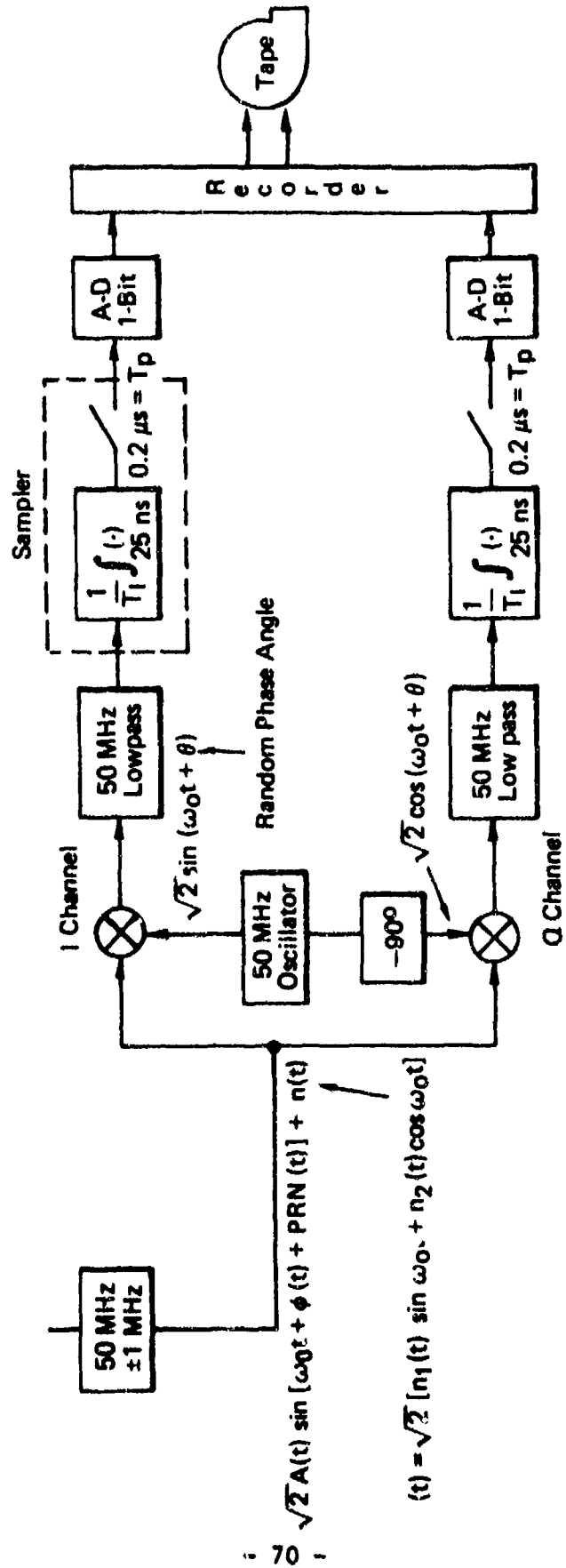


Fig. D-1 Preprocessing Aboard Range Ship

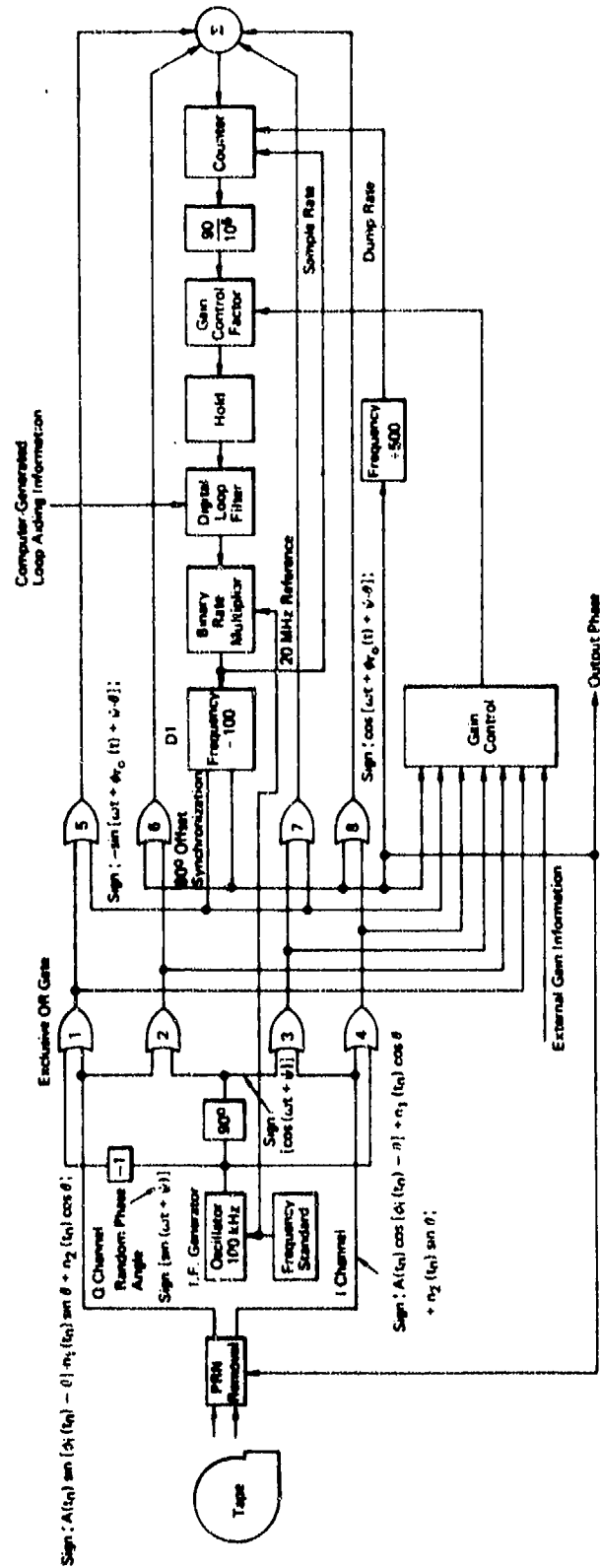


Fig. D-2 I.F. Mixer and Digital Phase-Locked Loop (DPLL)

input signal to the preprocessor is heterodyned to a center frequency of 0 Hz in order to allow sampling at as slow a rate as possible, while still somewhat above the Nyquist rate. The 1 MHz bandwidth on the signal is necessary because of the PRN present on the carrier signal (the doppler shift itself is expected to be less than 100 kHz on either side of the center frequency). The 50 MHz low-pass filter is used to reject the double angle signal and noise that results from the mixing operation. A frequency of 50 MHz is chosen for the shipboard intermediate frequency (IF) so as to avoid averaging the output of the mixer in the low-pass filter over any time period larger than that over which the low frequency component (1 MHz bandwidth) will change by 0.25 radians (Ref. D-1).

#### COMPONENTS AND NOISEFREE OPERATION OF THE DIGITAL PHASE-LOCKED LOOP

The principles of operation of the phase-locked loop shown in Fig. D-2 are next discussed without considering, for the moment, any of the various noises present. Note that the exclusive-OR (i.e., representing multiplication for sequences of  $\pm 1$ 's) gates 1 through 4 are used to heterodyne the input I and Q channels, centered at 0 frequency, up to an IF frequency of 100 kHz. First, the phase detector, which is composed of gates 5 through 8 followed by a counter, compares the phases of the heterodyned input square wave and the square wave generated by the frequency division of the binary rate multiplier (BRM) output. The latter square wave, in a perfect tracking situation, is at the frequency of the heterodyned input waveform and  $90^\circ$  offset from it.

To illustrate the above process take two square waves, both at a frequency of 100 kHz, which differ in phase by  $72^\circ$  (i.e.,  $18^\circ$  from perfect track) and imagine them to be put through any of the exclusive-OR gates in Fig. D-2. The resulting signals are shown in Fig. D-3. The counter, which samples 50 times in every cycle of Divider 1 (D-1) output, sums the samples and dumps its final answer (which is then held as input to the digital loop filter until the next dump) and resets to 0 count after exactly 500 cycles of the output of Divider 1. The total number of samples in every counter dump cycle is thus 25 000, and we would observe a net count of 5000 in this  $18^\circ$  offset situation. Note that

$$18^\circ = \frac{5000}{25\ 000} \times 90^\circ ,$$

so the phase detector, operating in the absence of noise (this is not true when noise is added), is in fact linear, unlike the phase detector in the analog phase-locked loop (Ref. D-2) which is sinusoidal in its response.

---

Ref. D-1. W. E. Larimore, "Design and Performance of a Second-Order Digital Phase-Locked Loop," Symposium on Computer Processing in Communications, Polytechnic Institute of Brooklyn, 1969, pp. 343-356.

Ref. D-2. A. J. Viterbi, Principles of Coherent Communication, McGraw-Hill Book Co., New York, 1966.

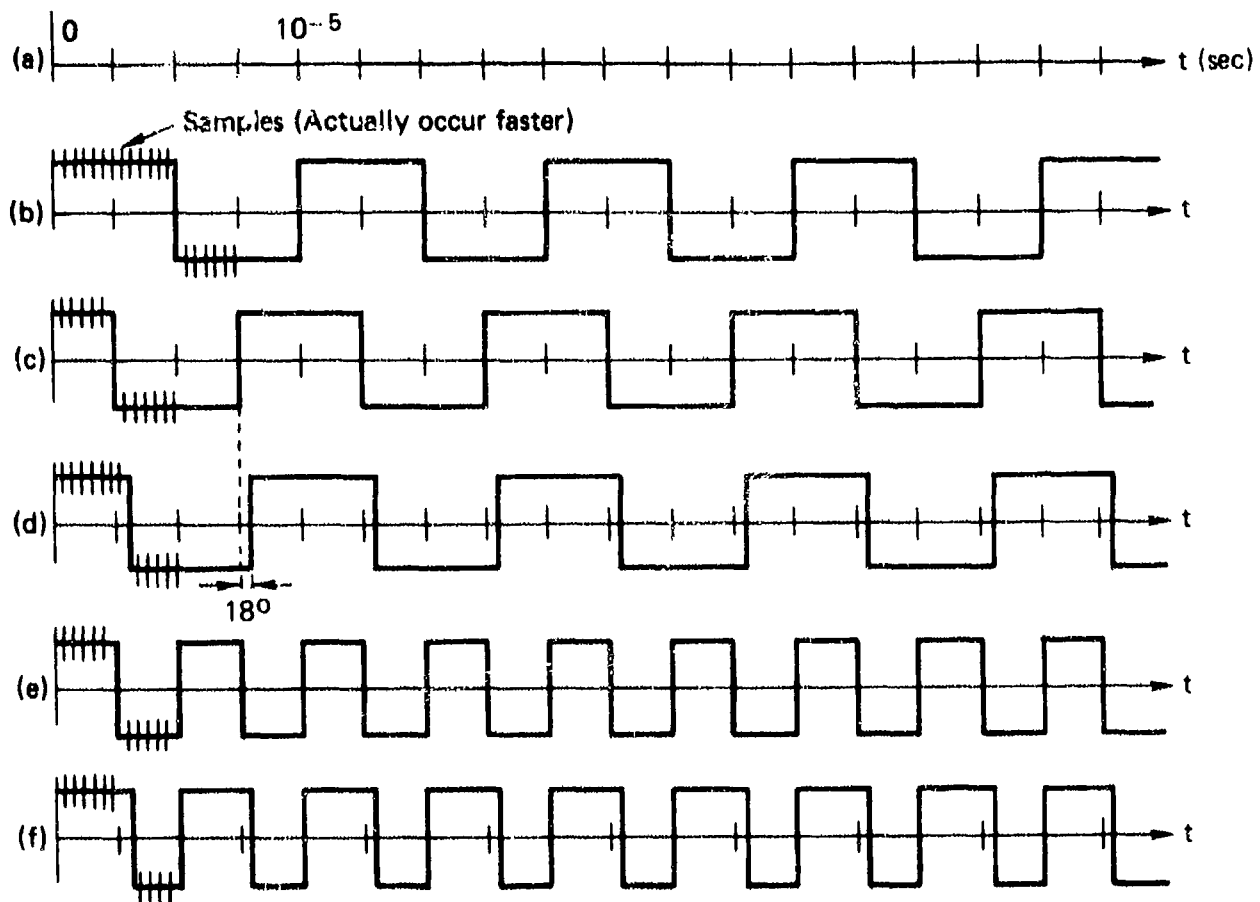


**Fig. D-3** Multiplication in a Phase Detector Gate: (a) Time Axis; (b) 100-kHz Sinusoid; (c) 100-kHz Sinusoid  $90^\circ$  Offset from b; (d) 100-kHz Sinusoid  $72^\circ$  Offset from b ( $18^\circ$  offset from perfect track); (e) Product of b and c in Phase Detector (sum of samples balanced to 0); (f) Product of b and d in Phase Detector (sum of samples is net positive, indicating relative position shift of b compared with d)

For a more mathematical explanation of this linearity see the section in this appendix, "Digital Phase Detector Linearity." The linearity of the phase detector response only holds for relative phase shifts between  $\pm 90^\circ$ . The overall response in the absence of noise is shown in Fig. D-4. The count also is quantized to  $(90/25\ 000)^\circ = (3.6 \times 10^{-3})^\circ$  because only a whole number of counts can be observed.

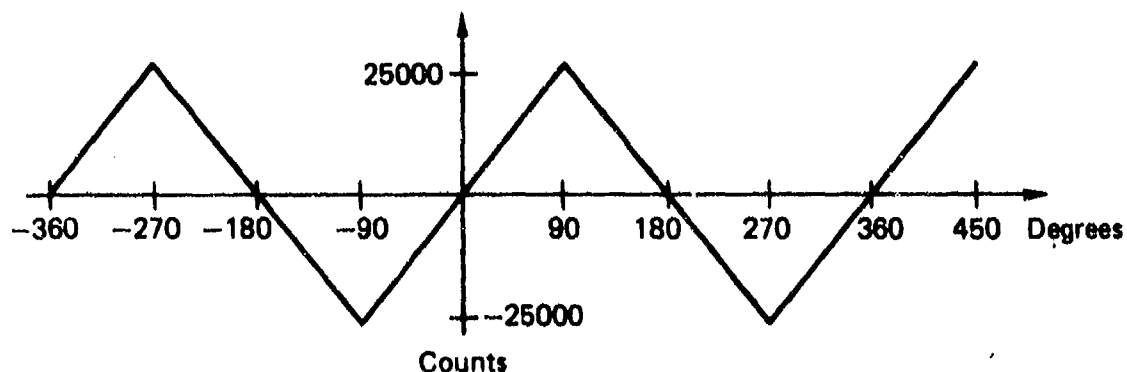


Fig. D-4 Response (In Counts) of the Phase Detector for Different Relative Phase Shifts of the Input Waves from Perfect Tracking ( $90^\circ$  Offset)

It is found, in fact, through computer simulation that in the absence of noise the digital phase detector will respond to inputs of sign  $\{\sin[2\pi fnT_p + \phi(nT_p)]\}$  and sign  $\{\cos[2\pi fnT_p + \phi_{r0}(nT_p)]\}$ ;

( $n = 1, \dots, 25\ 000$ ),  $T_p = 0.2\ \mu s$ , with a response of

$$(1/90) \times \sum_{n=1}^{25\ 000} [\phi(nT_p) - \phi_{r0}(nT_p)]$$

counts (assuming, of course,  $|\phi(nT_p) - \phi_{r0}(nT_p)| \leq 90^\circ$  for all  $n$ ), and is most accurate when the frequency  $f$  is not integrally related to the sampling rate, so that the samples are continually shifting in position with respect to the zero crossings of  $\cos 2\pi fnT_p$ . It is assumed, incidentally, that sampling is always done at a greater rate than the Nyquist rate.

Two input tape channels are processed for noise cancellation, which is needed because of the zero center frequency of the recorded signal. Four channels are processed in the DPLL in order to cancel double-angle terms and double-angle noise. Because the loop operates with a low IF compared to the input noise bandwidth, the double-angle noise terms would not otherwise be attenuated by loop smoothing. When noise is added, the phase detector becomes sinusoidal in its response. The performance of the phase detector in noise is discussed in the next section.

The phase detector counter could be designed to sample at a fixed 0.2  $\mu$ s rate and to dump every 5 ms, thus again giving 25 000 samples per dump cycle, but the counting would not then be done over an integral number of cycles of D1 output, causing a round-off error that is best avoided. For analytical purposes, however, it is henceforth assumed that sampling and dumping is done at the above fixed rates and the round-off effect is merely ignored. Because of the presence of the IF frequency, the effects on predicted loop performance of using this assumption are expected to be minimal.

The digital voltage-controlled oscillator (VCO) is a binary rate multiplier (BRM) followed by a frequency divider. The frequency of the BRM is controlled by the output of the digital loop filter, which in turn is a digital circuit chosen to make the performance of the overall loop be similar to that of a second-order analog phase-locked loop. The BRM operates at a frequency 100 times that of the output of D1, hence D1 smoothes over the "rough" output of the BRM, deleting pulses from its uniform pulse train reference frequency in order to have an overall pulse rate corresponding to the loop filter output. The effects of the nonuniformity of the BRM output will be discussed later.

Before discussing the digital loop filter, some concepts of phase locked analog loop design will be reviewed. A continuous-time analog loop that is optimal in its response to a step change in frequency has a linearized closed-loop frequency response (in terms of phase angle outputs to phase angle inputs) (Ref. D-3) of

$$H(s) = \frac{\tau s + 1}{\frac{\tau^2 s^2}{2} + \tau s + 1}, \quad (D-1)$$

---

Ref. D-3. R. Jaffee and E. Reichtin, "Design and Performance of Phase Lock Circuits Capable of Near-Optimum Performance Over a Wide Range of Input Signal and Noise Levels," IRE Trans. on Information Theory, Vol. IT-1, March 1955, pp. 66-72.

and an open-loop frequency response of

$$G(s) = \frac{2(\tau s + 1)}{\tau^2 s^2}, \quad (D-2)$$

where (Ref. D-4)

$$\tau = \frac{3}{2B_N}, \quad (D-3)$$

and  $B_N$  is the two-sided closed loop noise bandwidth (Hz). Let  $B_N$  be 2 Hz here.

In the design of the digital loop filter, the linearized open-loop frequency response of the analog second-order loop given by Eq. (D-2) can be expressed as two factors. One is a factor resulting from the analog loop filter and the other factor results from the analog VCO.

The factor resulting from the analog loop filter is

$$\frac{2K(\tau s + 1)}{\tau s}, \quad (D-4)$$

The step response of this filter is given in Fig. D-5. A combination of BRM's and counters has been formulated that responds to an input step function from the phase detector counter (i.e., a sequence of held counter dumps of equal magnitude) with a response approximately that in Fig. D-5b (aside from quantization, which will be discussed later).

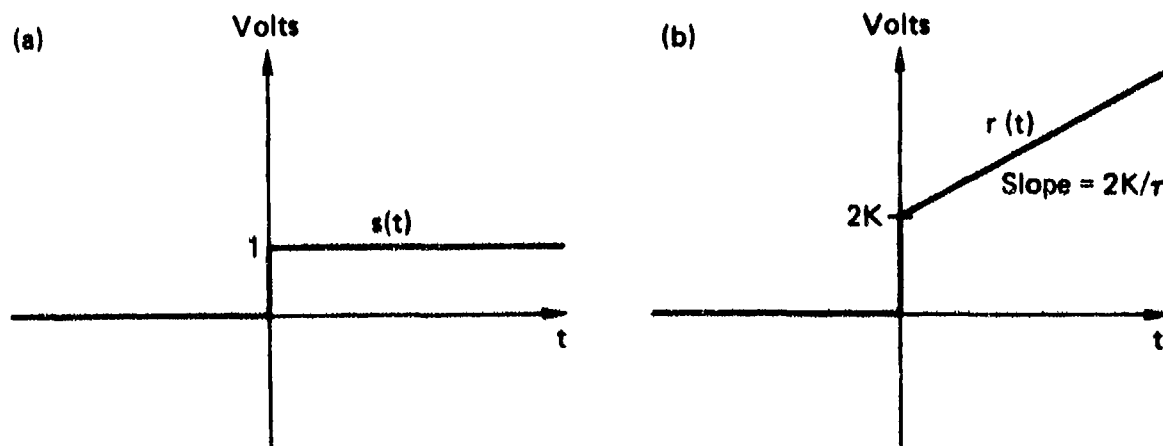


Fig. D-5 Response of Analog Loop Filter to a Step Function:  
 (a) Analog Step Function; (b) Step Response of Filter

Ref. D-4. R. Sydnor, J. J. Caldwell and B. E. Rose, "Frequency Stability Requirements for Space Communications and Tracking Systems," *Proc. IEEE*, Vol. 54, No. 2, February 1966, pp. 231-236.

The factor in Eq. (D-2) caused by the analog VCO is

$$1/K\tau \quad . \quad (D-5)$$

This response relates the VCO input to the phase of the VCO output. The phase of the step response of an analog VCO (the step response is a constant frequency starting at time 0) is given in Fig. D-6.

In response to a digital step function from the loop filter, the phase of the digital VCO output behaves in a manner quite similar to that of the analog VCO in Fig. D-6, but with some quantization (to be discussed later) imposed.

Thus aside from quantization and other noise sources the digital phase-locked loop may be modeled as an analog loop (Fig. D-7). The digital nature of the loop must be accounted for when both the causes and effects of the various noises that occur are analyzed. A linearized model (in terms of phase angle) for the DPLL is given in Fig. D-8 ( $T = 0.005$  s). The phase signal input to the loop in Fig. D-7 is assumed itself to be of low enough frequency that the sampling operation does not cause any aliasing, and merely represents a  $(1/T)$  factor in frequency response. Note that the input phase to the model in Fig. D-8,  $\phi(t)$ , is defined as the difference between the input phase of the actual loop in Fig. D-2 and the loop phase aiding information,  $\phi(t) = \phi_i(t) - \phi_{ref}(t)$ , which is expected to be low frequency in nature. Note also that the output phase in Fig. D-8,  $\phi_r(t)$ , is the difference between the output phase  $\phi_{r_o}(t)$ , of Fig. D-2 and  $\phi_{ref}(t)$ . The only places where the signals in Fig. D-8 do not correspond to those in Fig. D-2 are at the loop input and at the VCO input and output.

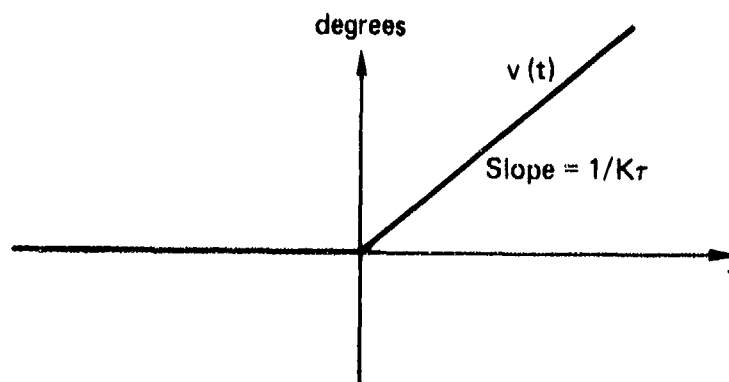


Fig. D-6 Phase of Step Response of Analog VCO and Digital VCO

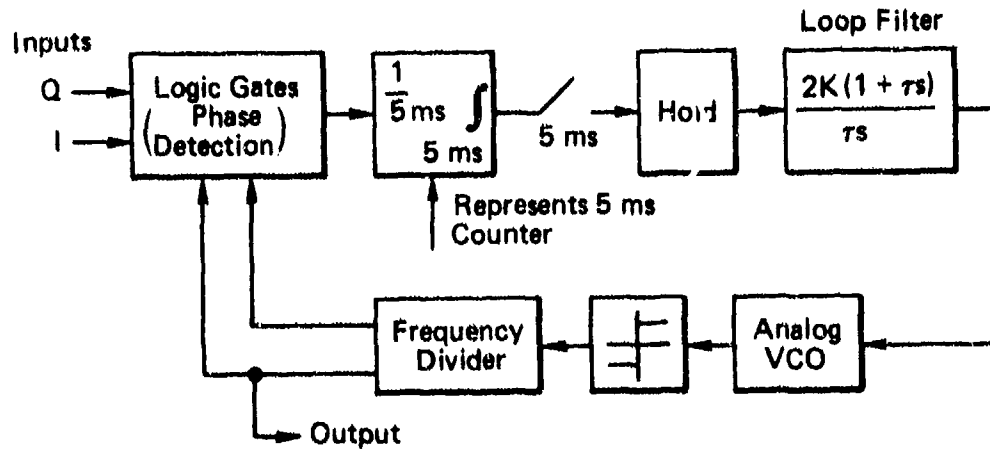


Fig. D-7 Model of Noise-Free Digital Phase-Locked Loop

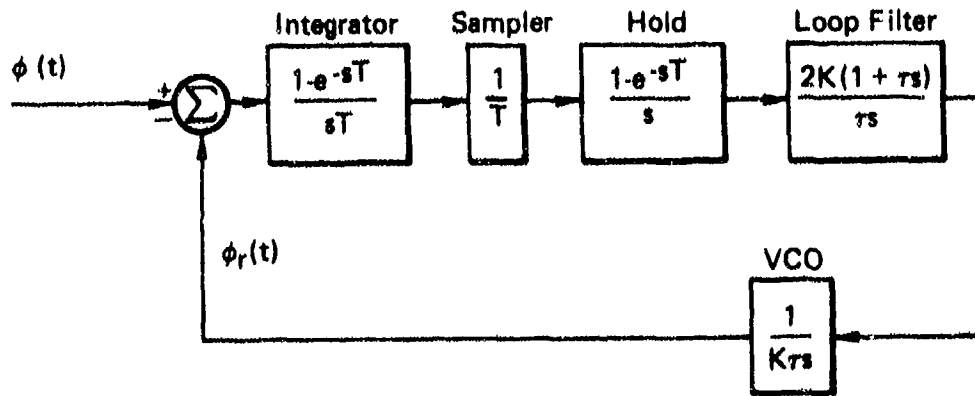


Fig. D-8 Linearized Model of Noise-Free Digital Phase-Locked Loop ( $r = 0.75$ )

Evaluation of the frequency response of the loop in Fig. D-8 ( $\tau = 0.75$ ) indicates that its magnitude is within 1% of the magnitude of the response of the second-order loop in Eq. (D-1) for all frequencies below 11 Hz, at which frequency the magnitude of the loop response is an attenuation of greater than 28 dB from the magnitude of the response at zero frequency. The phase of the frequency response of the loop in Fig. D-8 is within 5% of the phase of the response of the second-order loop in Eq. (D-1) for all frequencies below 2 Hz, which is more than twice the half-power frequency of the second-order loop. At about 2.6 Hz the phase response of the loop in Fig. D-8 crosses through  $-90^\circ$  and continues to fall off at  $1.8^\circ/\text{Hz}$  over all positive frequencies, while the phase response of the second-order loop is asymptotic to  $-90^\circ$  as the frequency increases. It is found in this manner that if the spectral composition of the signal  $\phi(t) - \phi_{\text{ref}}(t)$  is concentrated below 2 Hz the loop in Fig. D-8 may be modeled as being identical to the second-order loop of Eq. (D-1) (in the noiseless case). If the spectral composition has other significant components the more exact model (Fig. D-8) must be used instead.

#### NOISE SOURCES IN THE DIGITAL PHASE PROCESSING SCHEME

In this section the major noise sources present in the digital processing scheme are listed and briefly described.

1. Input Noise: The input noise is defined as the stochastic process  $n(t)$  which additively corrupts the carrier signal aboard the range ship (see Fig. D-1). This noise in turn is caused primarily by the noisy reception of the satellite signal aboard the missile, which transmits the signal to the range ship. In finding the effect of this noise, the much smaller errors over one 5 ms measurement interval (including phase quantization) are also accounted for because the ship records a sampled signal instead of a continuous time signal.
2. Shipboard Oscillator Instability: The phase noise caused by jitter of the oscillator controlling the I and Q channel processing and sampling of the carrier input signal on the range ship.
3. Instability in the APL Frequency Standard: The noise caused by stochastic irregularity in the cesium standard governing the frequency of the outputs of the IF mixer and BRM in Fig. D-2. Its effects will be shown to be nonexistent and are replaced by synchronous sampling noise (discussed next).

4. Synchronous Sampling Noise: The errors that result because the sampling in the phase detector counter is in synchronism with the frequency generation by the BRM.

5. Phase Texture Noise of Signal Recorded on Ship: The noise occurring because the waveform recorded on the ship denotes incremental phase displacements by changing the values of samples that are coarsely distributed in time over a number of 5-ms measurement intervals.

6. VCO Phase Texture Noise: The errors generated because the output phase of the VCO is "rough" in nature. This happens because the BRM output is formed by deleting positive pulses nonuniformly from a uniform pulse train, at a high frequency.

7. VCO Frequency Quantization Noise: The errors that result because the BRM output frequency is restricted to quantized levels.

8. Loop Filter Quantization Noise: The errors generated because operations in the loop filter can yield only quantized results.

A more detailed discussion of these noise sources follows.

#### DETAILED TREATMENT OF THE NOISE SOURCES

##### Input Noise

In SATRACK-GPS, the carrier power,  $A^2$ , received at the ship can range from -125 to -147 dBm. We shall choose the weakest level (-147 dBm) as the nominal level for our discussion. The input noise is a stationary random process with a two-sided PSD of  $N_0/2 = 10^{-17.2}$  mW/Hz, and is considered to be 2 MHz wide and centered at 50 MHz in Fig. D-1, after having been previously heterodyned down, along with the carrier, from the nominal transmission frequency of 2200 MHz.

The immediate effect of input noise is to change some of the samples recorded on the ship from positive to negative (or vice versa). Thus, given a sinusoidal carrier wave as in Fig. D-9a, that would generate the sequence of 1-bit quantized samples shown in Fig. D-9b, the

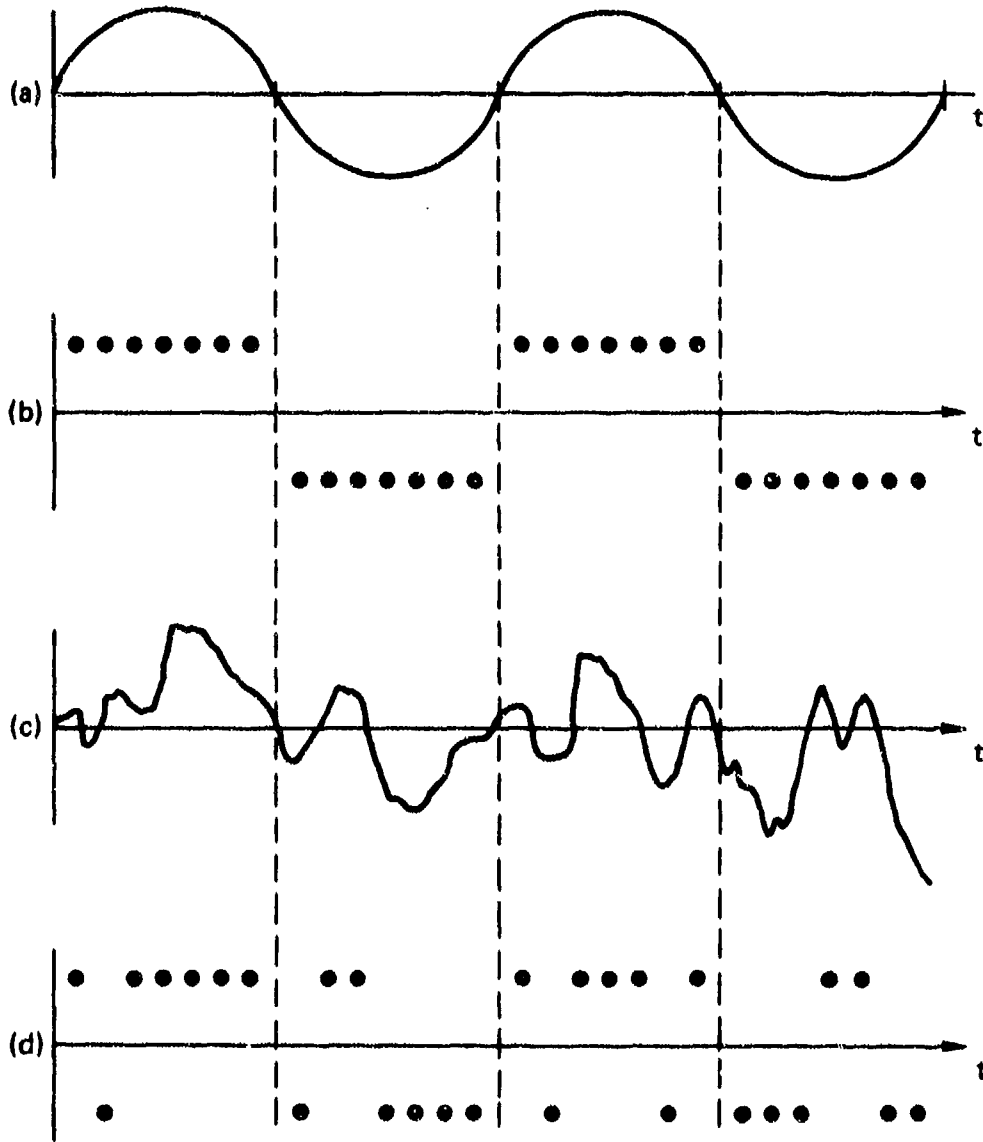


**Fig. D-9 Effect of Input Noise on Sampled Data: (a) Sinusoidal Carrier Wave; (b) 1-Bit Quantized Samples of Sinusoid; (c) Sinusoid with Additive Input Noise; (d) 1-Bit Quantized Samples of Sinusoid with Noise**

effect of the additive input noise might be to change the sinusoid to the signal shown in Fig. D-9c, which would, in turn, generate the sequence of samples shown in Fig. D-9d. Note that because the input noise  $n(t)$  is stationary and independent of the carrier wave, the likelihood of a given sample being changed by the noise varies with the height of the noiseless carrier signal at the precise time of the sample. In effect, instead of representing a pulse of a certain polarity, each sample now becomes a random variable with possible values of +1 or -1, each of these having certain probabilities. The sequence of random variables generated over a certain 5 ms measurement interval would have a joint probability distribution. The count observed at the phase detector counter output in Fig. D-2 at the end of the 5 ms would, in turn, also be a random variable with mean and variance depending on the phase relation of the VCO output to the IF-mixer input waveform to the DPLL (Fig. D-2). Investigation of the mean and variance of this random variable for different phase relations between the VCO output and DPLL input square wave will be pursued, but first heuristic discussion will be given.

If the VCO output is shifted  $\delta$  degrees from the DPLL input in the noiseless case, the total count at the output of the phase detector counter after 5 ms (with the nominal 0.2  $\mu$ s sampling rate) would be  $100\,000 \times (\delta/90)$ , one-fourth of this count coming from each of the four gates (5, 6, 7, 8). If the  $n$ th sample at the DPLL input would be a +1 in the noiseless case, it will now be a random variable with a mean of  $p(n) - [1 - p(n)]$ , where  $p(n)$  is the probability that the sample is still a +1 and  $1 - p(n)$  is the probability that the sample is now a -1. The mean of this random variable is  $2p(n) - 1$ , which is always  $\leq 1$  (it is equal to 1 when  $p(n) = 1$ , the noiseless case). In the presence of input noise, when all the samples occurring during the 5 ms interval are accumulated in the phase detector counter, the mean of the sum of all samples is equal to the sum of the means of each sample, hence the mean is scaled down by some factor from the number of counts that would have been observed without noise. It is possible to heuristically observe how this factor would change as the angle of offset of the VCO output and DPLL input from perfect lock ( $90^\circ$  difference) changes.

In Figs. D-10a, b, c, and d are plotted, respectively, a sinusoidal wave with no additive noise; a 1-bit-quantized version of this sinusoid, to be regarded as an input to the DPLL; a square wave signal tracking the input square wave ( $90^\circ$  offset); and a square wave signal slightly shifted ( $\delta^\circ$ ) from perfect tracking of the input square wave. In the phase comparator, a product would be formed between the input square wave and the tracking square wave. The phase comparator results are shown in Fig. D-10e for the perfect tracking square wave, and in Fig. D-10f for the tracking sinusoid with slight offset. Figure D-10g shows the original sinusoid from Fig. D-10a, with emphasis on the portions of the sinusoid which after 1-bit quantization and multiplication by the

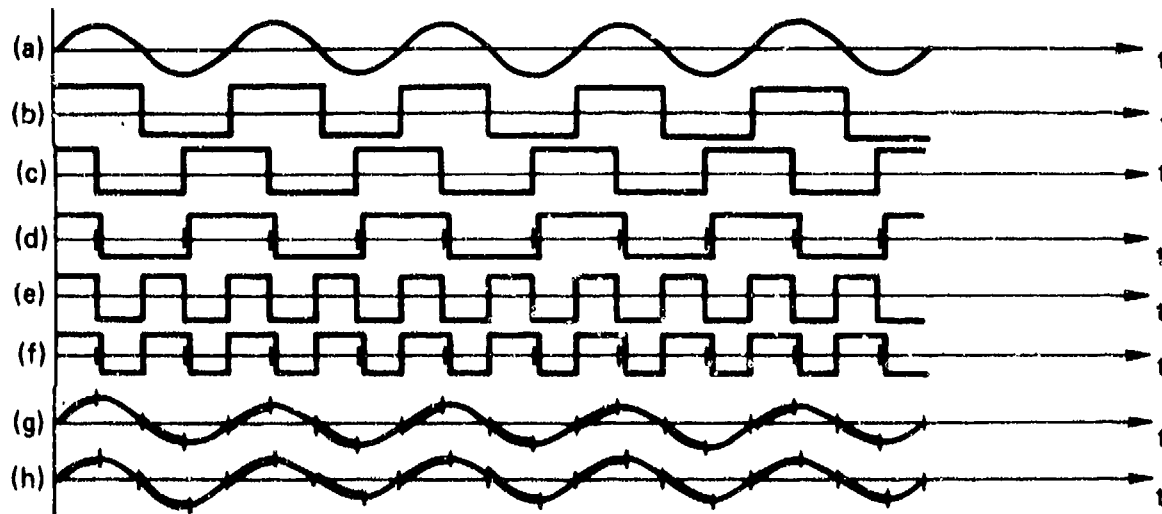


**Fig. D-10** Effect of Input Noise with Phase Comparator: (a) Noiseless Input Sinusoidal Wave; (b) 1-Bit Quantized Version of Sinusoid; (c) Squarewave Tracking Input Sinusoid; (d) Squarewave Slightly Offset in Phase from Perfect Track of Input Sinusoid; (e) Output of Phase Comparator for Inputs b and c; (f) Output of Phase Comparator for Inputs b and d; (g) Sinusoid from a, but Shaded Where Results of e is Positive; (h) Sinusoid from a, but Shaded Where Result of f is Positive

VCO output in Fig. D-10c in the phase comparator gave positive output in Fig. D-10e. Figure D-10h again shows the original sinusoid from Fig. D-10a, but now with emphasis on those portions of the sinusoid which after 1-bit quantization and multiplication by the VCO output in Fig. D-10d have given positive output in Fig. D-10f. The new portion of the sinusoid giving positive output in Fig. D-10h but not giving positive output in Fig. D-10g is the portion of the input to the DPLL that detects the phase shift of the VCO output. Note that the new portion of the sinusoid giving positive output in Fig. D-10h but not giving positive output in Fig. D-10g is near the peak of the wave, so that when noise is introduced only the most reliable samples are used to indicate the phase offset (an efficient technique). As the phase offset increases, the reliability of the samples used to indicate the additional offset decreases. Thus the net output of the phase detector counter every 5 ms is not a linear function of the phase offset between the DPLL input and the VCO output, but exhibits a decreasing slope as the absolute value of the offset increases. In fact this output is found to be sinusoidal for the input carrier level and noise in the SATRACK-GPS problem (as will be shown).

The mean and variance of the phase detector output count after a 5 ms measurement interval for various phase shifts between DPLL input and VCO output will now be evaluated. The narrowband input noise  $n(t)$  in Fig. D-1 may be written (Ref. D-2)

$$n(t) = \sqrt{2} [n_1(t) \cos \omega_0 t + n_2(t) \sin \omega_0 t] , \quad (D-6)$$

where the PSD's of  $n(t)$  and of  $n_1(t)$  are shown in Fig. D-11 ( $n_1(t)$  and  $n_2(t)$  have the same PSD's, and are independent). Considering the lowpass filter in Fig. D-1 to fully attenuate the double-angle terms resulting from the 50 MHz mixing operations, and considering the sampling following the low-pass filtering to be ideal, the inphase (I) and quadrature (Q) channels recorded on tape have the signals shown in Fig. D-2.

I channel:

$$\text{sign} \{ A(t_n) \cos[\phi_1(t_n) - \theta] + n_1(t_n) \cos \theta + n_2(t_n) \sin \theta \} \quad (D-7a)$$

Q channel:

$$\text{sign} \{ A(t_n) \sin[\phi_1(t_n) - \theta] - n_1(t_n) \sin \theta + n_2(t_n) \cos \theta \} \quad (D-7b)$$

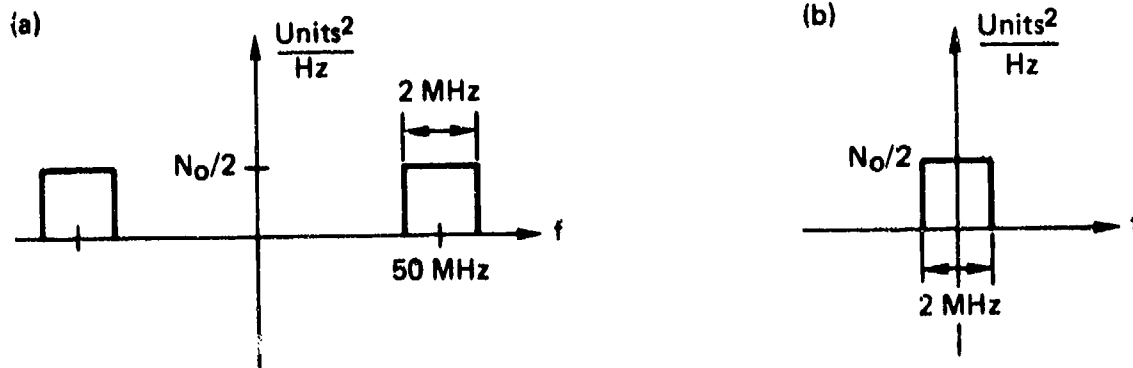


Fig. D-11 Comparison of Power Spectral Densities: (a) Power Spectral Density of  $n(t)$ ; (b) Power Spectral Density of  $n_1(t), n_2(t)$

The angle  $\theta$  is a random phase angle introduced by the mixing operation. It is assumed that  $\theta$  is uniformly distributed in probability between 0 and  $2\pi$  radians. The results of the IF mixing are next listed as the outputs of gates (1, 2, 3, 4) (Fig. D-2):

gate 1:

$$\text{sign} \left\{ \begin{array}{l} -A(t_n)\cos[\phi_1(t_n) - \psi - \theta - \omega t_n] + A(t_n)\cos[\phi_1(t_n) - \theta + \psi + \omega t_n] \\ -n_1(t_n)\cos(\theta + \psi + \omega t_n) - n_2(t_n)\sin(\theta + \psi + \omega t_n) \\ +n_1(t_n)\cos(\omega t_n + \psi - \theta) - n_2(t_n)\sin(\omega t_n + \psi - \theta) \end{array} \right\} \quad (\text{D-8a})$$

gate 2:

$$\text{sign} \left\{ \begin{array}{l} A(t_n)\sin[\phi_1(t_n) - \theta - \psi - \omega t_n] + A(t_n)\sin[\phi_1(t_n) + \psi - \theta + \omega t_n] \\ +n_1(t_n)\sin(\omega t_n + \psi - \theta) + n_2(t_n)\cos(\omega t_n + \psi - \theta) \\ +n_1(t_n)\sin(-\omega t_n - \psi - \theta) + n_2(t_n)\cos(\omega t_n + \psi + \theta) \end{array} \right\} \quad (\text{D-8b})$$

gate 3:

$$\text{sign} \left\{ \begin{array}{l} A(t_n) \cos[\phi_1(t_n) + \psi - \theta + \omega t_n] + A(t_n) \cos[\phi_1(t_n) - \psi - \theta - \omega t_n] \\ +n_1(t_n) \cos(\omega t_n + \psi + \theta) + n_2(t_n) \sin(\omega t_n + \psi + \theta) \\ +n_1(t_n) \cos(-\omega t_n + \theta - \psi) + n_2(t_n) \sin(-\omega t_n + \theta - \psi) \end{array} \right\} \quad (\text{D-8c})$$

gate 4:

$$\text{sign} \left\{ \begin{array}{l} A(t_n) \sin[\omega t_n + \psi + \phi_1(t_n) - \theta] + A(t_n) \sin[\omega t_n + \psi + \theta - \phi_1(t_n)] \\ +n_1(t_n) \sin(\omega t_n + \psi - \theta) + n_2(t_n) \cos(\omega t_n + \psi - \theta) \\ +n_1(t_n) \sin(\omega t_n + \psi + \theta) - n_2(t_n) \cos(\omega t_n + \psi + \theta) \end{array} \right\} \quad (\text{D-8d})$$

The angle  $\psi$  is another uniformly distributed random phase angle, introduced by the IF mixing operation. Finally, these DPLL inputs are mixed with the VCO outputs in gates 5, 6, 7, and 8 to yield (only the gate 5 answer will be given below):

gate 5:

$$\left\{ \begin{array}{l} A(t_n) \sin[\phi_1(t_n) - \phi_{r_0}(t_n)] - A(t_n) \sin[\phi_{r_0}(t_n) + \phi_1(t_n) - 2\theta + 2\psi + 2\omega t_n] \\ +A(t_n) \sin[\phi_{r_0}(t_n) + \phi_1(t_n) - 2\theta] + A(t_n) \sin[\phi_{r_0}(t_n) - \phi_1(t_n) + 2\psi + 2\omega t_n] \\ +n_1(t_n) \sin[\phi_{r_0}(t_n) - 2\theta] + n_2(t_n) \cos[\phi_{r_0}(t_n) - 2\theta] \\ +n_1(t_n) \sin[\phi_{r_0}(t_n) + 2\psi + 2\omega t_n] - n_2(t_n) \cos[\phi_{r_0}(t_n) + 2\psi + 2\omega t_n] \\ -n_1(t_n) \sin[\phi_{r_0}(t_n) + 2\psi - 2\theta + 2\omega t_n] - n_2(t_n) \cos[\phi_{r_0}(t_n) + 2\psi - 2\theta + 2\omega t_n] \\ -n_1(t_n) \sin[\phi_{r_0}(t_n)] + n_2(t_n) \cos[\phi_{r_0}(t_n)] \end{array} \right\}$$

(D-9)

Each of the three other gate outputs also contains  $A(t_n)\sin[\phi_1(t_n) - \phi_{r_0}(t_n)]$  as one term in their sign ( $\cdot$ ) function, and each contains the noise term  $-n_1(t_n)\sin[\phi_{r_0}(t_n)] + n_2(t_n)\cos[\phi_{r_0}(t_n)]$ . All other terms cancel between the four gate outputs (not exactly, of course, because of the presence of the sign ( $\cdot$ ), and the fact that  $\text{sign}(a) + \text{sign}(b) \neq 2 \text{sign}(a+b)$  in general). It is necessary to use all four gate outputs because the IF frequency is low compared to the bandwidth of the input noise, causing the double-angle noise terms to have frequency components overlapping zero frequency, that would not be removed by the loop, even though the loop is low-pass in nature. (For example, the PSD of the noise term

$$n_1(t_n)\sin[\phi_{r_0}(t_n) + 2\psi + 2\omega t_n] - n_2(t_n)\cos[\phi_{r_0}(t_n) + 2\psi + 2\omega t_n]$$

is plotted in Fig. D-12 for an IF frequency of 100 kHz.) The IF frequency cannot be raised high enough to completely prevent this overlap phenomenon if the sampling rate (5 MHz) is to be kept substantially above the Nyquist rate for the total signal (which would then be at a high frequency); also the PSD's of the various noises are not really square in shape (as was assumed for simplicity) but decay over wider frequency bands.

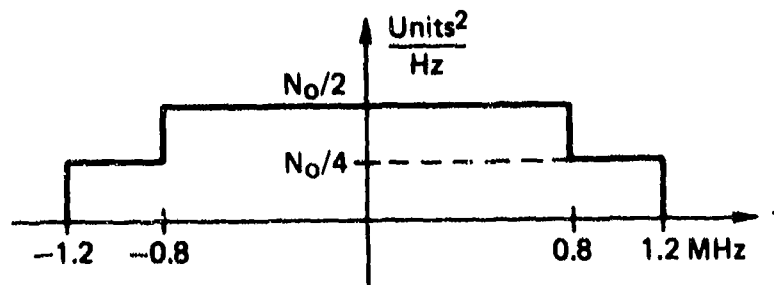


Fig. D-12 PSD of Double Frequency (200 MHz) Noise Term in the Output of Gate 5. (This noise is caused by the overlap of a box 2-MHz wide centered at 200 kHz and a box 2-MHz wide centered at -200 kHz.)

Using the distributions of the random phase angles, and assuming that the phase offset is constant over a 5  $\mu$ s time interval (i.e.,  $\phi_{r_0}(t_n) - \phi_1(t_n) = \delta^\circ (1 \leq n \leq 25\,000)$ ), the autocorrelation function of the outputs of gates 5 through 8, and the cross correlation functions of these outputs can be evaluated. In this computation it is assumed that the terms interior to the sign ( $\cdot$ ) functions are Gaussian (the

noise terms are, in fact, Gaussian, and do dominate the signal terms). Using the fact that for two jointly Gaussian random variables  $x$  and  $y$  (Ref. D-5):

$$E(\text{sign } x)(\text{sign } y) = \left(\frac{2}{\pi}\right) \arcsin\left(\frac{E(xy)}{\sigma_x \sigma_y}\right) \quad (D-10)$$

This information is then used to evaluate the mean-squared output of the phase detector counter (which is normalized to degrees through multiplication by 90/100 000 because there are 100 000 possible net counts in the 5 ms interval (with one count occurring every 0.2  $\mu$ s in each of the four channels), and a total count of 100 000 denotes a 90° phase shift (from a perfect tracking situation) in the noise-free case, as previously discussed).

Let  $y(\delta)$  denote the output (in degrees) of the phase detector, with input phase offset  $\delta^\circ$ . With the aid of a computer, it is found that to four digit accuracy as  $\delta$  is varied from perfect track,

$$E[y(\delta)]^2 = 0.16829 + [(0.45199) \sin \delta]^2 \quad (D-11)$$

Then,  $y(\delta, i)$ , the output of the phase detector for two inputs offset from perfect track by  $\delta^\circ$  over the  $i$ th 5 ms measurement interval, can be modeled as

$$y(\delta, i) = n_p(i) + m(\delta) \quad (D-12)$$

where the variance of the effective noise at the phase detector output is constant as  $\delta$  is varied, and the mean response of the phase detector to a  $\delta^\circ$  phase shift is

$$m(\delta) = 0.45199 \sin \delta \quad (D-13)$$

By Eq. (D-13), near zero phase offset the factor attenuating the mean response is given by

$$0.45199(\pi/180) = 7.8887 \times 10^{-3} \quad (D-14)$$

(Note that  $(\sin \delta^\circ)/\delta^\circ \rightarrow \pi/180$  for  $\delta \rightarrow 0$ )

and in order to have the remainder of the loop respond properly to a  $\delta^\circ$  phase shift, a multiplication by the inverse of the quantity

---

Ref. D-5. A. Papoulis, Probability, Random Variables, and Stochastic Processes, McGraw-Hill Book Co., New York, 1965, pp. 493-484.

in Eq. (D-14), the factor 126.76 must be introduced. This factor is dependent, of course, on the relative amplitude of the carrier  $A(t)$  and the noise  $n(t)$ . This dependency is the reason for the gain control in the loop; i.e., to adjust the relative amplitude when the input signal/noise ratio changes (see section on gain control design). Thus the effective noise variance at the phase detector output becomes

$$\bar{n}_d^2(t) = (126.76^2)(0.16829) = 2704.1 \text{ degrees}^2, \quad (\text{D-15})$$

which has an rms value of  $52.001^\circ$ . Henceforth this noise effectively added at the phase detector output shall be referred to as the "effective input noise".

Experimentation with different averaging interval lengths, noise PSD levels, noise bandwidths, and sampling rates (within a few orders of magnitude of the nominal values of these parameters) indicates that the factor by which the mean has been attenuated by the noise is proportional to the square root of input-noise-variance/carrier-power ratio, and is independent of averaging interval length or sampling rate. Thus the variable factor that is to be inserted in the loop must be proportional to  $1/\sqrt{\text{SNR}}$  (see section on gain control design).

With a fixed sampling rate, the variance of the effective noise at the phase detector output (before or after multiplication to correct the mean) is inversely proportional to the number of samples in the averaging interval (equivalently the number of input noise "correlation lengths" in the averaging interval), provided that the averaging interval is at least ten correlation lengths of the input noise ( $0.5 \mu\text{s}$  per correlation length, with input noise being 2 MHz wide at its center frequency). Thus the effective input noise may be considered white every 5 ms, because additive white noise would display this dependence on the averaging interval length (number of 5 ms samples in this case). After the holding operation following the phase detector counter dumping, the autocorrelation  $[R(\tau)]$  of this noise is triangular in form, having a maximum at  $\tau = 0$ , falling linearly to 0 at  $\tau = \pm T$  ( $T =$  averaging interval), and remaining at 0 for  $|\tau| > T$ . Thus the power spectral density of this noise, which then has a  $[(\sin f)/f]^2$  form, has a level at zero frequency independent of the interval length. Because of the low frequency nature of the loop [relative to  $1/(\text{averaging interval})$ ], only the zero-frequency level is important.

If the bandwidth of the input noise is decreased, and the averaging interval length held constant, less correlation lengths of the input noise are considered, hence the variance of the effective noise at the phase detector output before multiplication by the scale factor rises in proportion to the factor of noise bandwidth decrease. The scale factor, however, also decreases (because the total input noise variance decreases)

in proportion to the square root of the input noise bandwidth decrease. Thus the effective variance of the input noise after multiplication by the scale factor remains the same.

It may be concluded that the PSD of the effective input noise at the output of the hold circuit is dependent for its level near 0 frequency on the signal-power/input-noise-spectral-density ratio (+25 dB for SATRACK-GPS) precisely as in the analog processing case, where Ref. D-2 shows that the output phase variance of an analog phase-locked loop, of noise bandwidth  $B_N$ , is given by

$$E(N_d^2) = \left( \frac{N_0}{2A^2} \right) B_N \text{ radian}^2 \quad (D-16)$$

The variance in Eq. (D-15) results after the delay detector, which itself has a two-sided noise bandwidth of 200 Hz. When there is neither hard limiting or sampling of the input, the variance to be expected after filtering by a 200 Hz noise-bandwidth filter is given by Eq. (D-16) as

$$E[N_d^2(1)] = \left( \frac{10^{-16.9}}{2 \times 10^{-14.7}} \right) 200 = 0.6325 \text{ radian}^2, \quad (D-17)$$

$$E[N_d^2(1)] = 2076.38 \text{ degrees}^2, \quad (D-18)$$

The variance found by application of Eq. (D-16) is 1.15 dB less than the variance observed in Eq. (D-15). Thus the effect of 1-bit processing relative to input noise is a deterioration of 1.15 dB.

Using Eq. (D-16) for comparison, we now may state the dependence of the VCO output phase variance on input noise in the 1-bit case

$$E[N_d^2(1)] = \left( \frac{N_0}{2A^2} \right) B_N (1.3034) \text{ radian}^2 \quad (D-19)$$

This relation, plotted in Fig. D-13, applies as long as the loop is above threshold, and hence behaves linearly. Threshold for the DPLL will be discussed in later reports.

As the sampling rate is varied, keeping the averaging interval length at 5 ms, the effective noise at the phase detector output is asymptotically near  $51^\circ$  rms as the sampling rates become high compared to the Nyquist frequency. Analysis performed subsequent to the work described in this appendix shows that the deterioration decreases as the sampling rate increases, asymptotically approaching 0.77 dB. Thus the rms phase error would approach  $47.6^\circ$  (see Section 6). This effective noise remains relatively constant as the sampling rate is decreased

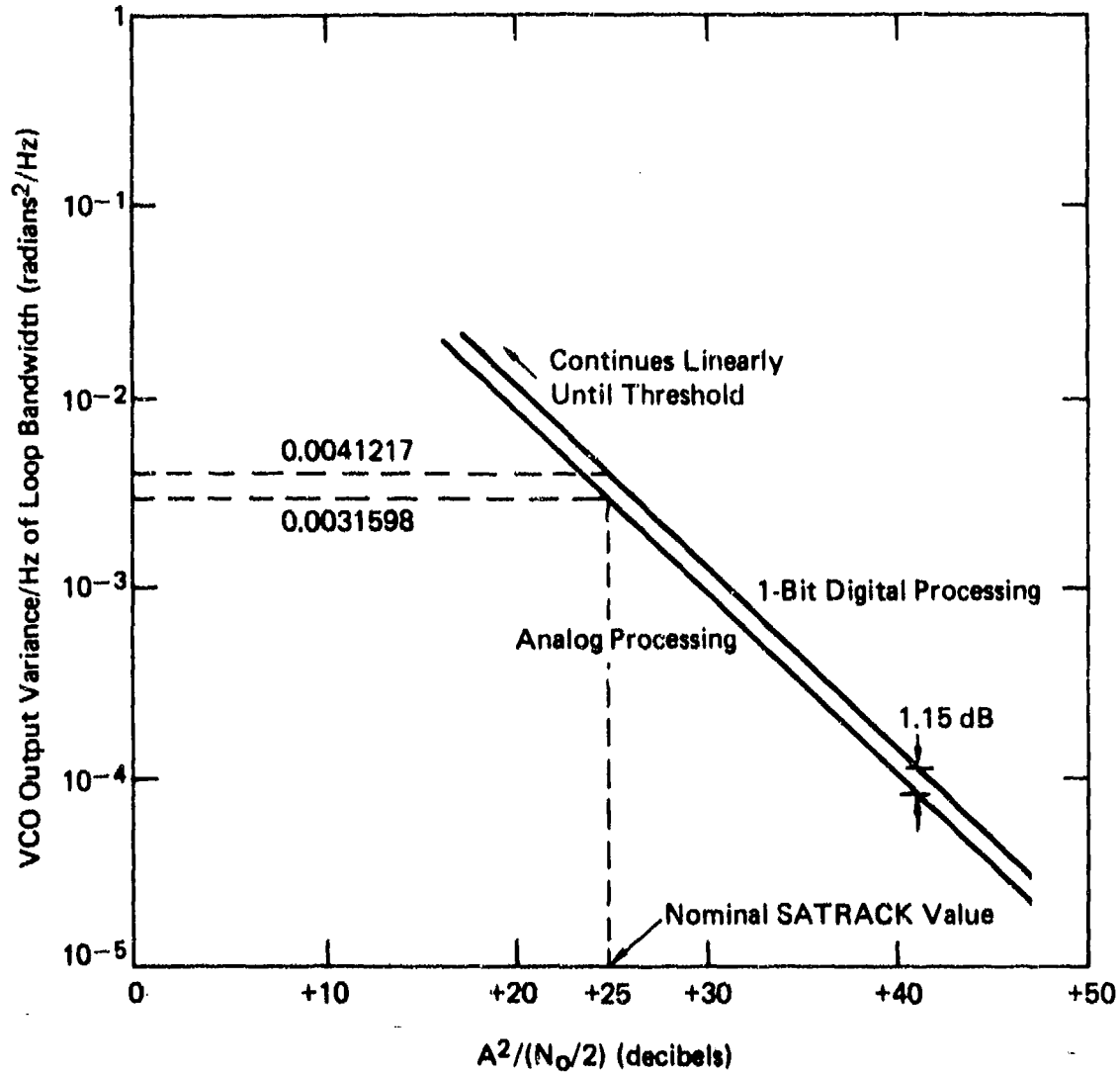


Fig. D-13 Relation Between the Phase Uncertainty (per hertz of loop bandwidth) at the VCO Output Caused by the Input and Input Noise (carrier power/noise spectral density) Ratio,  $A^2/(N_0/2)$ . (log-log scale)

(52.001° rms for 5 MHz sampling rate until the Nyquist frequency (2 MHz) is reached. With sampling rates lower than the Nyquist frequency, consecutive samples are almost uncorrelated, and the effective noise variance begins to rise in inverse proportion to the number of samples in the 5 ms averaging interval, which is decreasing as the sampling rate decreases. The exact dependence of output phase variance on sampling rate (for a 2 Hz loop) is shown in Fig. D-14.

If any of the outputs of gates 5 through 8 are deleted from the sum in the phase detector counter, the effective noise is increased because the double-angle noises overlap zero frequency and are not averaged by the loop. By deleting the signals from gates 5 and 7 the effective input noise variance doubles. The factor attenuating the mean remains the same, because the noise and signal levels in the gate 6 and 8 outputs are not changed. The number of samples processed, however, is smaller, so that less averaging takes place, causing an increase in the additive white noise variance at the output of the phase detector counter before multiplication by the scale factor.

Experimentation with different loop IF frequencies indicates that an IF frequency higher than the current 100 kHz will in fact result in slightly less effective input noise. This would not be true in analog processing, because the double-angle noise terms in the gate 5 through 8 outputs cancel each other. For one-bit processing, however, the sign (·) function prevents exact cancellation, so that as the frequency of the double-angle noise is raised the more they are attenuated both by the averaging in the phase detector counter and by the loop filter. At any rate, the attenuation in effective input noise caused by changing the IF frequency to 1 MHz is only 0.071 dB at the phase detector counter output.

In summary, the effect of input noise is to add a noise source at the output of the phase detector and to attenuate the mean output of the phase detector, making its response sinusoidal. Since in the noise-free case the response of the phase detector is linear, it is postulated that the mean phase detector response to phase offset behaves somewhat as in Fig. D-15, as the noise power grows in relation to the carrier power.

It was also found that the effective input noise at the phase detector output is 52.001° rms, with the nominal signal and noise levels in the SATRACK-GPS system. The gain control necessary to keep the mean output of the phase detector at the proper level (i.e., in degrees, for example) is developed in the section on gain control design. In terms of phase noise at the VCO output, the input noise causes 1.15 dB worse performance in the 1-bit case than in the analog processing case, and has variance at the output given by

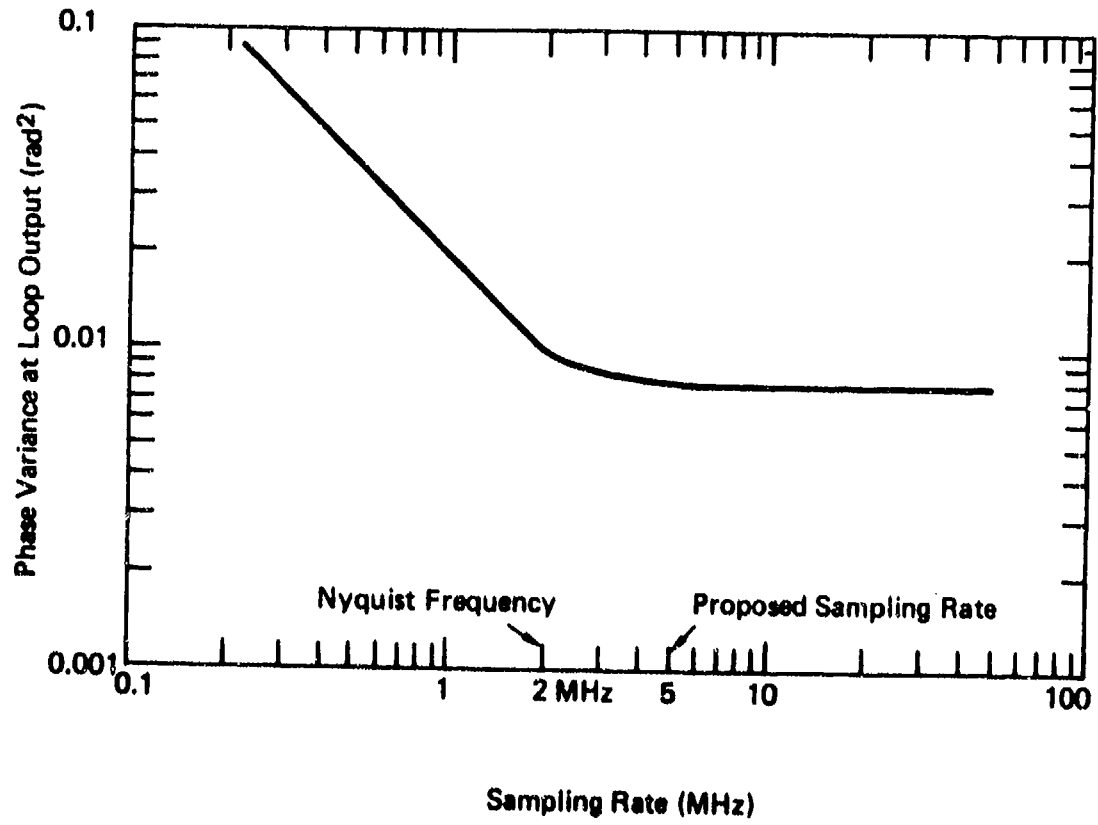


Fig. D-14 Phase Variance at Output of 2-Hz Loop as a Function of Shipboard Sampling Rate.

$$\frac{1.3034 N_o B_N}{2A^2} \text{ rad}^2 .$$

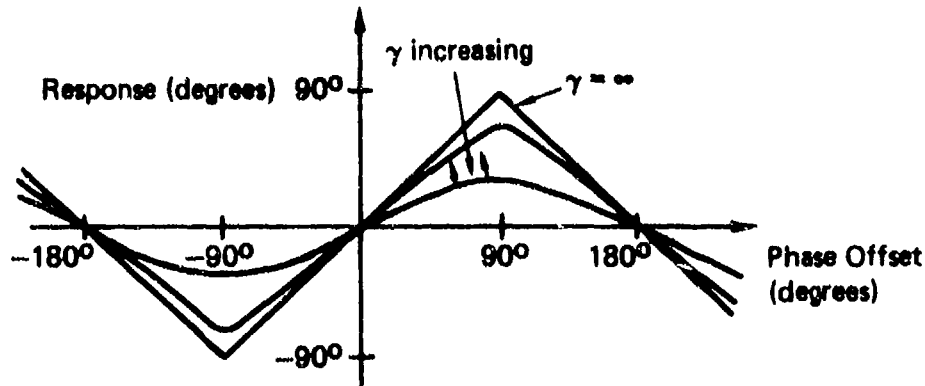


Fig. D-15 Postulated Mean Response of Phase Detector to Phase Offsets, with  $\gamma$  (= Input SNR) as a Parameter

#### Shipboard Oscillator Instability

The 50 MHz oscillator on the ship is subject to phase jitter affecting the signal recorded for processing at APL. As discussed in Ref. D-4, this jitter noise, as an additive phase angle, has a two-sided PSD of  $(c/|\omega|^3)$   $\text{deg}^2/\text{Hz}$ , where the constant,  $c$ , depends on the quality of the shipboard oscillator. Thus the signals generated by the shipboard oscillator in Fig. D-1 are in fact

$$\begin{aligned} & \sqrt{2} \sin [\omega_o t + \theta + n_{\text{osc}}(t)] \\ & \sqrt{2} \cos [\omega_o t + \theta + n_{\text{osc}}(t)] . \end{aligned} \quad (\text{D-20})$$

"Shiptime"  $t_s$ , a function of real time  $t$ , is defined as

$$t_s(t) \triangleq t + \frac{n_{\text{osc}}(t)}{\omega_o} \triangleq q(t) \quad (\text{D-21})$$

so that the signals generated by the shipboard oscillator may be written

$$\begin{aligned} & \sqrt{2} \sin (\omega_0 t_s + \theta) \\ & \sqrt{2} \cos (\omega_0 t_s + \theta) . \end{aligned} \quad (D-22)$$

Furthermore, the samples are not taken at real times  $t_n = n \times 0.2 \mu s$ , but at the real times when  $t_{s_n} = n \times 0.2 \mu s$ ; i.e.,  $q^{-1}(t_{s_n}) = n \times 0.2 \mu s$ . Thus the I and Q channel inputs to the IF mixer in Fig. D-1 are actually

I channel:

$$\text{sign} \left\{ \begin{aligned} & A[q^{-1}(t_{s_n})] \cos \left\{ \phi_1[q^{-1}(t_{s_n})] - \theta - n_{\text{osc}}[q^{-1}(t_{s_n})] \right\} \\ & + n_1[q^{-1}(t_{s_n})] \cos \left\{ \theta + n_{\text{osc}}[q^{-1}(t_{s_n})] \right\} \\ & + n_2[q^{-1}(t_{s_n})] \sin \left\{ \theta + n_{\text{osc}}[q^{-1}(t_{s_n})] \right\} \end{aligned} \right\}$$

Q channel:

$$\text{sign} \left\{ \begin{aligned} & A[q^{-1}(t_{s_n})] \sin \left\{ \phi_1[q^{-1}(t_{s_n})] - \theta - n_{\text{osc}}[q^{-1}(t_{s_n})] \right\} \\ & - n_1[q^{-1}(t_{s_n})] \sin \left\{ \theta + n_{\text{osc}}[q^{-1}(t_{s_n})] \right\} \\ & + n_2[q^{-1}(t_{s_n})] \cos \left\{ \theta + n_{\text{osc}}[q^{-1}(t_{s_n})] \right\} \end{aligned} \right\} \quad (D-23)$$

Note that in addition to additively corrupting the phase angle signal,  $\phi_1[q^{-1}(t_{s_n})]$ , the phase jitter also has an effect on the input noise.

It is assumed for the present that the latter effect is not significant because all noise terms involving  $n_{\text{osc}}[q^{-1}(t_{s_n})]$  cancel in the outputs of gates 5 through 8, presuming that the loop tracks the low frequency  $n_{\text{osc}}[q^{-1}(t_{s_n})]$  component of its input phase signal (i.e., the VCO output signals at time  $t_{s_n}$  are

$$\text{sign} \left( \cos \left\{ \omega q^{-1}(t_{s_n}) + \phi_{r_o} [q^{-1}(t_{s_n})] + \psi - \theta - n_{\text{osc}} [q^{-1}(t_{s_n})] \right\} \right)$$

and

$$\text{sign} \left( -\sin \left\{ \omega q^{-1}(t_{s_n}) + \phi_{r_o} [q^{-1}(t_{s_n})] + \psi - \theta - n_{\text{osc}} [q^{-1}(t_{s_n})] \right\} \right),$$

where  $t_{A_n}(t)$  is the "APL time," and  $t$  is real time). This assumption will be justified in the discussion below.

### Instability in the APL Frequency Standard

The frequency standard at APL is subject to the same type of instabilities as the shipboard oscillator discussed above. The reading of the input tape, which has recorded 1-bit entries every 0.2  $\mu$ s according to shipboard oscillator time, the oscillator in the loop IF mixer, the input reference frequency to the BRM, and the sampling occurring in the phase detector are all synchronously controlled by the same frequency standard. (For example, the frequency division following the BRM has a square wave transition for every 50 "down" transitions of the BRM output, and the sampling in the phase detector counter occurs for every second positive transition in the BRM output.) This fact has a number of consequences. First, because the input tape reading and the IF mixer oscillator are synchronous, the output sequence of the IF mixer is the same sequence that would have been observed had the APL frequency standard been synchronous with the shipboard oscillator. Next, if the frequency standard has a phase jitter this might cause a VCO output square wave transition to be delayed in time. If the sampling of the VCO output in the phase detector were asynchronous with the VCO output itself, a sample value of this output in the phase detector might be changed. But the sampling and the output are synchronous, so the sampling is delayed along with the VCO square wave output transition, hence the sequence of 0.2  $\mu$ s samples of the VCO output is exactly the sequence that would have been generated with a perfect frequency standard. Furthermore, when the output of the IF mixer is read into the phase detector to be compared with the VCO output, the reading of nominal 0.2  $\mu$ s samples is synchronous with the VCO frequency generation, hence there are no phase errors introduced in the sequence of 0.2  $\mu$ s samples of the comparison. In conclusion, the output of the DPLL is the same sequence that would be generated if the frequency standard at APL were synchronous with the shipboard oscillator. In other words, once the I and Q channel inputs have been determined on the ship, the remainder of the processing operates as though the APL frequency standard and the shipboard oscillator were in fact synchronous. All frequency instabilities can thus be modeled by considering only the

differences between shipboard oscillator time and real time (neglecting APL frequency standard time), and the output of the VCO at APL time  $t_{A_n}(t)$  is estimating phases that occurred at ship time  $t_{S_n}(t)$  [i.e., real time  $q^{-1}(t_{S_n})$ ], as claimed in the case of shipboard oscillator instability.

#### Synchronous Sampling Noise

As mentioned in the previous paragraph, the effects of APL frequency standard instabilities are not felt in the DPLL under consideration, because of the synchronous nature of the reading of the input tape, the IF frequency generation, the reference frequency input to the BRM, and the sampling in the phase detector. Analogously to the first law of thermodynamics, this loss of a noise source does not transpire without the introduction of another noise source. The synchronous sampling of the VCO output introduces a noise, which will be discussed next.

Because of the nature of the frequency division following the BRM (which causes a square wave transition for every 50 down transitions of the BRM output, and the sampling in the phase detector, which occurs for every second positive transition of the BRM) the sequence of 0.2  $\mu$ s sample pulses would be unchanged if the continuous time output of the divider were shifted any amount less than 0.025  $\mu$ s in either direction (the time interval between transitions of the reference input to the BRM). This 0.025  $\mu$ s shift is  $0.9^\circ$  at the nominal 100 kHz output of the divider (the IF frequency with no offset). The probability distribution of this error is modeled as uniform between  $-0.9^\circ$  and  $0.9^\circ$  for a given 5 ms measurement interval, and independent in successive measurement intervals. This probability distribution yields a variance of 0.27 degree<sup>2</sup>, hence an rms value of  $0.52^\circ$ . This noise source enters the loop at the frequency divider output.

#### Phase Texture Noise of Signal Recorded on Ship

It was mentioned earlier that the input noise computation also accounted for those errors over one 5 ms measurement interval because the ship records a sampled signal instead of a continuous time signal. However, there is also a lower frequency noise source present in the ship's output signal, which will now be described.

Imagine the input signal to the ship to be at a constant frequency, but suddenly shifted  $\delta^\circ$  in phase. In the absence of input noise the output 1-bit quantized pulse train from the ship will denote this phase shift by changing the sign of a fractional part ( $\delta/180$ ) of its samples to the nearest whole number of pulses. So, because there are 25 000 samples in 5 ms, a total of  $25\ 000 \times (\delta/180)$  samples will be changed. Thus one pulse every 5 ms will change for a phase shift of  $7.2 \times 10^{-3}$  degrees. If the pulse shift were instead

$$\frac{7.2 \times 10^{-3}}{200} = 3.6 \times 10^{-5} \text{ degree}$$

then one pulse in every two hundred 5-ms intervals would be changed (i.e., one sample would change in every second of record). The 5 ms interval containing the pulse that changed would (if considered alone) communicate a  $7.2 \times 10^{-3}$  degree phase shift. However, taken together with the other 199 intervals in which no pulses changed, the phase shift communicated is  $3.6 \times 10^{-5}$  degree. Thus there is a degree of time non-uniformity in the output from the ship in its communication of phase shift information. Calculation of this noise source as it would effectively appear at the output of the phase detector counter shows it to be more than two orders of magnitude smaller than the input noise. In fact, in the presence of the input noise this noise is attenuated even further, as will be shown next.

The mechanism (Fig. D-10) accounting for the phase detector output in the presence of input noise is the weighting of various portions of the input sinusoid as positive or negative after multiplication in the phase detector. When the input is slightly shifted positively in phase (the sampling times remaining constant) the shift might be too small to cause any samples to be changed in a 5 ms interval in the noise-free case, but in the presence of input noise the samples that after multiplication in the phase detector would give positive output become more reliable (are increased in magnitude on the input sinusoid), and the samples that would give negative output after multiplication become less reliable. Thus the mean phase detector response shows phase change even though in the noise-free case the change would not be seen. Further, if the shift were in fact great enough to cause a sample to change sign in the noiseless case this sample would be a very unreliable one when input noise is added, coming near a zero crossing of the input sinusoid. This apparent dither phenomenon, caused by the input noise, attenuates the phase texture noise of the signal recorded on the ship.

#### VCO Phase Texture Noise

The output of the BRM is obtained by selective deletion of positive pulses from a 20 MHz reference square wave (50% duty cycle) supplied by the frequency standard. The selection of pulses to be deleted is controlled by the BRM gate, which is set at the output count of the loop filter to control the BRM output frequency. In the present design the gate has 24 bits of precision, which means that the output frequency of the BRM may be set to quantized frequencies with spacing of 1.2 Hz between them  $(20 \times 10^6 \text{ Hz})/2^{24} = 1.2 \text{ Hz}$ .

To illustrate the operation of the BRM, if the gate were 6 bits in length, and were set to 101011 = 43, then the positive pulses corresponding to the 1's in the binary integer would be seen in the following

sense. First, consider the binary integer above to be reversed to obtain 110101. Next take the set of binary numbers from 0 through 63. In going from one number in the sequence to the next if any of the binary digits corresponding to a (1) in 110101 is converted from a (0) to a (1) then we see the corresponding positive pulse. So, in changing from 000000 to 000001 we see the positive pulse for #1, while in changing from 111111 to 000000 we see no pulse for #0. A portion of the input square wave reference to the BRM and the output for this gate setting are shown in Fig. D-16. After every 64 positive input pulses the pattern repeats, unless the number in the gate is changed. Thus the phase of the BRM output is nonuniform, and differs from that of a uniform 50-percent duty cycle square wave at a frequency of  $(43/64)f_0$ , where  $f_0$  is the reference frequency of the BRM. Phase nonuniformities of this type are analyzed by Levinge (Ref. D-6).

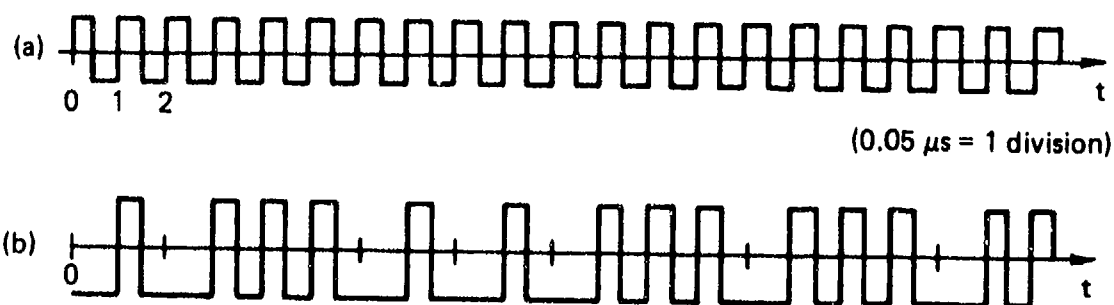


Fig. D-16 Relation of the Input Squarewave Reference to the BRM and the Output: (a) Input Squarewave Reference to BRM; (b) Output of 6-Bit BRM with Gate Set to 43

It is found that for a 4-bit gate the highest peak-to-peak phase error in a pattern period (16 cycles of the input reference waveform, for a 4-bit gate) for any possible gating number (0 to 15) is  $2.3\pi$  radians. Extrapolating a linear relation (between number of gating bits and highest peak-to-peak phase error in a pattern period for any possible gating number) given by Levinge, we find that the maximum peak-to-peak error with 24-bit gating is  $15.3\pi$  radians. Because of the frequency division of the BRM output by 100, this peak-to-peak error becomes  $15.3\pi/100$  rad, which is  $27.54^\circ$  at the output of the frequency divider.

Ref. D-6. R. W. Levinge, "Frequency Control Using Binary Rate Multipliers for Automatic Testing on CW Radar Systems," Proc IEE, Vol. 121, No. 10, October 1974, pp. 1059-1066.

The actual value of the phase error at any given time for the particular gating number causing the maximum peak-to-peak value moves between the peak values of  $13.77^\circ$ .

From Levinge (Ref. D-6), given the number of gating bits, the peak-to-peak phase error in a pattern period averaged over the possible gating numbers is about one-half of the maximum, for small numbers of gating bits. We assume that this relation holds for larger numbers of gating bits, specifically the 24-bit case of interest, hence an approximate model is used, which says that the peak-to-peak phase error for a particular gating number is proportional to the gating number, with a high value of  $27.54^\circ$  for gating number  $2^{24} - 1$ .

We imagine, to find the largest possible effect of this noise, that the output of the BRM is given a new frequency by changing of the gating number only once every 5 ms, and thus starts at a random place on the phase error pattern for that frequency (beginning with zero phase error at that place and following the time evolution of the phase error curve for that gating number in order to incrementally generate phase error). The 5 ms interval is 0.00596 part of one pattern period, which is  $2^{24} \times 0.05 \mu\text{s} = 0.8389 \text{ s}$ . From the phase-error time response given by Levinge (scaled in time axis and also in peak-to-peak error to fit each of our gating number peak-to-peak values) we estimate that the phase error (i.e., the difference between the phase generated and the phase that would be generated by a uniform square wave at the proper frequency) accumulated in 5 ms for gating #n will be  $[1.0719n/(2^{24} - 1)]^\circ$  in either the positive or negative direction. This error averaged over the 5 ms interval is  $[0.53595n/(2^{24} - 1)]^\circ$  in either the positive or negative direction, each with a probability of 0.5. The rms value of this two-point distribution is also  $[0.53595n/(2^{24} - 1)]^\circ$ . If each gating number were equally probable, the overall rms value would be  $0.3094^\circ$ , which would be a noise source uncorrelated every 5 ms and added at the frequency divider output. The actual noise is less because the gating number is changed more often.

#### VCO Frequency Quantization Noise

The allowable output frequencies of the VCO are governed by the fact that the BRM is gated by 24 bits. The input frequency to the BRM from the standard is 20 MHz, thus the quantization is  $(20 \times 10^6/2^{24}) = 1.2 \text{ Hz}$ . There is a frequency division by 100 following BRM, so the output of the VCO is quantized to  $1.2/100 = 0.012 \text{ Hz}$ . In one 5 ms averaging interval the average phase error that would be introduced by a frequency error of this size is  $0.012 \text{ Hz} \times (0.005/2) \text{ s} \times 360^\circ = 0.0108^\circ$ . The probability density distribution of this error is taken as uniform

between  $-0.0054^\circ$  and  $+0.0054^\circ$ . The variance caused by this noise source is  $9.72 \times 10^{-6}$  degrees<sup>2</sup>, or an rms value of  $3.118 \times 10^{-3}$  degrees at the output of the digital VCO. This noise is modeled as uncorrelated every 5 ms.

#### Loop Filter Quantization Noise

The loop filter quantization noise described briefly earlier is not treated in this discussion. It is not expected to be at all significant in comparison with, for example, the input noise.

#### SUMMARY OF THE NOISE SOURCES

The various noise sources (as calculated using the nominal SATRACK-GPS parameters given in the previous section) and their places of entry into the DPLL can be summarized as follows:

1. Input Noise: Effective input noise is introduced at the output of the phase detector counter. The input noise necessitates the introduction of a multiplication by 126.76 at the phase detector counter output because of attenuation that it causes in the mean output of the phase detector. The effective input noise has an rms value of  $52.001^\circ$  following this multiplication, and is uncorrelated every 5 ms. The effective input noise with 1-bit processing is 1.15 dB worse than in the analog case. This same number holds for the increase in the 1-bit case of the phase noise variance at the VCO output caused by input noise.
2. Shipboard Oscillator Instability: This noise source is introduced into the phase of the input signal, and has a PSD of  $c/|\omega|^3$  [in (phase angle)<sup>2</sup>/Hz]. Also it causes the samples taken on the ship to be recorded at times offset from the intended times.
3. Instability in the APL Frequency Standard: In the digital phase-locked loop design no errors are caused by this instability. The loop functions as though the APL standard were synchronous with the shipboard oscillator.
4. Synchronous Sampling Noise: This noise has an rms value of  $0.52^\circ$  and is introduced at the output of the frequency divider. It is uncorrelated every 5 ms.

5. Phase Texture Noise of Signal Recorded on Ship: Negligible because of dither caused by the input noise.
6. VCO Phase Texture Noise: The VCO phase texture noise has as rms value of  $0.3094^\circ$ , and is introduced at the output of the frequency divider. It is uncorrelated every 5 ms.
7. VCO Frequency Quantization Noise: This noise has an rms value of  $3.118 \times 10^{-3}$  degrees, and is introduced at the output of the frequency divider. It is uncorrelated every 5 ms.
8. Loop Filter Quantization Noise: The quantization noise from the loop filter is not treated here because it is not expected to be significant in comparison to input noise.

#### DIGITAL PHASE DETECTOR LINEARITY

In this section a more mathematical explanation is given for the fact that the output of the digital phase detector is in fact linear in its response to the phase shift between the two input square waves, while in the analog case the response is sinusoidal.

In the analog case, if two sinusoids  $\sqrt{2} \sin(\omega t + \theta)$  and  $\sqrt{2} \cos(\omega t + \phi)$  are multiplied, we obtain

$$y(t) = 2 \sin(\omega t + \theta) \cos(\omega t + \phi) = \sin(\theta - \phi) + \sin(2\omega t + \theta + \phi) \quad (D-24)$$

This output is plotted in Fig. D-17. If this output is applied to a low-pass filter the result is,

$$y_{LP}(t) = \sin(\theta - \phi), \quad (D-25)$$

which is sinusoidally related to the phase difference between the two input sinusoids. However, if the input sinusoids are 1-bit quantized before multiplication the result is

$$\begin{aligned} y_q(t) &= \text{sign}[\sqrt{2} \sin(\omega t + \theta)] \times \text{sign}[\sqrt{2} \cos(\omega t + \phi)] \\ &= \text{sign}[2 \sin(\omega t + \theta) \cos(\omega t + \phi)] \\ y_q(t) &= \text{sign}[\sin(\theta - \phi) + \sin(2\omega t + \theta + \phi)], \quad (D-26) \end{aligned}$$

which is a square wave. This output is also shown in Fig. D-17.

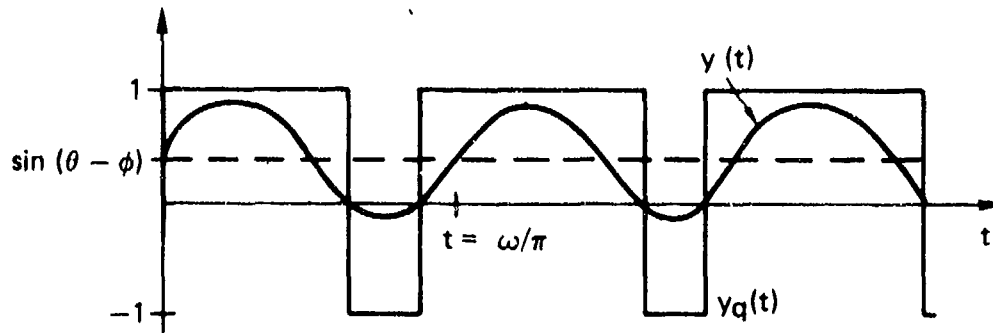


Fig. D-17 Output of Multiplier for Sinusoidal Inputs  $[y(t)]$ , and for 1-Bit Quantized Sinusoidal Inputs  $[y_q(t)]$ .

The probability density function for the amount of time that a sinusoidal wave spends at various levels is given by

$$p(y) = \begin{cases} \frac{1}{\pi} \left( \frac{1}{\sqrt{1-y^2}} \right); & |y| \leq 1 \\ 0 & ; \text{otherwise} \end{cases} \quad (\text{D-27})$$

Equation D-27 may be deduced from the following argument. Given a function  $f(t)$  that is strictly monotonic over a segment  $[c,d]$ , and for which  $f(c) = a$ ,  $f(d) = b$ , then the amount of time the function spends between  $a$  and  $b$  is given by  $(d - c)$ , which may be written as  $f^{-1}(b) - f^{-1}(a)$ . If, over the segment  $[c,d]$ ,  $f(t)$  has a continuously differentiable inverse function  $f^{-1}(\cdot)$ , then we know that

$$\int_a^b \frac{d}{dy} f^{-1}(y) dy = f^{-1}(b) - f^{-1}(a) = d - c \quad (\text{D-28})$$

So if  $[e,g] \subset [a,b]$  (or  $[e,g] \subset [b,a]$  if  $f(t)$  is decreasing), the probability measure for the amount of time spent between  $e$  and  $g$  is given by:

$$P[e, g] \propto \left\{ \begin{array}{l} \int_e^g \left( \frac{d}{dy} f^{-1}(y) \right) dy \quad ; \text{ if } f(\cdot) \text{ is increasing} \\ \int_g^e \left( \frac{d}{dy} f^{-1}(y) \right) dy \quad ; \text{ if } f(\cdot) \text{ is decreasing} \end{array} \right\}, \quad (D-29)$$

which may be abbreviated

$$P[e, g] \propto \int_e^g \left| \frac{d}{dy} f^{-1}(y) \right| dy, \quad (D-30)$$

where the integration is always in the positive direction. Thus the probability density function for the amount of time that  $f(\cdot)$  spends at various levels is proportional to

$$\left| \frac{d}{dy} f^{-1}(y) \right|,$$

where the constant of proportionality is determined by the requirement that the total probability over all levels be unity. This argument is easily applied to the case  $f(t) = \sin(t)$ , where the function is strictly monotonic over wide regions.

By Eq. (D-27), the portion of time during  $y_q(t)$  in Fig. D-17 is below zero is given by

$$\begin{aligned} \int_{-1}^{-\sin(\theta - \phi)} \frac{1}{\pi} \left( \frac{1}{\sqrt{1 - y^2}} \right) dx &= \frac{1}{\pi} \{ \arcsin[-\sin(\theta - \phi)] - \arcsin(-1) \} \\ &= \frac{1}{\pi} \left[ \phi - \theta + \frac{\pi}{2} \right] \\ &= \frac{\phi - \theta}{\pi} + \frac{1}{2}. \end{aligned} \quad (D-31)$$

The portion of time during which  $y_q(t)$  is above zero is thus given by

$$1 - \left( \frac{\phi - \theta}{\pi} + \frac{1}{2} \right) = \frac{1}{2} + \frac{\theta - \phi}{\pi}. \quad (D-32)$$

Finally, when averaging (low-pass filtering) is done over many cycles of  $y_q(t)$ , the average value is

$$y_{q,LP}(t) = 1 \left( \frac{1}{2} + \frac{\theta - \phi}{\pi} \right) + (-1) \left( \frac{\phi - \theta}{\pi} + \frac{1}{2} \right)$$

$$y_{q,LP}(t) = \left( \frac{\theta - \phi}{\pi/2} \right) . \quad (D-33)$$

So that the output of the phase detector counter is a linear function of the phase angle difference of the two input square waves.

#### DESIGN FOR THE GAIN CONTROL FUNCTION

Here a design is described for the gain control function that will maintain the scale factor following the phase detector in the digital phase-locked loop. The scale factor is at a level that ensures that the mean output of the phase detector (after multiplication by 90/100 000) is the phase offset (in degrees) of the VCO output from the DPLL input.

The output,  $y(\delta, i)$  of the phase detector (discussed earlier in this appendix), given two inputs offset by  $\delta^\circ$  from perfect track during the  $i$ th measurement interval, is given by (after multiplication by 90/100 000):

$$y(\delta, i) = m(\delta) + n_p(i) , \quad (D-34)$$

where

$$m(\delta) = 0.45199 \sin \delta \quad (D-35)$$

and  $n_p(i)$  is a random variable with variance equal to (0.16829) for the nominal S/N ratio, sampling rate, and phase detector counter averaging interval of 5 ms in the SATRACK-GPS system. The changes in the S/N ratio must be detected so compensation can be made for the resultant changes in phase detector mean output attenuation. If the VCO output square waves are mixed with the DPLL input waves with  $0^\circ$  nominal offset phase instead of  $90^\circ$  offset phase as in the four gates (5 through 8) of Fig. D-2, the count that should be received after multiplication by 90/100 000 is

$$y_o(\delta, i) = 0.45199 \cos \delta + n_{p_o}(i) , \quad (D-36)$$

where, for the ranges of S/N of interest the coefficient in front of  $\cos \delta$  is proportional to  $\sqrt{S/N}$ , and the variance of  $n_{p_0}(i)$ , (0.16829), is independent of S/N.

If it is assumed that the loop is close to a perfect tracking condition, then  $\delta \approx 0$ , and

$$y_o(i) \approx 0.45199 \sqrt{\frac{(S/N)_{\text{actual}}}{(S/N)_{\text{nominal}}}} + n_{p_0}(i), \quad (D-37)$$

where  $(S/N)_{\text{nominal}}$  is the nominal SATRACK-GPS signal/noise ratio (-41 dB in a 2 MHz bandwidth), and  $(S/N)_{\text{actual}}$  is the actual signal/noise ratio.

If multiplication by 90/100 000 is now omitted, a net number of counts should be observed every 5 ms, given by

$$y_{\text{count}}(i) = 502.21 \sqrt{\frac{(S/N)_{\text{actual}}}{(S/N)_{\text{nominal}}}} + n_{p_{\text{count}}}(i),$$

where the variance of  $n_{p_{\text{count}}}(i)$  is 207 765.4 counts<sup>2</sup>. If the S/N ratio is assumed to change slowly enough to be considered constant over, say, 1-second intervals, then  $y_{\text{count}}(i)$  may be averaged over two hundred 5-ms intervals to get, for the jth second:

$$y_{\text{count,av.}}(j) = 502.21 \sqrt{\frac{(S/N)_{\text{actual}}}{(S/N)_{\text{nominal}}}} + n_{\text{count,av.}}(j),$$

where, because  $n_{p_{\text{count}}}(i)$  is white every 5 ms, the variance of  $n_{\text{count,av.}}(j)$  is 207 765.4/200 = 1038.827 counts<sup>2</sup>, an rms of 32.23 counts, not enough to significantly disturb the measurement of the mean value of 502.21 counts that would be observed if the S/N ratio were at the nominal SATRACK-GPS level.

As was mentioned earlier in this appendix, we wish to introduce a multiplier into the DPLL, having a nominal value of 126.76 that is inversely proportional to

$$\sqrt{\frac{(S/N)_{\text{actual}}}{(S/N)_{\text{nominal}}}}.$$

Thus we use

$$\frac{6.366 \times 10^4}{y_{\text{count, av.}}(j)}$$

as the multiplier, which would then be changed once per second, to provide the loop gain control. Any externally supplied gain information that may be available, of course, can be used to aid in the determination of the loop gain control factor.

#### A NOTE ON EXPERIMENTAL VERIFICATION

Relative to the phase noise present at the VCO output, caused by input noise, the performance predicted for the processing scheme discussed here (in terms of the signal-power/noise-density ratio) is also predicted for a scheme in which the input carrier is not beat to 0 frequency, but directly sampled and 1-bit quantized. For this latter scheme, processing is carried out using only one channel of information provided the sampling rate is at least as high as the Nyquist rate. Such implementation would require sampling that is too fast for our problem, but that can be used conveniently with lower frequencies to experimentally check the theoretical results.

Appendix D

REFERENCES

- D-1. W. E. Larimore, "Design and Performance of a Second Order Digital Phase-Locked Loop," Symposium on Computer Processing in Communications, Polytechnic Institute of Brooklyn, 1969, pp. 343-356.
- D-2. A. J. Viterbi, Principles of Coherent Communication, McGraw-Hill Book Co., New York, 1966.
- D-3. R. Jaffe and E. Reichtin, "Design and Performance of Phase Lock Circuits Capable of Near-Optimum Performance Over a Wide Range of Input Signal and Noise Levels," IRE Trans. on Information Theory, Vol. IT-1, March 1955, pp. 66-72.
- D-4. R. Sydnor, J. J. Caldwell, and B. E. Rose, "Frequency Stability Requirements for Space Communications and Tracking Systems," Proc. IEEE, Vol. 54, No. 2, February 1966, pp. 231-236.
- D-5. A. Papoulis, Probability, Random Variables, and Stochastic Processes, McGraw-Hill Book Co., New York, 1965, pp. 483-484.
- D-6. R. W. Levinge, "Frequency Control Using Binary Rate Multipliers for Automatic Testing on CW Radar Systems," Proc. IEE, Vol. 121, No. 10, October 1974, pp. 1059-1066.

## Appendix E

### PERFORMANCE ANALYSIS OF THE COHERENT BINARY DELAY-LOCKED LOOP FOR THE SATRACK DIGITAL RECEIVER

This Appendix continues the investigation of the digital receiver, begun in Appendix D. The coherent binary delay-locked loop is analyzed. A receiver for the SATRACK suppressed carrier signals was discussed in Appendix C. It was an analog receiver that would perform the combined code and carrier tracking. The received signal  $x(t)$  is in fact heterodyned by 2200 MHz to a nominal zero center frequency (bandwidth  $\pm 1$  MHz) by the shipboard preprocessor, hard limited, sampled at 5 MHz (2.5 times the Nyquist frequency), and recorded for later processing by the post-flight receiver (Appendix D). The postflight receiver, then, is a digital receiver, with somewhat different performance than the analog receiver that has been discussed, although the digital receiver is designed to perform in a manner similar to the analog receiver. Our concern in this appendix is the second stage of the digital receiver (Appendix C, Fig. C-4), the phase-locked loop/delay-locked loop. Specifically, having already discussed the digital phase-locked loop (Appendix D) the performance of the coherent binary delay-locked loop following hard limiting of the input signal is now discussed.

#### THE BINARY DELAY-LOCKED LOOP PRECEDED BY SHIPBOARD HARD LIMITING AND HETERODYNING

The binary delay-locked loop and associated SATRACK receiver processing is illustrated in Fig. E-1. As in Appendix C, in discussing the receiver for the signal from the  $i$ th satellite, the effects of interference from signals transmitted by the other  $N-1$  in-view satellites is ignored for the present. The signal received by the ship is thus assumed to be given by

$$x_i(t) = \sqrt{2P_{s1}} \text{PRN}_i(t - \lambda_i) m_i(t - \lambda_i) \sin [\omega_0 t + \phi_i(t)] + n(t), \quad (\text{E-1})$$

where  $\lambda_i$  denotes the total time delay from transmission of the signal from satellite ( $f$ ) to its final reception by the ship. The function  $\text{PRN}_i(t)$  is a pseudorandom sequence of  $\pm 1$ 's with a chip length of  $\Delta = (10^{-6}/1.023)$  second and an epoch rate of 1 kHz (i.e., 1023 chips per epoch). The function  $m_i(t)$  is also a sequence of  $\pm 1$ 's that carries data from the  $i$ th satellite. The chip length of  $m_i(t)$  is  $\Delta_m = 20$  ms. The phase function  $\phi_i(t)$  is due to the doppler shifts caused by satellite, missile, and range ship movement. The noise function  $n(t)$  is Gaussian white noise that has been bandlimited by the shipboard receiver to  $\pm 1$  MHz about the missile transmission frequency of  $f_0 = 2200$  MHz. The PSD of  $n(t)$  is given by  $N_0/2 = 10^{-17.2}$  mW/Hz. The noise function  $n(t)$  may also be written as

$$n(t) = \sqrt{2} [n_1(t) \sin \omega_0 t + n_2(t) \cos \omega_0 t], \quad (E-2)$$

where  $n_1(t)$  and  $n_2(t)$  are independent Gaussian white noise processes, bandlimited to  $|f| \leq 1$  MHz, with PSD's of  $N_0/2$ . The nominal carrier power for the  $i$ th signal,  $P_{s_i}$ , is given as  $10^{-14.7}$  mW, although a wide variation may be observed in the signal power received from the different satellites. The nominal signal/noise density ratio is thus given by  $2P_{s_i}/N_0 = 25$  dB-Hz. The code sequences,  $PRN_i(t)$ , and their epoch times, as transmitted by the satellites, are known by the postflight receiver, although the delays ( $\lambda_i$ ) are not known a priori. In the GPS program a set of 37 Gold codes have been chosen as the PRN codes to be used by the various satellites. The doppler shifts ( $\phi_i(t)$ ) are also not known a priori; however, telemetry and ground station data are available to the receiver, and are converted into aiding information for the various receiver tracking loops.

In this appendix only the received signal emanating from one satellite is dealt with, therefore the subscript (1) in Eq. (E-1) will be dropped. Also, the small effect on the delay-locked loop of errors in the estimation of  $m_i(t - \lambda_i)$  in the first stage of the receiver will be ignored here. Thus we take for the shipboard received signal:

$$x(t) = \sqrt{2P_s} PRN(t - \lambda) \sin [\omega_0 t + \phi(t)] + n(t) \quad (E-3)$$

The shipboard processing is of the form given in Appendix D, Fig. D-1. The in-phase and quadrature (I and Q) channel signals received on tape from the ship are heterodyned up to an IF frequency of 100 kHz before processing (gates 1, 2, 3, 4). The exclusive-OR gates represent straightforward multiplication for sequences of  $\pm 1$ 's. The principle of operation of the delay-locked loop is discussed in Ref. E-1. The delay detector counter dumps its output and resets at a nominal rate of 1 kHz, after adding together 40 000 pulses from gates 9 through 16 (the pulses are taken at 0.2  $\mu$ s intervals). When the loop input is not hard limited, Gill (Ref. E-2) shows that the mean delay detector output is linear in the clock delay error ( $\epsilon$ ),  $e(t) \hat{=} \lambda(t) - \hat{\lambda}(t)$ , for  $|\epsilon| \leq \Delta/2$ , with a half maximum reading for  $\epsilon = \Delta/2$ . That is

$$m(\epsilon) = 2\sqrt{P_s} \left(\frac{\epsilon}{\Delta}\right); \quad |\epsilon| \leq \frac{\Delta}{2} \quad (E-4)$$

Ref. E-1. J. J. Spilker, Jr., "Delay Lock Tracking of Binary Signals," IEEE Trans. on Space Electronics and Telemetry, Vol. SET-9, March 1963, pp. 1-8.

Ref. E-2. W. J. Gill, "A Comparison of Binary Delay-Lock Tracking Loop Implementations," IEEE Transactions on Aerospace and Electronic Systems, Vol. AES-2, No. 4, July 1966, pp. 415-424.

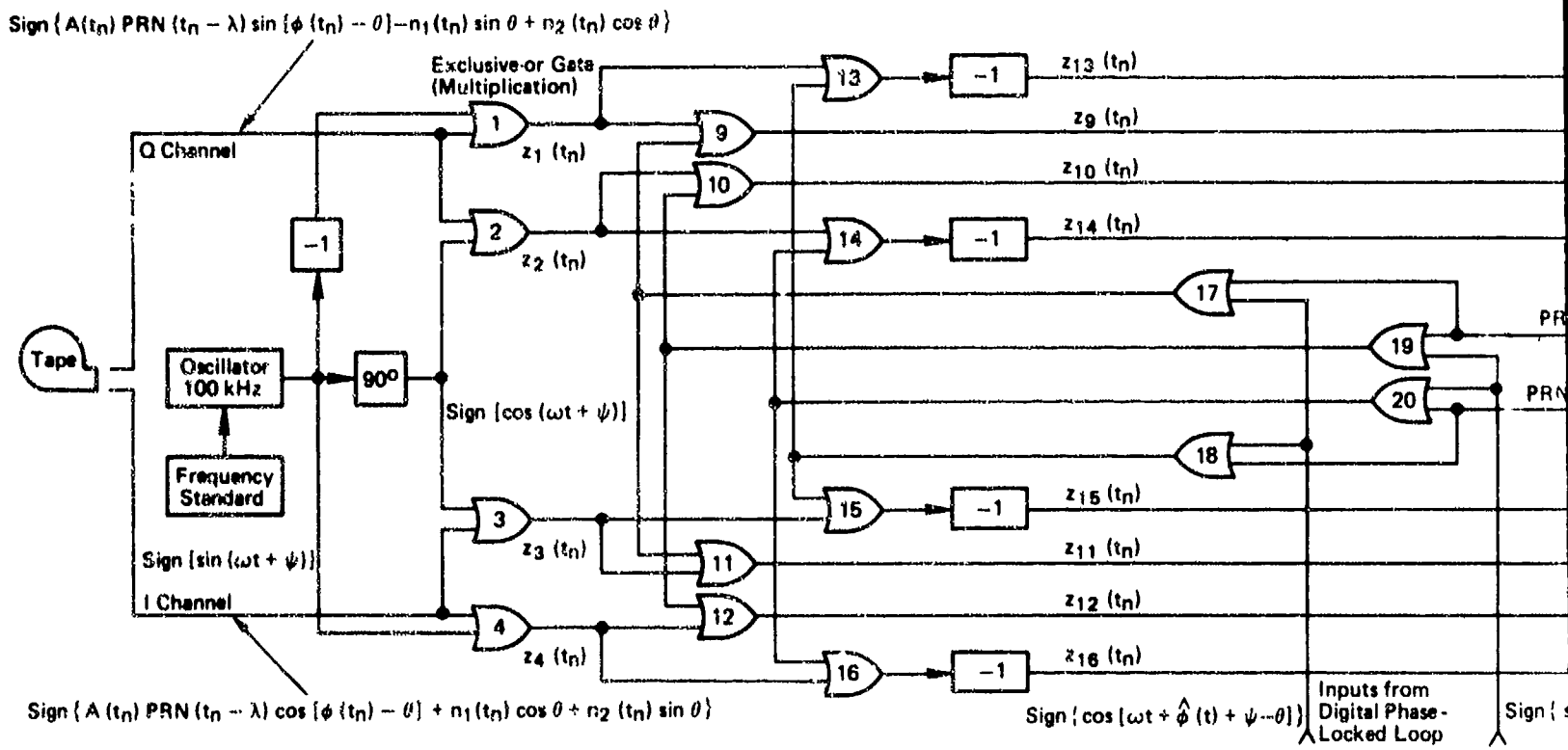
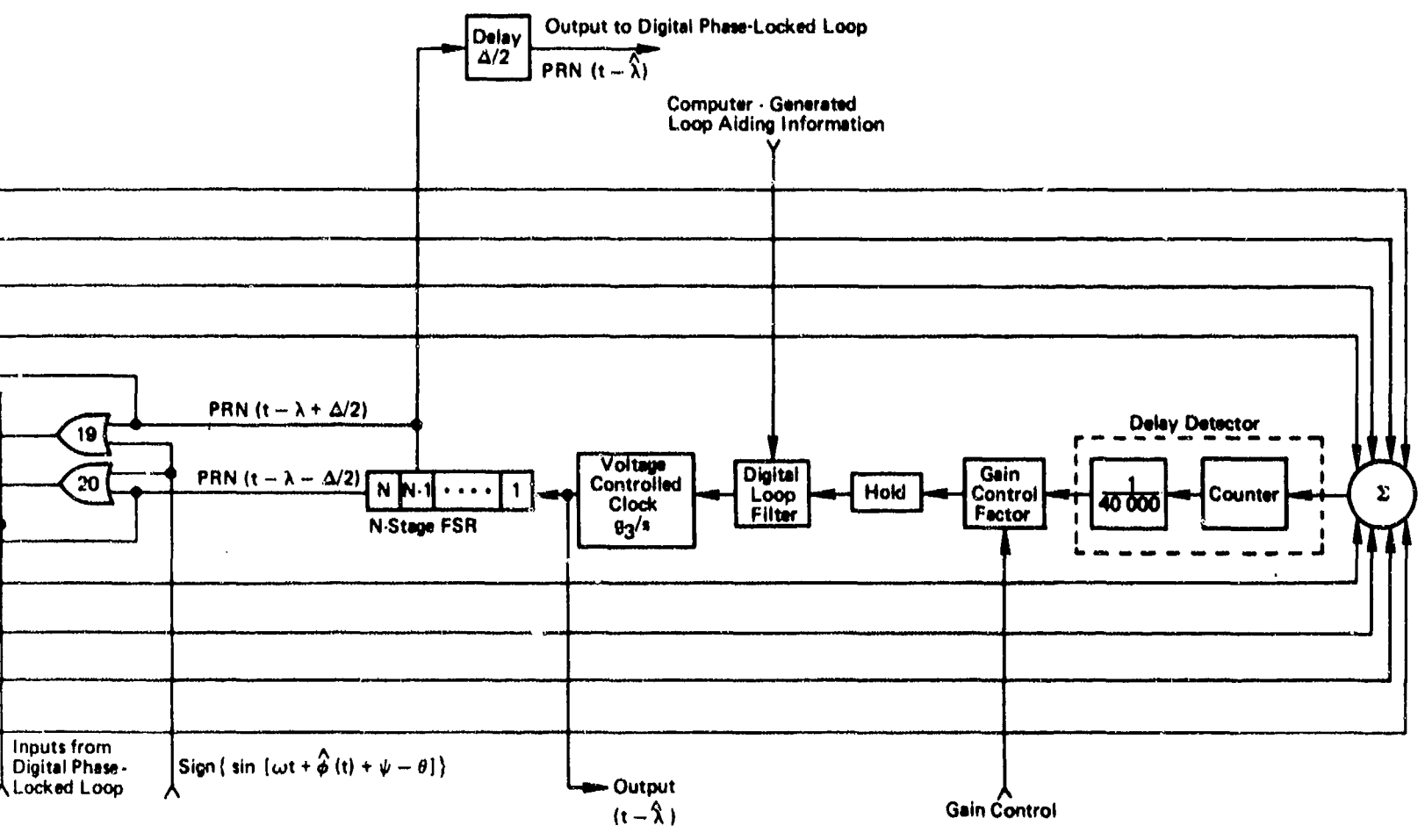


Fig. E-1 Binary Delay-Locked Loop and Associated Circuitry



Locked Loop and Associated Processing

2

With hard limiting preceding the loop, a half maximum reading would be 20 000 counts at the delay detector counter output after 1 ms. The digital loop filter is designed so that the closed loop response is given approximately by

$$H(s) = \frac{\tau s + 1}{\frac{\tau^2 s^2}{2} + \tau s + 1} \quad (E-5)$$

This response is optimal in terms of the total mean-squared delay error for ramp inputs of delay in the presence of noise. The two-sided noise bandwidth of the loop,  $B_N$ , is then given (Ref. E-3) by

$$B_N = \frac{3}{2\tau} \quad (E-6)$$

The necessity for the abundance of signals in our loop is (a) the input signal has been heterodyned to a low frequency on the ship, causing input noise terms to overlap in the power spectrum, and (b) the IF frequency (100 kHz) used in the postprocessing is not high enough to ensure that double-angle noise terms found at the outputs of gates 9 through 16 do not overlap zero frequency. For these reasons, extra signal terms are carried to allow some of the noise terms to cancel each other.

Gill (Ref. E-2) shows that the normalized output delay error of the loop, when the input is not hard limited, is given by

$$E \left( \frac{\epsilon}{\Delta} \right)^2 = \frac{N_0}{2P_s} \times \frac{B_N}{2} \quad (E-7)$$

where only the errors caused by input noise have been assessed. Attention here will be restricted to the errors caused by input in the anticipation that the loop bandwidth used will be sufficiently wide to attenuate those noises generated within the loop. In this case, the corresponding result to Eq. (E-7) is to be determined where hard limiting has been done on the ship.

From Fig. E-1 it is easy to calculate the outputs of gates 9 through 16. For example, the output of gate 9 is given by

---

Ref. E-3. R. Syndor, J. J. Caldwell, and B. E. Rose, "Frequency Stability Requirements for Space Communications and Tracking Systems," Proc. IEEE, Vol. 54, No. 2, February 1966, pp. 231-236.

$$z_g(t) = \left\{ \begin{aligned} & \left[ \text{PRN}(T_n - \hat{\lambda} + \frac{\Delta}{2}) \right] \left\{ \left( \sqrt{P_s(t_n)} \right) \cos[\phi(t_n) - \hat{\phi}(t_n)] + \cos[\phi(t_n) + \hat{\phi}(t_n) - 2\theta + 2\psi + 2\omega t_n] \right. \\ & - \cos[\phi(t_n) - \hat{\phi}(t_n) - 2\psi - 2\omega t_n] - \cos[\phi(t_n) + \hat{\phi}(t_n) - 2\theta] \text{PRN}(t - \lambda) \\ & - n_1(t_n) \cos[2\omega t_n + 2\psi + \hat{\phi}(t_n)] - n_2(t_n) \sin[2\omega t_n + 2\psi + \hat{\phi}(t_n)] \\ & - n_1(t_n) \cos[\hat{\phi}(t_n) - 2\theta] + n_2(t_n) \sin[\hat{\phi}(t_n) - 2\theta] \\ & + n_1(t_n) \cos[2\omega t_n + 2\psi + \hat{\phi}(t_n) - 2\theta] - n_2(t_n) \sin[2\omega t_n + 2\psi + \hat{\phi}(t_n) - 2\theta] \\ & \left. + n_1(t_n) \cos[\hat{\phi}(t_n)] + n_2(t_n) \sin[\hat{\phi}(t_n)] \right\} \end{aligned} \right\} \quad (\text{E-8})$$

It is assumed that the delay error  $\epsilon(t) \triangleq \lambda(t) - \hat{\lambda}(t)$  and the phase-locked loop error  $\phi_e(t) \triangleq \phi(t) - \hat{\phi}(t)$  are constant over a 1 ms counting interval. The output of the delay detector counter at the end of this interval (after being divided by 40 000 for normalization) is given by

$$y = \frac{1}{40\,000} \sum_{j=9}^{16} \sum_{i=1}^{5000} z_j(t + i \times T_p); \quad (T_p = 0.2 \mu\text{s}) \quad (\text{E-9})$$

(see Fig. E-1). We evaluate the mean-squared value of  $y$ :

$$\begin{aligned} E(y^2) &= E \left\{ \left( \frac{1}{40\,000} \right)^2 \left[ \sum_{j=9}^{16} \sum_{i=1}^{5000} z_j(t + i \times T_p) \right]^2 \right\} \\ E(y^2) &= \left( \frac{1}{40\,000} \right)^2 \left[ 5000 \sum_{j=9}^{16} R_{z_j z_j}(0) + \sum_{k,j=9}^{16} \sum_{i=1}^{4999} 2(5000 - i) R_{z_j z_k}(i \times T_p) \right], \end{aligned} \quad (\text{E-10})$$

where  $R_{z_j z_k}(\tau)$  represents a cross-correlation function defined by

$$R_{z_j z_k}(\tau) = E[z_j(t) z_k(t - \tau)]. \quad (\text{E-11})$$

In the evaluation of  $R_{z_j z_k}(\tau)$  the following facts and approximations are used:

1.  $P_s(t)$ ,  $\epsilon(t)$ , and  $\phi_e(t)$  are approximated as constant over the delay ( $\tau$ ) of interest.
2.  $\theta$  and  $\psi$  are uniformly distributed random phase angles.

3. The terms interior to the sign  $[\cdot]$  functions are approximated as Gaussian (the noise terms are, in fact, Gaussian and do dominate the signal terms).
4. PRN(t) is approximated as Gaussian, in the sense that the Gaussian Moment Factoring Theorem (Ref. E-4) is applied to products involving this function (see example below).
5. The "(3,7) Gold code"<sup>\*\*</sup> is used for PRN(t), and its autocorrelation function  $[R_{PRN(3,7)}(\tau)]$ <sup>\*\*</sup> is used in the evaluation of  $E[y^2]$ .
6.  $n_1(t)$  and  $n_2(t)$  are zero mean independent processes, with identical correlation functions.

Assumption 3 allows use of the fact that for two jointly Gaussian random variables  $x$  and  $y$  (Ref. E-5);

$$E[\text{sign}[x] \cdot \text{sign}[y]] = \frac{2}{\pi} \arcsin \frac{E[xy]}{\sigma_x \sigma_y} \quad (\text{E-12})$$

As an example of the evaluation of  $R_{z_j z_k}(\cdot)$ , we find (see last section of this Appendix) that

$$R_{z_9 z_9}(\tau) = \left[ P_s R_{PRN}^2(c + \frac{\Delta}{2}) + R_{PRN}^2(\tau) + R_{PRN}(c + \frac{\Delta}{2} + \tau) \times R_{PRN}(c + \frac{\Delta}{2} - \tau) \right] \\ \times \left[ \cos^2(\phi_e) + \cos(2\omega\tau) + \left(\frac{1}{2}\right) \right] + R_{n_1}(\tau) \left[ 4 \cos^2(\omega\tau) \right] R_{PRN}(\tau) \quad , \quad (\text{E-13})$$

where  $R_{n_1}(\tau)$  is the autocorrelation function of  $n_1(t)$ , given by

$$R_{n_1}(\tau) = \frac{N_0}{2} \times 2 \times 10^6 \times \frac{\sin(2 \times 10^6 \pi \tau)}{2 \times 10^6 \pi \tau} \quad , \quad (\text{E-14})$$

\*ITT recommendations

\*\*Private communication with G. Jamison, APL.

Ref. E-4. J. M. Wozencraft and L. M. Jacobs, Principles of Communication Engineering, John Wiley & Sons, New York, 1967,

Ref. E-5. A. Papoulis, Probability, Random Variables, and Stochastic Processes, McGraw-Hill Book Co., New York, 1965, pp. 483-484.

and the Gaussian Moment Factoring Theorem has been used to make the approximation that

$$E[\text{PRN}(t - \hat{\lambda} \pm \frac{\Delta}{2}) \times \text{PRN}(t - \lambda) \times \text{PRN}(t - \hat{\lambda} + \frac{\Delta}{2} - \tau) \times \text{PRN}(t - \tau - \lambda)] \approx R_{\text{PRN}}^2(\epsilon + \frac{\Delta}{2}) + R_{\text{PRN}}^2(\tau) + R_{\text{PRN}}(\epsilon + \frac{\Delta}{2} + \tau) \times R_{\text{PRN}}(\epsilon + \frac{\Delta}{2} - \tau) \quad (\text{E-15})$$

Given a fixed value of  $\epsilon$ , this approximation (Eq. (E-15)) can be seen to be inaccurate for certain specified values of  $\tau$ . Nonetheless, averaging over the full range of 5000 values of  $\tau$  in an averaging period, the PRN terms involved heuristically should exhibit Gaussian behavior, justifying the approximation. Another possible approximation in Eq. (E-15) used in a different context by Spilker (Ref. E-1), is to take analytically a low frequency average of the signal components of the gate outputs in anticipation of the averaging to be performed by the counter and subsequent division by 40 000. Thus, for example, in Eq. (E-8) we would make the approximation

$$\text{PRN}(t - \hat{\lambda} - \frac{\Delta}{2}) \text{PRN}(t - \lambda) \approx R_{\text{PRN}}(\epsilon + \frac{\Delta}{2}) \quad (\text{E-16})$$

This method leads to results within 2% of those obtained using Eq. (E-15), with the delay detector counting interval of 1 ms.

Using a computer program to evaluate the quantity in Eq. (E-10) (actually a scaled-down version of this quantity), it is found that as  $\epsilon$  is varied (letting the phase-locked loop error  $\phi \equiv 0$ , for the present analysis):

$$E[y^2(\epsilon)] = 4.5225 \times 10^{-5} + \left[ 5.0496 \times 10^{-3} \left( \frac{\epsilon}{\Delta} \right)^2 \right] ; |\epsilon| \leq \frac{\Delta}{2} \quad (\text{E-17})$$

Thus  $y(\epsilon, j)$ , the output of the delay detector for a clock offset of  $\epsilon$  over the  $j$ th 1-ms counter interval, may be modeled as:

$$y(\epsilon, j) = n_{d_a}(j) + m(\epsilon) \quad (\text{E-18})$$

where the variance of the effective noise at the delay detector output is constant as  $\epsilon$  is varied.

$$E \left[ n_{d_a}(j) \right]^2 = 4.5225 \times 10^{-5} \quad (\text{E-19})$$

and the mean response of the delay detector to a delay shift  $\epsilon$  in the input signal is given by

$$m(\epsilon) = (5.0496 \times 10^{-3}) \left(\frac{\epsilon}{\Delta}\right) ; \quad |\epsilon| \leq \frac{\Delta}{2} \quad (\text{E-20})$$

In order to reobtain the half-maximum reading at  $\epsilon = \Delta/2$ , which occurs at the delay detector output when no hard limiting is done, gain control multiplication by  $198.04 = (5.0496 \times 10^{-3})^{-1}$  must be introduced. This factor is dependent on the relative power of the carrier  $P_s(t)$  and the noise  $n(t)$ , which is the reason for putting the gain control in the loop [the gain control adjusts this constant when the input signal/noise ratio changes (see Appendix D)]. Note that the scale factor of 198.04 is approximately  $\pi/2$  times the scale factor 126.76 which was used in the digital phase-locked loop (Appendix D). This difference is caused by the fact that phase information in the hard-limited signal is contained in the relatively reliable samples recorded near carrier sinusoid peaks (see Appendix D), while delay information is contained in samples spread uniformly over the carrier sinusoid. Note that each heterodyning operation performed on the signal doubles the number of noise terms associated with each signal [there are 8 in Eq. (E-8)], and also doubles the number of channels that are carried (one signal received by the ship, two channels recorded on the ship after heterodyning to zero frequency, four channels carried after the post-processing IF heterodyning operation). Each of these operations has the canceling effects of raising the scale factor by  $\sqrt{2}$ , and doubling the total number of available samples. From Eq. (E-19), the effective noise variance after gain control multiplication is

$$E[n_d(t)]^2 = (198.04)^2 (4.5225 \times 10^{-5}) = 1.7737. \quad (\text{E-21})$$

This variance results after the delay detector, which itself has a two-sided noise bandwidth of 1 kHz. In the case without hard limiting, the variance to be expected following filtering by a 1 kHz noise bandwidth filter is given by Eq. (E-7) as

$$E\left(\frac{\epsilon}{\Delta}\right)^2 = \left(\frac{N_0}{2P_s}\right) \left(\frac{10^3}{2}\right) = 1.5811. \quad (\text{E-22})$$

Thus the hard limiting has resulted in a variance degradation of

$$\frac{1.7737}{1.5811} = 1.1218 = 0.4991 \text{ dB}. \quad (\text{E-23})$$

Thus for the delay-locked loop under consideration, with shipboard hard limiting, we find that the output delay error caused by input noise has variance given by:

$$E \left( \frac{\epsilon}{\Delta} \right)^2 = \left( \frac{N_0}{2P_2} \right) \left( \frac{B}{2} \right) (1.1218) . \quad (E-24)$$

The above answer was obtained using a shipboard sampling rate of 5 MHz (2.5 times the Nyquist frequency). A study was made of the effects of changing this sampling rate. Graphs of the normalized delay variance at the loop output (for a 0.5 Hz loop) are given on different scales in Figs. E-2 and E-3. Note that as the sampling rate is increased the variance approaches a lower limit ( $\approx 8 \times 10^{-4}$ ), as expected, because unquantized sampling at the Nyquist rate would be sufficiently fast to reconstruct the entire received signal. The lower limit variance is very close to the variance that would be predicted using Eq. (E-7) for a loop with no prior hard limiting or sampling. Yet Spilker (Ref. E-1) predicts a 0.4 dB degradation in the case where band-limited white noise is directly added to a binary PRN sequence that is then hard limited (not sampled) before being input to a binary delay-locked loop. The fact that the result is more optimistic is likely because of the assumption by Gill (in the derivation of Eq. (E-7)) that the bandwidth of the loop input is substantially wider than the PRN bandwidth, causing the PRN  $\times$  input noise terms to have higher spectral density than in this case, where the input to the loop is band limited so as only to include the main lobe of the PRN spectrum ( $\pm 1$  MHz). Also, for rates lower than the Nyquist rate the variance is inversely proportional to the sampling rate, because the noise components of consecutive samples are then almost uncorrelated. It may be noted from Fig. E-2 that if the shipboard sampling rate were lowered from 5 MHz to 2 MHz (the Nyquist rate), the deterioration in coherent delay-locked loop performance would be approximately 1.33 dB.

Incidentally, use of a maximal length feedback shift register sequence (Ref. E-1) for the PRN function instead of the Gold code introduces less than 0.2% change in the answers. The difference is expected to be more significant in terms of intersignal interference, which has not been discussed here, since the Gold codes have been chosen for the GPS program due in part to their low cross-correlation properties.

#### EVALUATION OF THE AUTOCORRELATION FUNCTION $R_{z_9 z_9}(\tau)$

$$R_{z_9 z_9}(\tau) = E[z_9(t) z_9(t - \tau)] . \quad (E-25)$$

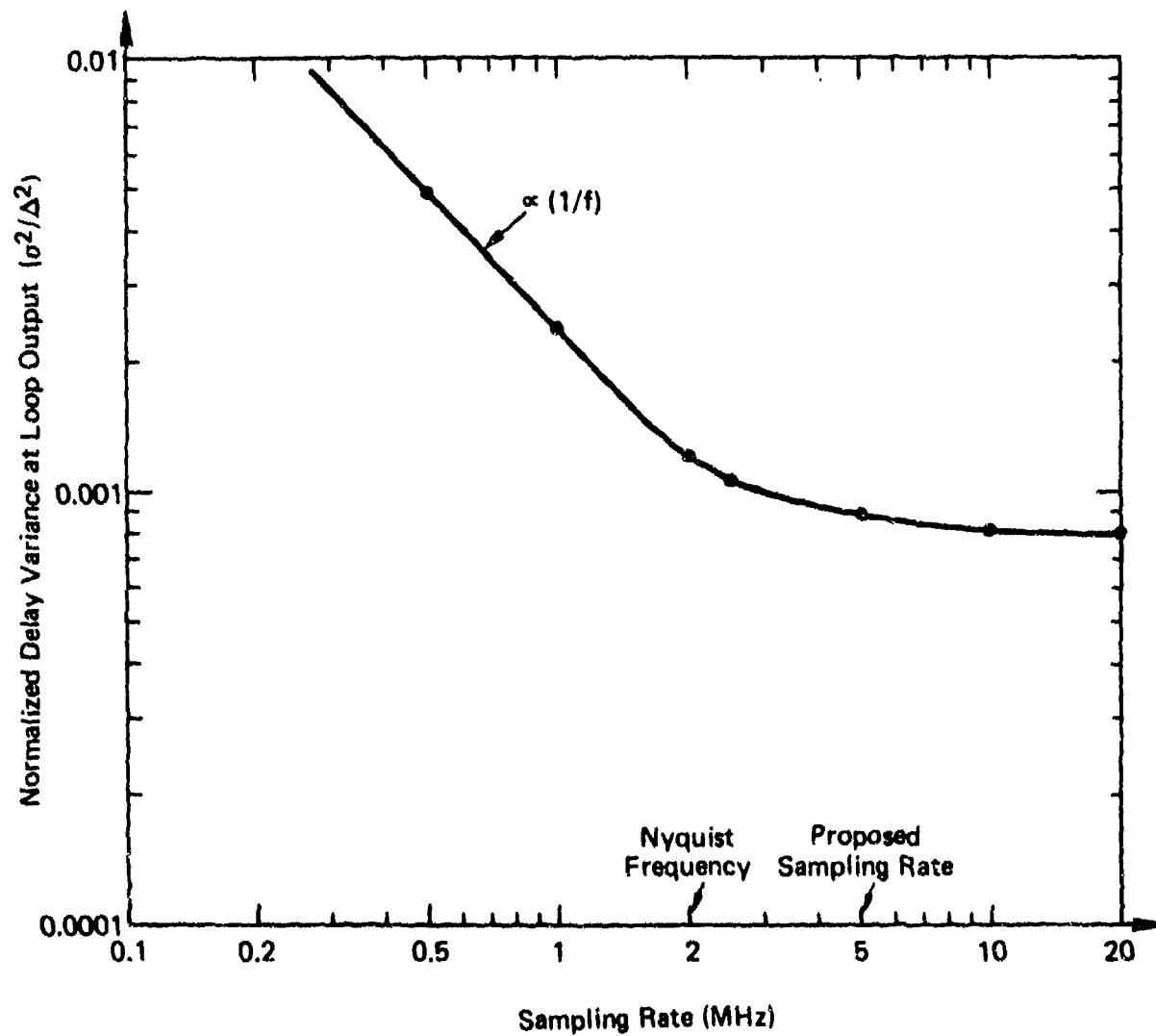


Fig. E-2 Normalized Delay Variance at Output of 0.5-Hz Loop as a Function of Shipboard Sampling Rate. (log-log scale)

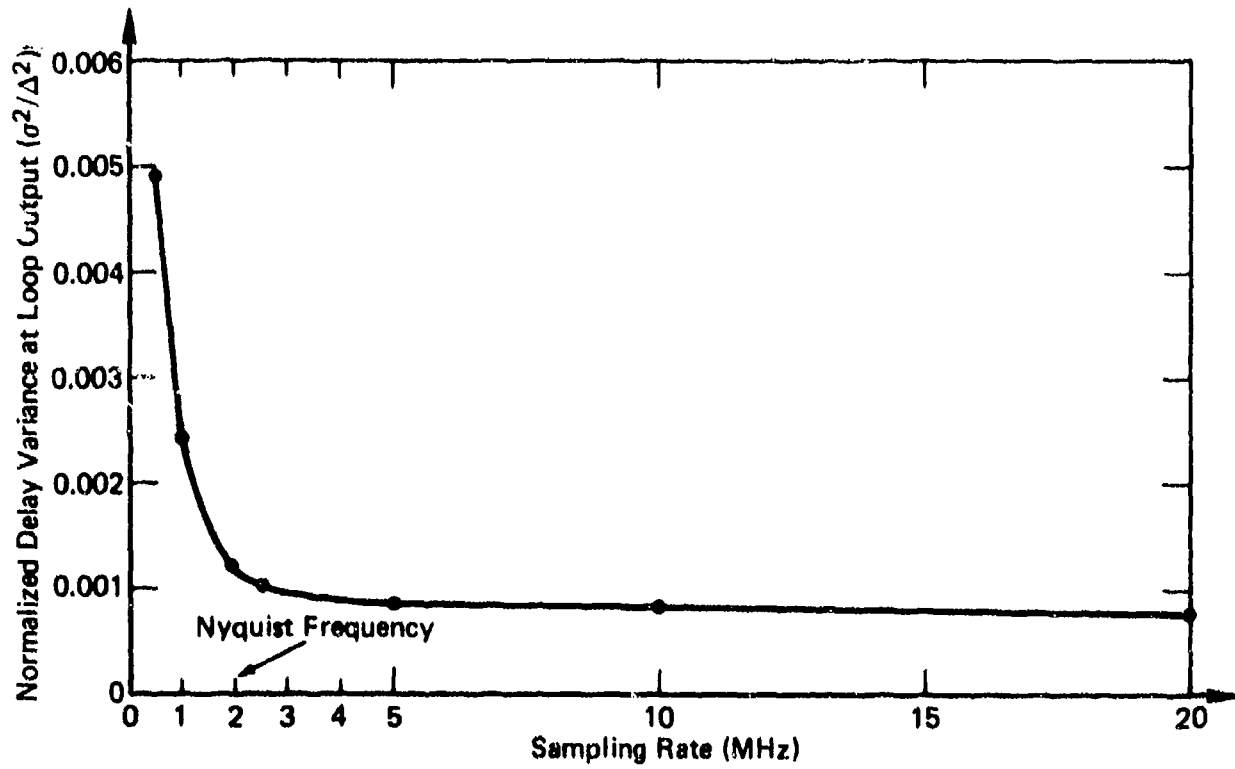


Fig. E-3 Normalized Delay Variance at Output of 5-Hz Loop as a Function of Shipboard Sampling Rate. (linear scale)

From Eq. (E-8) of the text, Eq. (E-25) may be written as (use assumptions 1, 2, and 6

$$R_{z_9 z_9}(\tau) = \left\{ \begin{aligned} & [\text{PRN}(t - \hat{\lambda} + \frac{\Delta}{2}) \text{PRN}(t - \tau - \hat{\lambda} + \frac{\Delta}{2})] \{ P_{\theta} [\cos^2 \hat{\phi}_{\theta} + \frac{1}{2} \cos 2\omega\tau \\ & + \frac{1}{2} \cos 2\omega\tau + \frac{1}{2}] [\text{PRN}(t - \lambda) \text{PRN}(t - \lambda - \tau)] \\ & + R_{n_1}(\tau) \cos^2(\hat{\phi} - 2\theta) + \frac{1}{2} R_{n_1}(\tau) \cos 2\omega\tau + \frac{1}{2} R_{n_2}(\tau) \cos 2\omega\tau \\ & + R_{n_2}(\tau) \sin^2(\hat{\phi} - 2\theta) + \frac{1}{2} R_{n_1}(\tau) \cos 2\omega\tau + \frac{1}{2} R_{n_2}(\tau) \cos 2\omega\tau \\ & + R_{n_1}(\tau) \cos^2 \hat{\phi} + R_{n_2}(\tau) \sin^2 \hat{\phi} \} \end{aligned} \right\} \quad (\text{E-26})$$

Using the fact that  $n_1(t)$  and  $n_2(t)$  have identical correlation functions, and the approximation in Eq. (E-15), Eq. (E-13) is quickly obtained.

Appendix E

REFERENCES

- E-1. J. J. Spilker, Jr., "Delay Lock Tracking of Binary Signals," IEEE Trans. on Space Electronics and Telemetry, Vol. SET-9, March 1963, pp. 1-8.
- E-2. W. J. Gill, "A Comparison of Binary Delay-Lock Tracking Loop Implementations," IEEE Transactions on Aerospace and Electronic Systems, Vol. AES-2, No. 4, July 1966, pp. 425-424.
- E-3. R. Sydnor, J. J. Caldwell, and B. E. Rose, "Frequency Stability Requirements for Space Communications and Tracking Systems," Proc. IEEE, Vol. 54, No. 2, February 1966, pp. 231-236.
- E-4. J. M. Wozencraft and L. M. Jacobs, Principles of Communication Engineering, John Wiley & Sons, New York, 1967.
- E-5. A. Papoulis, Probability, Random Variables, and Stochastic Processes, McGraw-Hill Book Co., New York, 1965, pp. 483-484.

## Appendix F

### PERFORMANCE ANALYSIS OF THE NONCOHERENT CARRIER AND CODE TRACKING LOOPS FOR THE SATRACK DIGITAL RECEIVER

#### INTRODUCTION

This appendix continues the analysis done in Appendixes C, D, and E. The performance of the first stage of the digital receiver is investigated. In Appendix C a receiver for the SATRACK suppressed carrier signals was discussed. The discussion included an analog receiver that would perform the combined code and carrier tracking. The received signal  $x(t)$  is in fact heterodyned by 2200 MHz to a nominal zero center frequency (bandwidth  $\pm 1.073$  MHz) by the shipboard preprocessor. It is then hard limited, sampled at 5 MHz (2.33 times the Nyquist frequency), and recorded for later processing by the postflight receiver (Appendix D). A  $\pm 1$  MHz bandwidth was considered in Appendix D, but  $\pm 1.073$  MHz is used henceforth, as this is the actual code width, plus possible doppler shift. The postflight receiver, then, is a digital receiver, with somewhat different performance than the analog receiver that has been discussed, although the digital receiver is designed to perform in a manner similar to the analog receiver. In Appendix D and Appendix E the performance to be expected from the component loops of the second stage of the digital receiver was treated. This appendix discusses the component loops of the first stage of the digital receiver, the noncoherent delay-locked loop, and the suppressed-carrier tracking loop, and then evaluates the overall performance to be expected of this stage of the receiver.

#### The Noncoherent Delay-Locked Loop Preceded by Shipboard Hard Limiting and Heterodyning

A diagram of the noncoherent delay-locked loop for the SATRACK digital receiver is given in Fig. F-1. The shipboard preprocessing is of the form given in Appendix D, Fig. D-1. The exclusive-OR gates represent straightforward multiplication for sequences of  $\pm 1$ 's. The input signal to the ship is assumed to be of the form given in Appendix E, Eq. (E-3).

$$x_1(t) = \sqrt{2} A_1(t) \text{PRN}_1(t - \lambda_1) m_1(t - \lambda_1) \sin[\omega_0 t + \phi_1(t)] + n(t), \quad (\text{F-1})$$

where interfering signals have been ignored, but the data,  $m_1(t - \lambda_1)$ , are included. Discussion of the factors and parameters in this signal is given in Appendix E. Note that the input I and Q channels are

heterodyned down to a nominal 0 Hz in the loop multiplication, and that the mixing frequency contains aiding information obtained from telemetry and ground station data. The resulting frequency is intended to be 0 Hz  $\pm$  20 Hz, where a 20 Hz error in the aiding frequency is allowed here. A shipboard recording IF frequency of 100 kHz is used, instead of the zero IF frequency mentioned in the introduction. Such a shipboard IF frequency ( $\omega_2 = 2\pi \times 100$  kHz) simplifies the second-stage processing. The I and Q recorded channels thus change from those given in Appendix D, Eq. (D-7) to the following:

I channel:

$$\text{sign} \left\{ A_1(t_n) \text{PRN}(t_n - \lambda_1) m_1(t_n - \lambda_1) \cos[\phi_1(t_n) + \omega_2 t_n - \theta] \right. \\ \left. + n_1(t_n) \cos(\omega_2 t_n - \theta) - n_2(t_n) \sin(\omega_2 t_n - \theta) \right\}$$

Q channel:

$$\text{sign} \left\{ A_1(t_n) \text{PRN}(t_n - \lambda_1) m_1(t_n - \lambda_1) \sin[\phi_1(t_n) + \omega_2 t_n - \theta] \right. \\ \left. + n_1(t_n) \sin(\omega_2 t_n - \theta) + n_2(t_n) \cos(\omega_2 t_n - \theta) \right\}$$

The necessity for the multiple signals in Fig. F-1 is caused by the fact that we have heterodyned the input signal on the ship to a low frequency, causing input noise terms to overlap in the power spectrum.

In the noncoherent delay-locked loop shown in Appendix C, Fig. C-2, there is only one input signal, and the bandwidths of  $\text{PRN}_1(t)$  and  $n(t)$  are assumed narrow in comparison with the IF frequency. Reference F-1 discusses the principal of operation of the noncoherent delay-locked loop given in Appendix C, Fig. C-2. The digital loop in Fig. F-1 works on the same principles as this loop, but suffers some degradation in performance because of the 1-bit quantization and sampling prior to the shipboard recording. The level of this degradation will be determined next.

The signal at the output of the center bandpass filter in Appendix C, Fig. C-2 is given by (see Ref. F-1)

$$A_1 R_{\text{PRN}_1} (\lambda_1 - \hat{\lambda}_1) m_{1\text{LP}}(t - \lambda_1) \cos[\phi_{d_1}(t)] + n_r(t), \quad (\text{F-2})$$

---

Ref. F-1. W. J. Gill, "A Comparison of Binary Delay-Lock Tracking Loop Implementations," IEEE Transactions on Aerospace and Electronic Systems, Vol. AES-2, No. 4, July 1966, pp. 415-424.

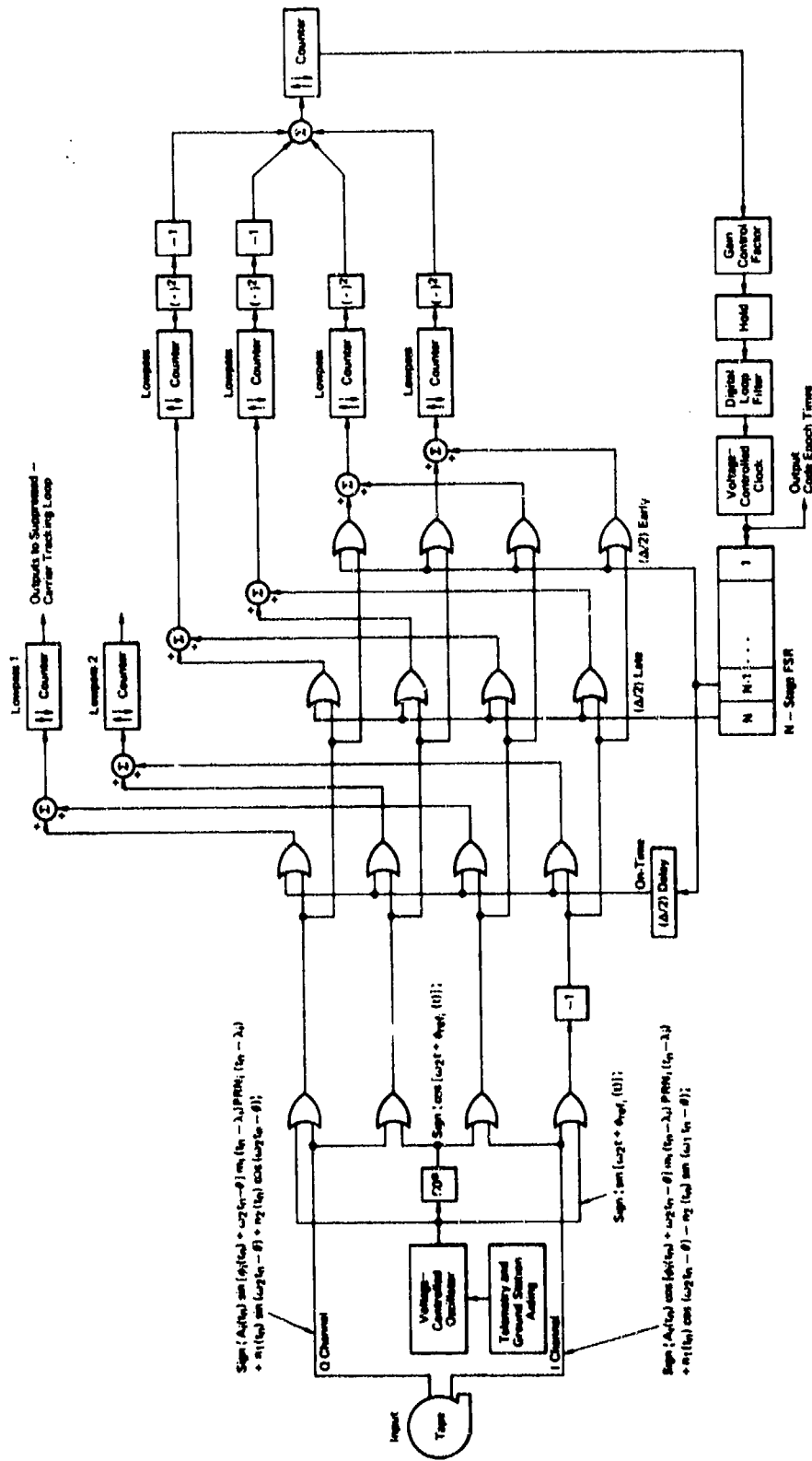


Fig. F-1 The Noncoherent Delay-Locked Loop

where  $R_{PRN_1}(\cdot)$  is the autocorrelation function of  $PRN_1(t)$ , and  $\phi_{d_1}(t)$  is the error in the phase-aiding reference signal in Appendix C

$$\phi_{d_1}(t) \triangleq \phi_1(t) - \phi_{ref_1}(t) .$$

The term  $m_1(t - \lambda_1)$  is changed to  $m_{1LP}(t - \lambda_1)$  to account for the effect low-pass filter on the data.  $n_r(t)$  is white noise of spectral height  $N_0/4$ , which is bandlimited to  $f_1 - B_1/2 \leq |f| \leq f_1 + B_1/2$ . The signal corresponding to this one in the digital case is found at the output of Lowpass ① in Fig. F-1. Analysis is done similar to that in Appendix E in the case where  $m_1(t - \lambda_1)$  is ignored and ( $\omega_1 \equiv 0$ ,  $\phi_{d_1}(t) \equiv \phi_0$ ). This signal, after summing for 1/139.997 second (a total of 71 430 possible counts), is given by

$$461.8626 R_{PRN_1}(\lambda_1 - \hat{\lambda}_1) \cos \phi_0 + n_s(t) , \quad (F-3)$$

where  $n_s(t)$  has a variance of 124326.4 counts<sup>2</sup>. A summation interval of 1/40 second (i.e., a 70 Hz low-pass filter) was picked here because a low-pass filter was needed that passes the data  $m_1(t - \lambda_1)$ , whose spectrum is significant to 50 Hz past the highest frequency (20 Hz) that the aided carrier can assume. A short explanation of the result in Eq. (F-3) is given in the last section of this appendix. Because  $d_1(t)$  will be a frequency within the passband of the low-pass filter following the multiplication, we infer that in the digital case the signal corresponding to Eq. (F-2) will be

$$461.8626 m_{1LP}(t - \lambda_1) R_{PRN_1}(\lambda_1 - \hat{\lambda}_1) \cos[\phi_{d_1}(t)] + n_{r_1}(t) , \quad (F-4a)$$

where  $n_{r_1}(t)$  has a variance of 124326.4 counts<sup>2</sup>. This signal contains noise terms overlapping 0 frequency. Thus we keep a quadrature version of Eq. (F-4a) (output of Lowpass ② in Fig. F-1).

$$461.8626 m_{1LP}(t - \lambda_1) R_{PRN_1}(\lambda_1 - \hat{\lambda}_1) \sin[\phi_{d_1}(t)] + n_{r_2}(t) , \quad (F-4b)$$

where  $n_{r_2}(t)$  is in quadrature with  $n_{r_1}(t)$ . The signal/noise density ratio of each of the quadrature signals of Eq. (F-4) is given by

$$\frac{(1/2) (461.8626)^2}{(124326.4) (1/139.997)} = 120.102 = 20.7955 \text{ dB}\cdot\text{Hz} . \quad (F-5)$$

This ratio is 1.1942 dB worse than the signal/noise density ratio of  $A_1^2/N_0 = 21.9897$  dB · Hz that would be obtained if the processing were done in continuous time without quantization (using a 0 IF frequency, as we have, and keeping I and Q channels). The signals in Eq. (F-4) correspond to the DLL (delay-locked loop) estimate of the PRN epoch times. These signals are sent to the next loop for further processing. The corresponding signals with early and late code multiplication are processed in the DLL. Using analysis similar to that of Gill (Ref. F-1), it is found that the loop rms delay error in our case is given by

$$\frac{\sigma_{\epsilon}}{\Delta} = \left( \frac{\epsilon_1}{\Delta} \right)_{\text{rms}} = \left[ \left( \frac{N_0 (10^{0.11942})}{2A_1^2 [E(m_{LP}^2)]} + \frac{[N_0 (10^{0.11942})]^2 (2B_w)}{A_1^4 [E(m_{LP}^2)]^2} \right) \left( \frac{B_{NI}}{2} \right) \right]^{1/2} \quad (\text{F-6})$$

where  $B_w$  is the bandwidth of the low-pass filters ( $B_w = 70$  Hz) following the multiplication. The factors of  $(10^{0.11942})$  in Eq. (F-6) represent the 1.1942 dB loss due to digital processing. Otherwise, the result is identical to Gill's (see Appendix C, Eq. (C-8)), with  $2B_w$  replacing the IF filter bandwidth in his result. The derivation, however, is changed because the I and Q signals are present. An approximation of  $E(m_{LP}^2)$  may be obtained by approximating  $m_{1,p}(t - \lambda_1)$  as the result of passing  $m_1(t - \lambda_1)$  through a 50 Hz low-pass filter. The worst performance can be expected if the data are a square wave with a 40 ms cycle time. In that case  $E(m_{LP}^2) = 0.81059$ . If the data are more random in nature, the corresponding autocorrelation function might be a triangle, extending to  $\tau = \pm 20$  ms. Then  $E(m_{LP}^2) = 0.9029$ . The latter will be used for the present approximation. If the former is a better approximation, then  $B_w$  could be widened to pass the data more effectively, hence increasing  $E(m_{LP}^2)$ .

The discussion above has been based on a sampling rate of 5 MHz. Lowering the sampling rate results in additional degradation. In Fig. F-2 the factor increase in the signal/noise density ratio of Eq. (F-4) is plotted as a function of the sampling rate. Observe that the line in Fig. F-2 that refers to the +21.9897 dB · Hz signal/noise density ratio obtained by continuous time processing without any quantization; also, note that with 5 MHz sampling the result falls 1.1942 dB below this line, as derived above. This is the factor  $10^{0.11942}$  in Eq. (F-6), with 2.5 MHz sampling ( $0.16 \times$  Nyquist rate), Fig. F-2 shows that the degradation is 1.9991 dB. Much storage could be saved by sampling at this lower rate. Equation (F-6) then becomes

$$\frac{\sigma_{\epsilon}}{\Delta} = \left( \frac{\epsilon_1}{\Delta} \right)_{\text{rms}} = \left[ \left( \frac{N_0 (10^{0.19991})}{2A_1^2 [E(m_{LP}^2)]} + \frac{[N_0 (10^{0.19991})]^2 (2B_w)}{A_1^4 [E(m_{LP}^2)]^2} \right) \left( \frac{B_{NI}}{2} \right) \right]^{1/2} \quad (\text{F-7})$$

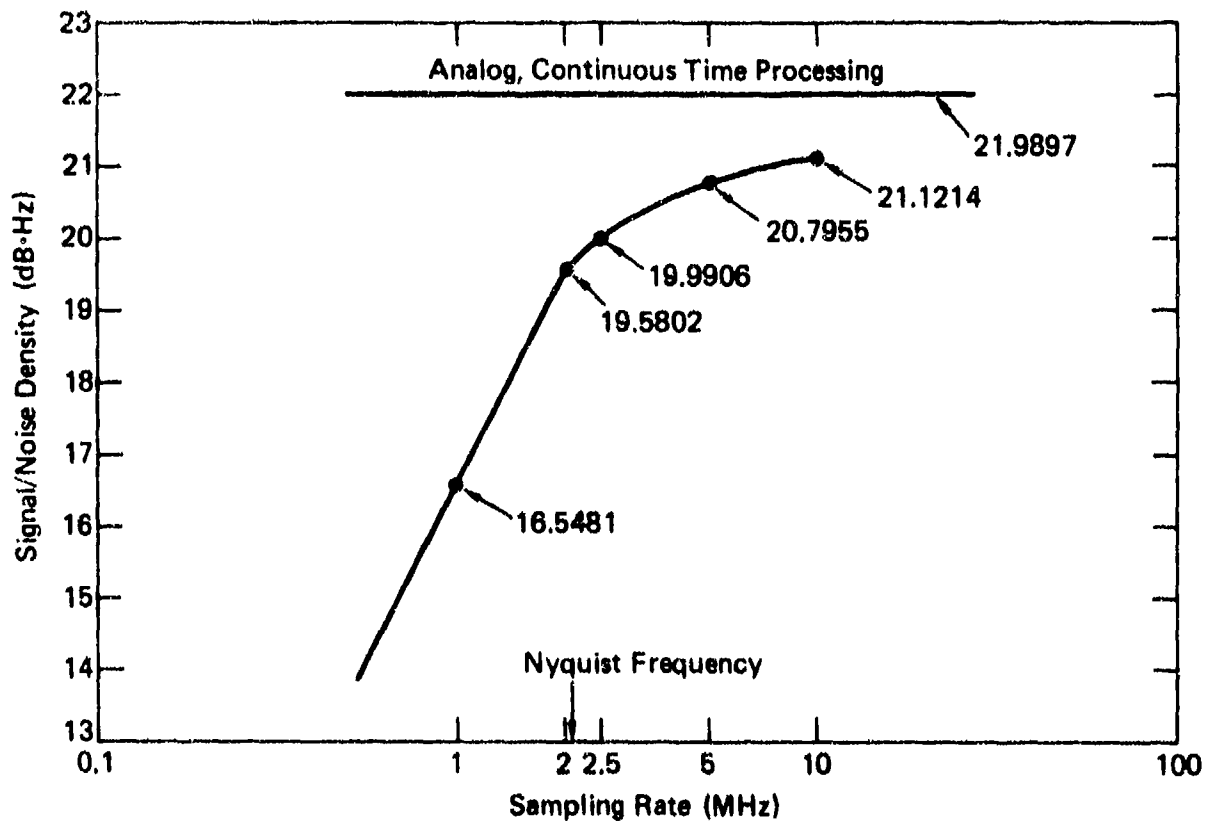


Fig. F-2 Degradation of Signal/Noise Density Ratio in Eq. F-4 as a Function of Sampling Rate

Next the form that Eq. (F-4a) would assume will be determined for a 2.5 MHz sampling rate. Recall that summing is over 1/139.997 second. Previously (with 5 MHz sampling) there was a maximum possible net count (from two channels) of  $(5 \times 10^6)(1/139.997)(2) = 71\,430$  counts. Observe the I and Q answers given in Eq. (F-4): In the no-noise case the mean of the signal in Eq. (F-4a) would be given by  $(71\,430) m_{1LP}(t - \lambda_1) R_{PRN_1}(\lambda_1 - \hat{\lambda}_1)$  for  $\phi_{d_1}(t) \equiv 0$ . Thus the scale factor is  $71\,430/461.8626 = 154.6564$ . As mentioned in Appendix D, this scale factor is a function of the signal/noise variance ratio, not of sampling rate. Thus, for sampling at a 2.5 MHz rate, with a total possible net count of 35 715 in 1/139.997 second, the mean value of the count is given by

$$\begin{aligned} & \left( \frac{35\,715}{154.6564} \right) m_{1LP}(t - \lambda_1) R_{PRN_1}(\lambda_1 - \hat{\lambda}_1) \cos \phi_{d_1}(t) \\ & = (230.9313) m_{1LP}(t - \lambda_1) R_{PRN_1}(\lambda_1 - \hat{\lambda}_1) \cos \phi_{d_1}(t) \end{aligned} \quad (F-8)$$

We have observed that the signal/noise density ratio would be degraded by 1.9991 dB from the continuous time processing case with no quantization (the latter case has  $A_1^2/N_0 = 21.9897$  dB · Hz). Thus we may solve for the variance of the noise,  $n_{r_3}(t)$ , which would be added to the mean count in Eq. (F-8).

$$\text{var. } (n_{r_3}(t)) = \frac{(139.997)(230.9313)^2}{10(2.19897 - 0.19991)} = 74821.14 \text{ counts}^2 \quad (F-9)$$

Thus, with 2.5 MHz sampling, the signal corresponding to Eq. (F-4a) is given by

$$(230.9313) m_{1LP}(t - \lambda_1) R_{PRN_1}(\lambda_1 - \hat{\lambda}_1) \cos \phi_{d_1}(t) + n_{r_3}(t) \quad (F-10a)$$

and

$$(230.9313) m_{1LP}(t - \lambda_1) R_{PRN_1}(\lambda_1 - \hat{\lambda}_1) \sin \phi_{d_1}(t) + n_{r_4}(t), \quad (F-10b)$$

where  $n_{r_3}(t)$  is characterized by Eq. (F-9). The performance of the non-coherent delay-locked loop with 2.5 MHz sampling was given in Eq. (F-7). Let  $B_w = 70$  Hz (50 Hz for the data, 20 Hz for the aiding uncertainty), and let  $B_{N1} = 1$  Hz in Eq. (F-7). We then obtain that

$$\sigma_\epsilon = (\epsilon_1)_{\text{rms}} = 0.10676 \Delta = 104.36 \text{ ns} \quad (F-11)$$

For convenience, scale the results in Eq. (F-10) by a factor to obtain (let  $\epsilon_1 \hat{=} \lambda_1 = \hat{\lambda}_1$ ):

$$A_1 m_{i_{LP}}(t - \lambda_1) R_{PRN_1}(\epsilon_1) \cos \phi_{d_1}(t) + n_{r_5}(t) \quad (F-12a)$$

and

$$A_1 m_{i_{LP}}(t - \lambda_1) R_{PRN_1}(\epsilon_1) \sin \phi_{d_1}(t) + n_{r_6}(t), \quad (F-12b)$$

where  $n_{r_5}(t)$  and  $n_{r_6}(t)$  are low frequency quadrature noise terms of one-sided bandwidth 70 Hz, and of spectral height 1.9991 dB greater than  $N_0/2$  [as was discussed; i.e.,  $(1.5846) N_0/2$ ]. These noise terms could be written as

$$n_{r_5} = n_a(t) \cos \phi_{d_1}(t) + n_b(t) \sin \phi_{d_1}(t)$$

and

$$n_{r_6} = n_a(t) \sin \phi_{d_1}(t) - n_b(t) \cos \phi_{d_1}(t) \quad (F-13)$$

where  $n_a(t)$  and  $n_b(t)$  are independent Gaussian low frequency noise terms, of bandwidth 70 Hz, and spectral density  $(1.5846) (N_0/2)$ . The next phase of the tracking is a noncoherent suppressed-carrier loop, to be discussed next. The intent is to track the phase angle in Eq. (F-12) in order to remove the sinusoids from the data modulation.

#### The Suppressed-Carrier Tracking Loop

The suppressed-carrier tracking loop is shown in Fig. F-3. The output signals of the noncoherent delay-locked loop are first heterodyned up to an IF frequency, so the suppressed-carrier loop will not have to track through zero frequency. The loop itself is a combination of a squaring loop and a Costas loop. The combination is used because the input noises on the recorded signal overlap zero frequency. Analysis of the combined loop indicates that its performance is analogous to the performance of the squaring loop (see under "Suppressed Carrier Tracking Loops" in Appendix C). The loop output is two signals given by

$$y_{2i}(t) = \cos[\omega_1 t - \phi_{d_1}(t) + n_3(t)]$$

and

$$y_{2i,q}(t) = \sin[\omega_1 t - \phi_{d_1}(t) + n_3(t)] \quad (F-14)$$

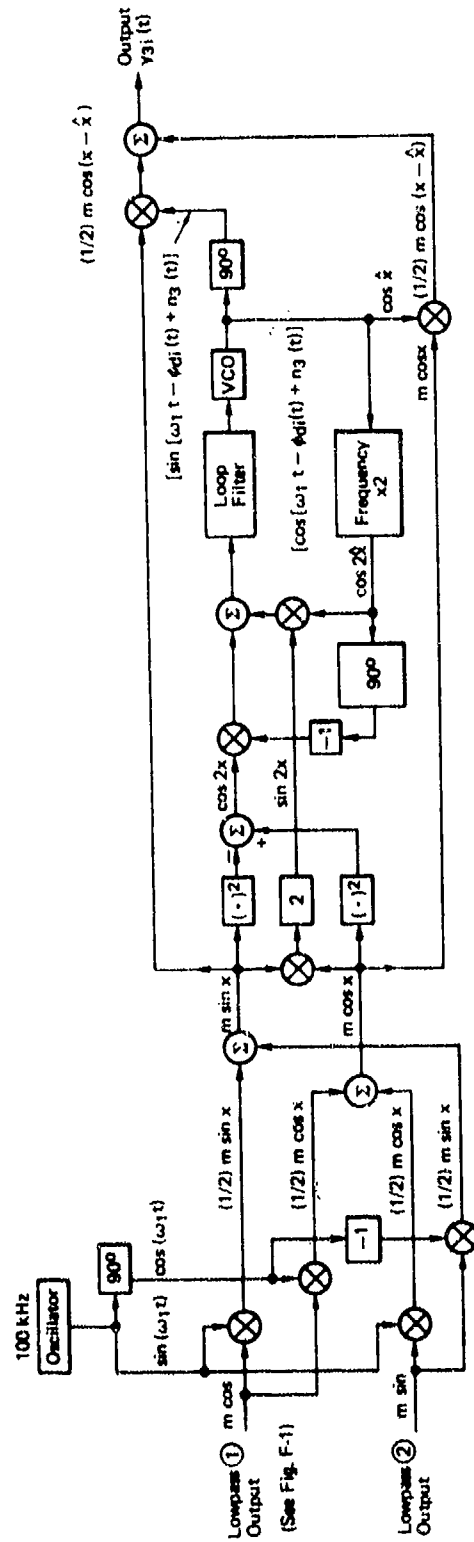


Fig. F-3 The Suppressed-Carrier Tracking Loop. (Abbreviated signal components are included in diagram to aid in reading.)

where  $n_3(t)$  is the phase tracking error. Analysis indicates that the rms value of  $n_3(t)$  is given by (for 2.5 MHz sampling)

$$[n_3(t)]_{\text{rms}} = \left\{ \left[ \left( \frac{N_o (10^{0.19991})}{2A_1^2 \{E[R_{\text{PRN}_1}(\epsilon_1)]\}^2 E(m_{\text{LP}}^2)} \right) + \left( \frac{N_o (10^{0.19991})}{2A_1^2 \{E[R_{\text{PRN}_1}(\epsilon_1)]\}^2 E(m_{\text{LP}}^2)} \right)^2 (2B_w) \right] B_{N2} \right\}^{1/2} \quad (\text{F-15})$$

The effect of different sampling rates on Eq. (F-15) is analogous to the effects on Eq. (F-7).

To evaluate Eq. (F-15),  $E[R_{\text{PRN}_1}(\epsilon_1)]$  must be evaluated first. The term  $\epsilon_1$  is modeled as Gaussian, and uses the fact that  $R_{\text{PRN}_1}(x)$  is given approximately by

$$R_{\text{PRN}_1}(x) \approx \begin{cases} (1 - \frac{|x|}{\Delta}); & |x| \leq \Delta \\ 0 & ; \text{ otherwise} \end{cases} \quad (\text{F-16})$$

We then find that (using Eq. (F-11))

$$E[R_{\text{PRN}_1}(\epsilon_1)] = 1 - \left( \frac{2}{\sqrt{2\pi}} \right) \left( \frac{\sigma(\epsilon_1)}{\Delta} \right) \quad (\text{F-17})$$

$$= 1 - \left( \frac{2}{\sqrt{2\pi}} \right) (0.10676) = 0.91482 \quad (\text{F-18})$$

Substituting Eq. (F-18) into Eq. (F-15), and letting loop bandwidth  $B_{N2} = 1$  Hz, we obtain

$$[n_3(t)]_{\text{rms}} = 0.11308 \text{ rad} = 6.479^\circ. \quad (\text{F-19})$$

The outputs of the carrier loop are mixed with the quantities in Eq. (F-12) as shown in Fig. F-3. This mixing attempts to remove the sinusoids from the data. The result is given by

$$y_{31}(t) = A_{1\text{LP}} m_1(t - \lambda_1) \cos[n_3(t)] R_{\text{PRN}_1}[\epsilon_1(t)] + n_4(t), \quad (\text{F-20})$$

where  $n_4(t)$  is a low-pass Gaussian process of bandwidth 70 Hz and power spectral density  $10^{0.19991} (N_o/2)$ . Appendix C describes the technique for estimating the bits in  $m_1(t - \lambda_1)$  given Eq. (F-20), and evaluates the probability of data estimation error, given Eq. (F-20). Because the low-pass filter effects  $m_1(t - \lambda_1)$ , we must compensate for the fact that

$E(m_{LP}^2) = 0.9029$ . The probability of estimating the  $k^{\text{th}}$  bit in the data sequence incorrectly is given by

$$P(\hat{m}_1(t - \lambda_1) \neq m_1(t - \lambda_1) | \#k) \approx 1/2 \left( 1 - \text{erf} \left\{ \sqrt{R_{bi}} E[R_{PRN}(c_1)] E \cos n_3(t) \right\} \right), \quad (F-21)$$

where

$$R_{bi} = \frac{[(0.9029) A_1^2] (20 \times 10^{-3} - 104.36 \times 10^{-9})}{N_o (10^{0.19991})} \quad (F-22)$$

$$R_{bi} = 1.8019 . \quad (F-23)$$

If  $n_3(t)$  is modeled as Gaussian, we obtain

$$E\{\cos[n_3(t)]\} = \exp \left\{ - (1/2) \sigma^2 [n_3(t)] \right\} = 0.99363 \quad (F-24)$$

If Eqs. (F-18), (F-23), and (F-24) are substituted into Eq. (F-21) the value obtained is

$$P(\hat{m}_1(t - \lambda_1) \neq m_1(t - \lambda_1) | \#k) \approx (1/2) [1 - \text{erf}(1.2202)] = 0.042208 . \quad (F-25)$$

#### EXPLANATION OF EQUATION (F-3) RESULTS

A short explanation of the derivation of the result given in Eq. (F-3) is in order here. In Appendix E the output of a coherent delay detector was analyzed. In that detector, a difference between early and late channel outputs was made. In the present situation, only one channel is considered; one channel is deleted from the earlier analysis. Also, in that analysis each channel is a sum of four signals instead of two signals (because of the extra heterodyning operation that was made in that analysis and use of the approximation given in Appendix E, Eq. (E-16)). If the four channels are summed for 1/139.997 second (a total of 142 860 possible counts) and divided by 142 860, the output is found to be

$$(4.811685 \times 10^{-3}) R_{PRN_1} (\lambda_1 - \hat{\lambda}_1) \cos(\phi_o) + n_{ra}(t) , \quad (F-26)$$

where  $n_{ra}(t)$  has a variance of  $1.218352 \times 10^{-5}$ . In the no-noise case, the mean response would have been

$$R_{\text{PRN}_1}(\lambda_1 - \hat{\lambda}_1) \left( 1 - \left| -\pi + [\phi_{d_1}(t) + \pi] \bmod 2\pi \right| \left( \frac{2}{\pi} \right) \right)$$

(the second factor is a cosine with triangular lobes), which is just  $R_{\text{PRN}_1}(\lambda_1 - \hat{\lambda}_1)$ , when  $\phi_{d_1}(t) = 0$ . So the scale factor is

$$\frac{1}{4.811685 \times 10^{-3}} = 207.8274 . \quad (\text{F-27})$$

The signal/noise density ratio is

$$\frac{(4.811685 \times 10^{-3})^2 (139.997)}{1.218352 \times 10^{-5}} = 266.036 = 24.2494 \text{ dB} \cdot \text{Hz} . \quad (\text{F-28})$$

With one less heterodyning operation, the scale factor is multiplied by  $1/\sqrt{2}$ . This is because the signal/noise variance ratio in each component signal is 3.01 dB higher (Appendix D). Thus, with a possible total of 71 430 counts, and division by 71 430, the output is given by

$$(6.80475 \times 10^{-3}) R_{\text{PRN}_1}(\lambda_1 - \hat{\lambda}_1) \cos \phi_0 + n_{\text{rb}}(t) , \quad (\text{F-29})$$

where the variance of  $n_{\text{rb}}(t)$  may be determined by the fact that the signal/noise density ratio is unchanged by the deletion of a heterodyning operation.

$$\text{var} [n_{\text{rb}}(t)] = \frac{[6.80475 \times 10^{-3}]^2 (139.997)}{266.036} = 2.43670 \times 10^{-5} \quad (\text{F-30})$$

If Eq. (F-29) is translated into counts through multiplication by 71 430, we obtain

$$(486.0633) R_{\text{PRN}_1}(\lambda_1 - \hat{\lambda}_1) \cos \phi_0 + n_s(t) , \quad (\text{F-31})$$

where  $n_s(t)$  has a variance of 124326.4 counts<sup>2</sup>.

A signal degradation of 0.4436 dB caused by the input signal to the ship being bandpass filtered ( $\pm 1.073$  MHz) must also be added (perfect bandpass is assumed for analytical ease). The degradation may be derived approximately by multiplying a sequence of  $\pm 1$ 's (with a triangular autocorrelation function) by another sequence that has been low-pass filtered at the chip rate (here, 1.023 MHz), the product has a mean-squared value 0.4436 dB down from unity. (The code autocorrelation

is approximated as triangular even though Gold codes are actually used here.) This effect was not accounted for in the analytical model used to obtain Eq. (F-26); however, the effect of the bandlimiting on the input noise was taken into account. Thus in practice Eq. (F-31) would become

$$(461.8626) R_{\text{PRN}_1} (\lambda_1 - \hat{\lambda}_1) \cos \phi_0 + n_g(t) , \quad (\text{F-32})$$

where  $n_g(t)$  has a variance of  $124326.4 \text{ counts}^2$ . Incidentally, the effects of bandlimiting of signal and noise on system performance approximately cancel each other. Thus Eq. (F-3) of the text has now been derived.

Appendix F

REFERENCE

- F-1. W. J. Gill, "A Comparison of Binary Delay-Lock Tracking Loop Implementations," IEEE Transactions on Aerospace and Electronic Systems, Vol. AES-2, No. 4, July 1966, pp. 415-424.

## Appendix G

### SOME PRACTICAL SIMPLIFICATIONS

In this appendix, we present some practical simplifications and their effects based on Fig. A-4.

First, note that the operations of Lowpass ① and Lowpass ② in Fig. A-3 may be performed after the heterodyning operations in Fig. A-4. This will permit the redundant heterodyning operations on Output ⑤ and Output ⑥ to be combined with the other heterodyning operations in Fig. A-4.

Second, note that the outputs of the suppressed-carrier tracking loop are low frequency ( $< 45$  Hz). The outputs of the heterodyning operations on Output ⑤ and Output ⑥ are also low frequency. Thus, we could reduce the internal sampling rate in the suppressed-carrier tracking loop, and accumulate samples of Output ⑤ and Output ⑥ before mixing these outputs with the suppressed-carrier loop outputs. The accumulation time,  $T_s$ , would have to satisfy  $T_s \ll 0.01$  s in order not to cause extensive intersymbol interference. The signal  $y_{31}(t)$ , which is sent to the data estimator, would no longer change value at the ship-board sampling rate,  $T_p$ , but every  $T_s$  second instead.

We not determine the intersymbol effects of the above procedure. We assume that the number of accumulated samples per data bit interval

is a fixed whole number ( $N_s = \frac{\Delta}{T_s}$ ). The proper choice of which  $N_s$  sam-

ples belong to each data bit is the function of the data clock synchronizer. The synchronizer uses the estimated code epochs to determine which of the 20 code epochs per data interval is aligned with the data bit epoch. Accumulated samples that fall less than  $(T_s/2)$  second after the estimated data epoch are ascribed to the previous bit in the bit-value estimation. The synchronizer uses the estimated code epochs to determine which of the 20 code epochs per data interval is aligned with the data epoch. The absolute value of the offset,  $k_e$ , between the exact data-bit boundaries and the interval over which the  $N_s$  samples integrate lies approximately between 0 and  $(T_s/2) + \sigma(\epsilon_1)$ . The data bits are estimated by adding together the  $N_s$  samples over a given data bit interval to obtain a positive or negative answer. The effective signal power degradation factor,  $d_s$ , to be put into Eq. 15 is a function of  $k_e$ . If the bit stream is a pair-wise uncorrelated sequence, this factor is given by:

$$d_s = \left(\frac{1}{2}\right) \cdot 1 + \left(\frac{1}{2}\right) \left[ 1 - 2 \left( \frac{|k_e|}{\Delta_m} \right) \right]^2 . \quad (G-1)$$

Thus, if  $T_s = 5 \times 10^{-4}$  and  $\Delta_m = 20$  ms, we would insert  $d_s$  as a multiplicative factor in Eq. 15, where  $d_s$  lies between 1 (for  $k_e = 0$ ) and 0.975 [for  $k_e = 2.5 \times 10^{-4} + \sigma(\epsilon_1) \approx 2.5 \times 10^{-4}$ ]. We could utilize either the mean value of  $d_s$ , calculated by assuming a probability density function for  $k_e$ , or we could just use the lower limit (0.975 in this case).

Note that according to discussion there should be a factor of  $d_s$  in Eq. 15 as it stands in Section 5 (with  $T_s = T_p$ , the shipboard sampling rate). However, this factor would be very close to unity, and so has been deleted.

# INITIAL DISTRIBUTION EXTERNAL TO THE APPLIED PHYSICS LABORATORY\*

The work reported in TG 1283 was done under Navy Contract N00017-72-C-4401. This work is related to Task P810, which is supported by Strategic Systems Project Office.

ORGANIZATION	LOCATION	ATTENTION	No. of Copies
<b>DEPARTMENT OF DEFENSE</b>			
DDR&E	Washington, D.C.		1
Weapons Systems Evaluation Group	Arlington, Va.	Director	1
Advanced Research Projects Agency	Arlington, Va.	Director	1
Inst. for Defense Analyses	Alexandria, Va.	Director	1
Defense Mapping Agency	Washington, D.C.	Director	1
DDC	Alexandria, Va.		12
<u>Department of the Navy</u>			
Ass't. Secretary of the Navy (R&D)	Washington, D.C.	Dr. Marcy	1
CNO	Washington, D.C.	OP 352	1
		OP 05	1
		OP 506D	1
		OP 98	1
		OP 986	1
		OP 95	1
CNM	Washington, D.C.	Commander	1
Strategic Systems Project Office	Washington, D.C.	MMAT-32	1
		SP-25	1
		SP-250	1
		SP-2531	1
Office of Naval Research	Arlington, Va.	Code 492	1
		Code 463	1
		Code 480	1
NAVSEASYSOM	Washington, D.C.	SEA-09G3	2
NAVELEXSYSOM	Washington, D.C.	Code 052	1
NAVPRO	Silver Spring, Md.		1
<u>Centers</u>			
NWC	China Lake, Cal.	Library	1
NAVELEXCEN	San Diego, Cal.	Director	1
Naval Surface Weapons Ctr.	White Oak, Md.	Tech. Library	1
	Dahlgren, Va.	Director	1
Naval Warfare Research Ctr.	Menlo Park, Cal.	R. Hill, Code KAS	1
CNA	Arlington, Va.	Commanding Officer	1
		Commanding Officer	1
<u>Laboratories</u>			
NRL	Washington, D.C.	Director	1
<u>Schools</u>			
U.S. Naval Academy	Annapolis, Md.	Supt. Library	1
<u>Department of the Air Force</u>			
SAMSO	Los Angeles, Cal.	Attn. JPO-YE	1
<b>CONTRACTORS</b>			
Interstate Electronics Corp.	Anaheim, Cal.	H. Baggot	1
Requests for copies of this report from DoD activities and contractors should be directed to DDC, Cameron Station, Alexandria, Virginia 22314 using DDC Form 1 and, if necessary, DDC Form 56.			

\*Initial distribution of this document within the Applied Physics Laboratory has been made in accordance with a list on file in the APL Technical Publications Group.